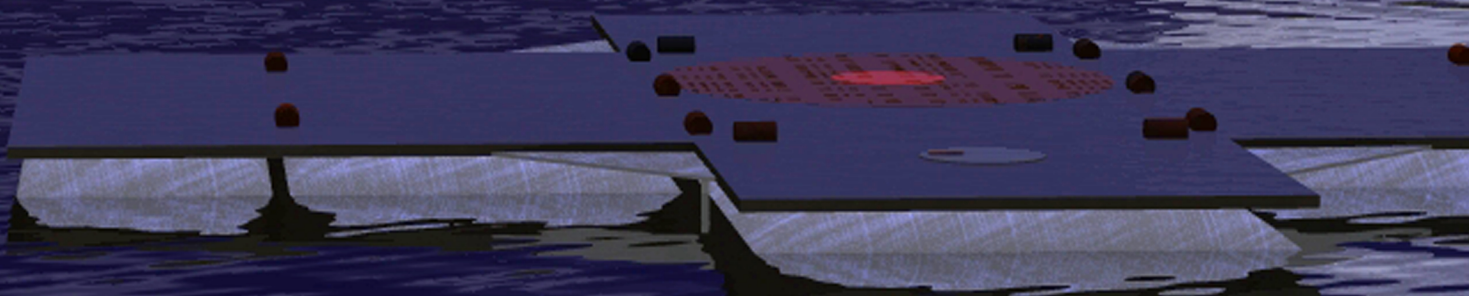University of Maryland

TRITON

ADVANCED DEPLOYABLE COMPACT ROTORCRAFT
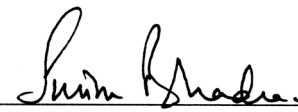
JUNE 1, 2007

University of Maryland

Alfred Gessow Rotorcraft Center

Department of Aerospace Engineering
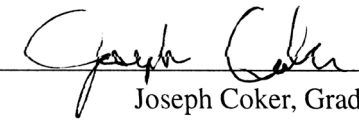
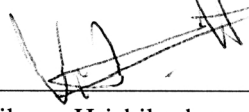University of Maryland

College Park, Maryland 20742

TRITON

ADVANCED DEPLOYABLE COMPACT ROTORCRAFT
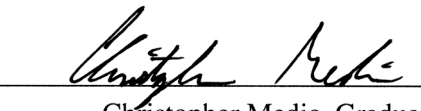
In response to the 2007 American Helicopter Society

Student Design Competition - Graduate Category

June 1, 2007
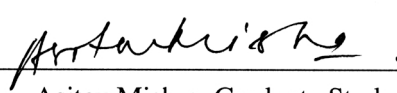
Benjamin Silbaugh - Graduate Student (Team Leader)
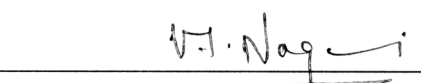
Smita Bhadra, Graduate Student

Joseph Coker, Graduate Student

Vikram Hrishikeshavan, Graduate Student

Christopher Medic, Graduate Student

Asitav Mishra, Graduate Student

Dr. Vengalattore T. Nagaraj - Faculty Advisor

Dr. Inderjit Chopra - Faculty Advisor

Acknowledgements

The TRITON design team would like to acknowledge the following people and thank them for their advice and assistance:

Contents

List of Figures

List of Tables

List of Symbols and Abbreviations

Symbol	Description	Symbol	Description
σ	Solidity	μ	Advance Ratio
AHS	American Helicopter Society	ARV	Approach and Recovery Vehicle
BVI	Blade-Vortex-Interactions	DL	Disk Loading
CG	Center of Gravity	C_T	Thrust Coefficient
FCS	Flight Control System	c.g.	Center of Gravity
DOC	Direct Operating Cost	FAR	Federal Aviation Regulation
UEV	unmanned escort vehicle	θ	Blade Pitch
HOGE	Hover Out of Ground Effect	FADEC	Full Authority Digital Electronic Control
HUMS	Health and Usage Monitoring System	AR	Blade Aspect Ratio
HPP	Half Peak-to-Peak	MRP	maximum rated power
ISA	International Standard Atmosphere	GPS	Global Positioning System
IBC	individual blade control	GTOW	Gross Take Off Weight
INS	Inertial Navigation System	DGPS	Differential Global Positioning System
LHLRS	Light Harpoon Landing Restraint System	MPT	Magnetic Particulate Trap
MFD	Multi-Functional Display	MCP	Maximum Continuous Power
NOTAR	No Tail Rotor	Nb	Number of Blades
RFP	Request for Proposals	Ω	Angular Velocity
RPM	Rotations Per Minute	RTM	Resin Transfer Molding
RTM	Resin Transfer Molding	SLRP	Submersible Launch and Recovery Pod
SMR/TR	Single Main Rotor, Conventional Tail Rotor	SMR	Single Main Rotor
SSGN	Submersible Ship, Guided missile, Nuclear-powered	SSCN	Submersible Ship, Aircraft Carrier, Nuclear-powered
SHP	Shaft Horsepower	SFC	Specific Fuel Consumption
IOC	Indirect Operating Cost	TE	Trailing Edge
UMARC	Univ. of Maryland Adv. Rotor Code	USN	United States Navy
TO	Take Off	UCARS	Unmanned Air Vehicle Common Automatic Recovery System
TCS	Tactical Command System	IR	Infrared
VTOL	vertical takeoff and landing	VVI	vortex-vortex-interactions

RFP Requirements and Compliance

Table 1: Common UEV and ARV RFP requirements

Requirment	Action Taken	Section
Deployable from submerged sub at periscope depth (-50 ft)	SLRP design	Section 2.1.2
VTOL capable	TRITON is a rotory wing craft	Throughtout the report and Section 1.2
Automatic take-off and landing with manual take-off abort and landing wave-off (both land and sea)	Autonomous Control System enables these features	Section 7.1and 9.1
Automatic recovery to predesignated location	Flight Control System enables	Section 9.1 and 9.2
Automatic folding of blades/wings	Automatic Blade Fold System	Section 4.6
Critical system components and subsystems are protected (to the extent possible) against combat damage	Ceramic matrix composite CRYSTALOY used to protect skin	Section 6.4
Impervious to the effects of sea water	Advanced composite material selection	Chapter 6 and Section 6.5
Able to remain afloat in sea state 3 for no less than 30-minutes	Specially designed hull and water tight fuselage	Section 6.3
High degree of availibility and reliability	Affordable proven state-of-the-art	Section 6.5, 7, 4.2.2
HOGE at 6000 ft, 95° F	TRITON designed for high HOGE performance	Chapter 11 and section 11.2
Capable of safe operation at low cruise altitude of less than 50-ft *AGL*	Autorotation capability and Automatic Nap-of-Earth Guidance System	Sections 4.2.5 and 9.2
Mission range of 280-nm	TRITON sized for this requirement including reserves	Chapter 3
100% Mission capable in maritime, arctic, tropical and desert climates	Main rotor has good de-icing, erosion resistant capability	Section 4.2.3
Launch capable within 30-minutes of tasking	SLRP concept design	Section 2.1.2
Maximum of 10-minutes from vehicle surfacing to take-off	SLRP concept design	Section 2.1.2
Maximum of 10-minutes from water landing to submersion below water's surface	SLRP concept design	Section 2.1.2
Transportable by C-130J: 40 x 10.25 x 9 ft	Small overall size of TRITON enables transportability of two vehicles at a time in C-130J	Section 3.2.2

Table 2: ARV specific RFP requirements

Requirement	Action Taken	Section
Payload capacity of 800 lbs (assumed minimum)	incorporated in Sizing of *Triton*	Chapter 10
Crash worthy fuel system	Self-sealing, crash worthy tanks used	Section 6.3
Configurable to allow transport of one or both crew members as injured personnel	Taken care in internal cabin configuration	Section 7.3.1
Lighting compatible with night vision goggles	TCS has night vision goggles compatible displays	Section 7.1.2
IR/Low light imaging	FLIR Systems BriteStar II provides this	Section 7.2.1
All weather, day-night, pilotage	FLIR Systems BriteStar II ensures this	Section 7.2.1
Compatible with all net-centric services (real-time information exchange)	Compatibility achieved through Future Combat System (FCS)	Section 7.1.3
Over the horizon, jam resistant com (voice, data, imaging).	Incorporated in Autonomous Constrol System (ACS) and FCS	Sections 7.1 and 7.1.3
Wireless com (voice, data, imaging) between other ARVs or personnel up to ranges of 100 meters	Incorporated in ARV control system	Section 7.1.2

Table 3: UEV specific RFP requirements

Requirement	Action Taken	Section
Payload capacity of 600-lbs (assumed minimum)	incorporated in TRITON sizing	Chapter 3
Capable of programming mission prior to launch	Autonomous Control System	Section 7.1
Capable of re-planning mission prior to launch	Autonomous Control System	Section 7.1
Incorporate tactical data link to provide command, control commnunications (C3) and data exchange: video, data and telemetry between UEV and ARV, and only video and data commnunications to the network.	Autonomous Control System	Section 7.1
Incorporates TCDL (Tactical Command Data Link)	Autonomous Control System	Section 7.1
Has embeded VHF and UHF radio relay capability to augment system's tactical comm (i.e. address line-of-sight problems)	Autonomous Control System	Section 7.1

Table 4: LRS RFP requirments

Requirement	Action Taken	Section
Faciliates vehicle launch capability of no greater than 30-minutes of tasking	SLRP design	Chapter 2 and Section 2.3.1
Capable of recovering vehicle from water surface to hanger in less than 10-minutes	SLRP design	Section 2.3.1
Permits vehicle to take-off in less than 10-minutes from time of surfacing	SLRP design	Section 2.3.1

Table 5: Hanger conversion RFP requirements

Requirement	Action Taken	Section
Hanger does not require the conversion of more than 20 trident missle silos	Sub hangar configuration	Chapter 2
Number of converted missle silos is kept to a minimum	Sub hangar configuration	Chapter 2

10.5

4.0°

14.0°

21.98

6.56

5.38
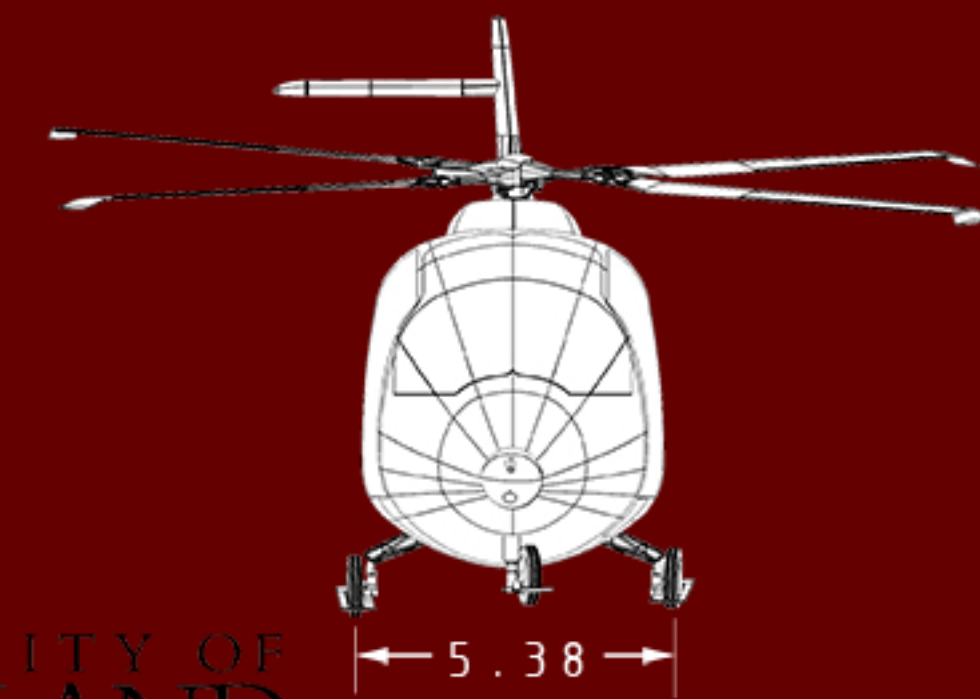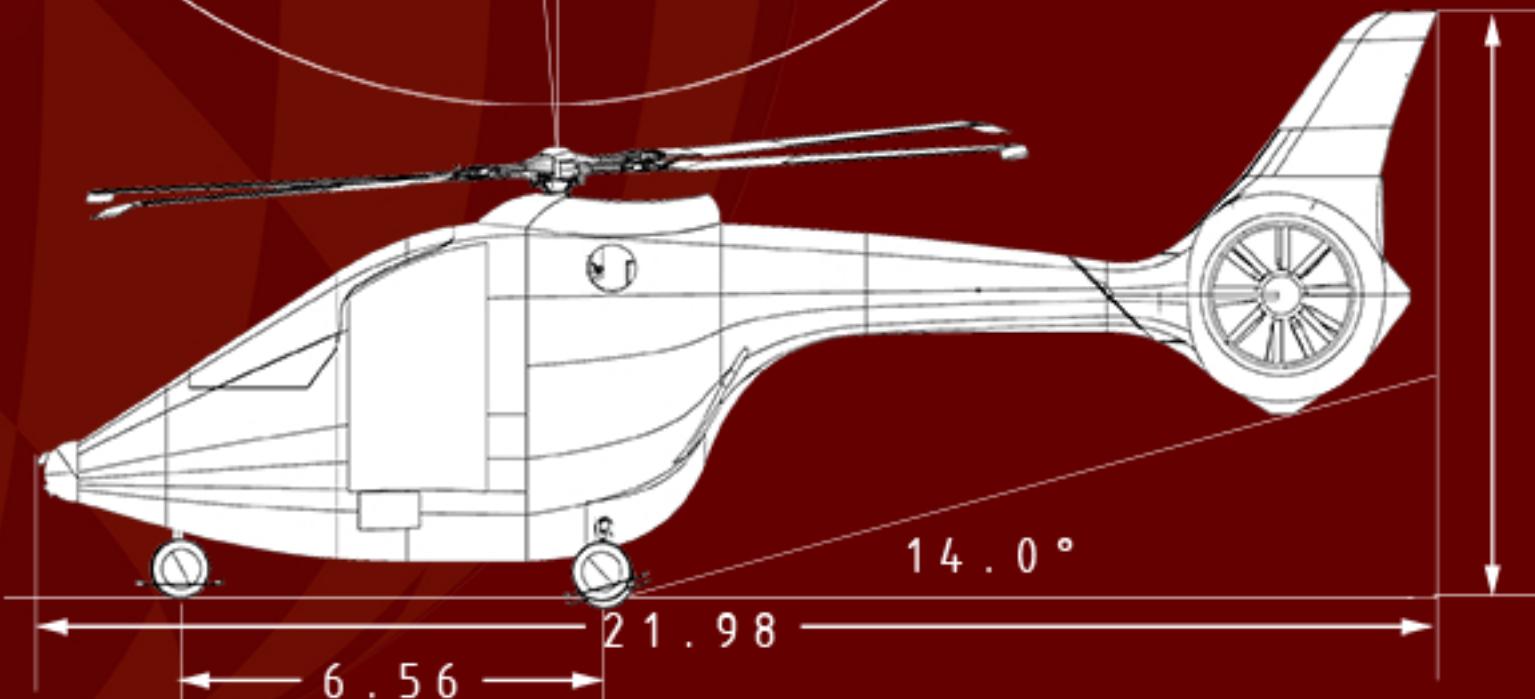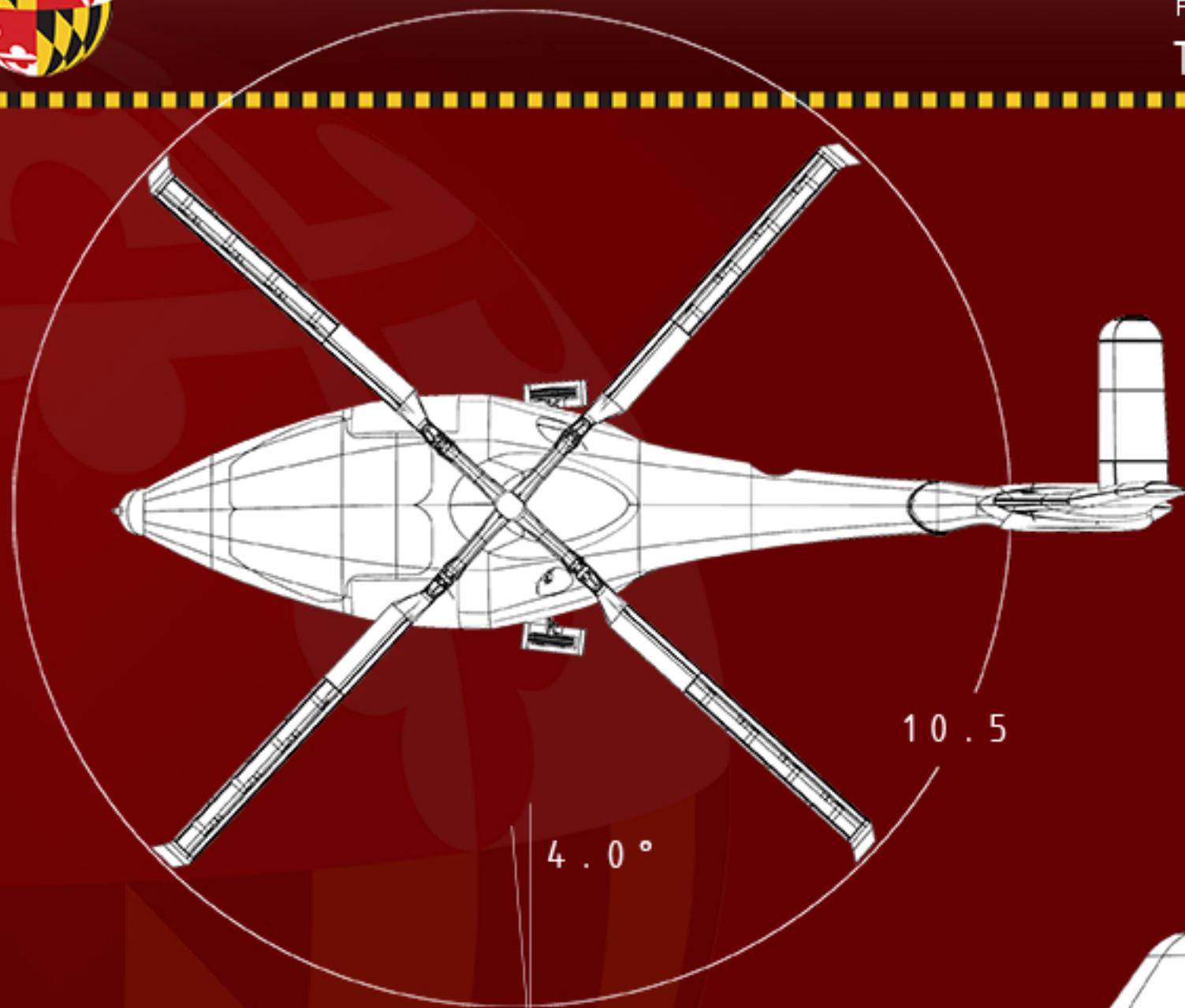
ALL DIMENSIONS IN FEET

UNIVERSITY OF
MARYLAND

CRASHWORTHY SEATS

HOIST SYSTEM

TCS INSTALLATIONS

TRITON ARV
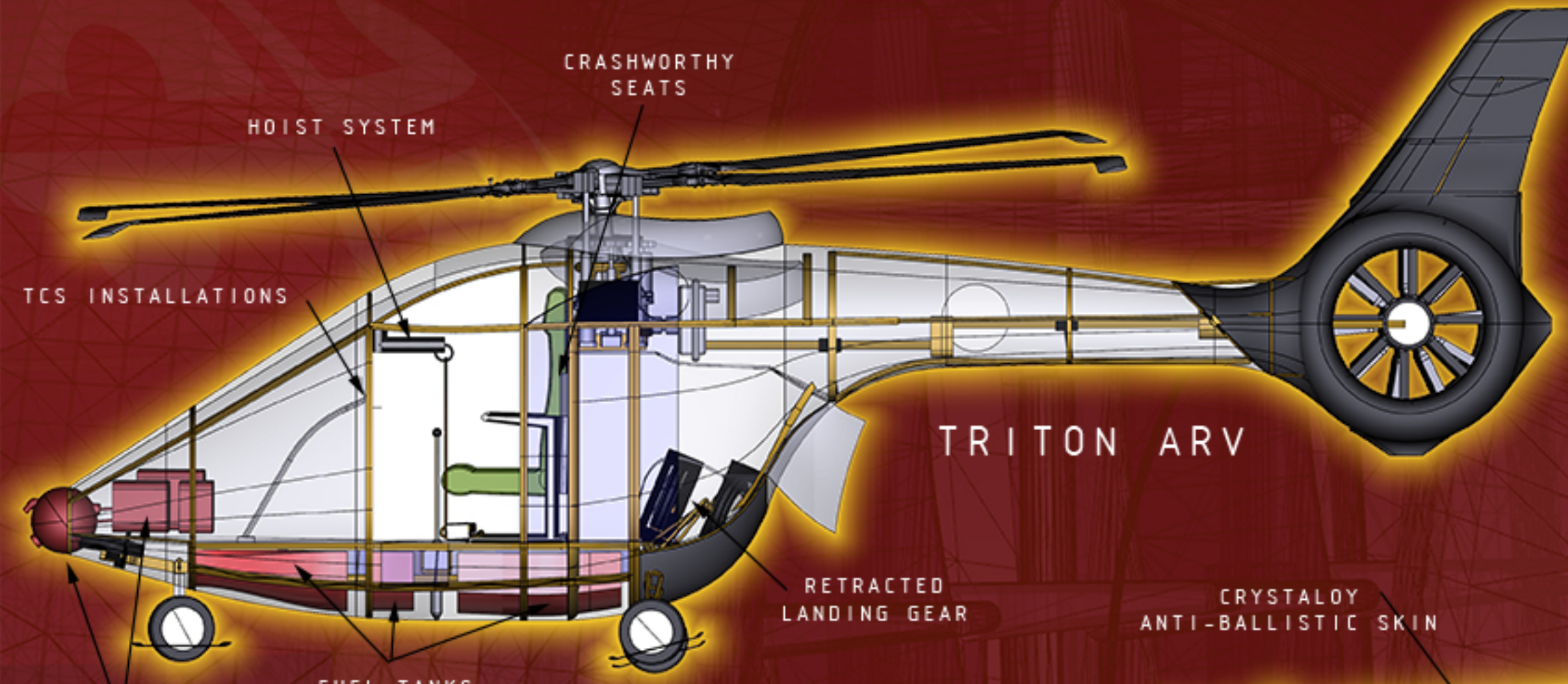
ARV EMPTY WEIGHT: 1110 lb
ARV FUEL: 320 lb
ARV PAYLOAD: 800 lb
ARV GTOW: 2230 lb

RETRACTED LANDING GEAR

CRYSTALOY ANTI-BALLISTIC SKIN

FUEL TANKS

AVIONICS SUITE

ADDITIONAL FUEL TANKS

TRITON UEV

CLAM-SHELL CARGO DOORS
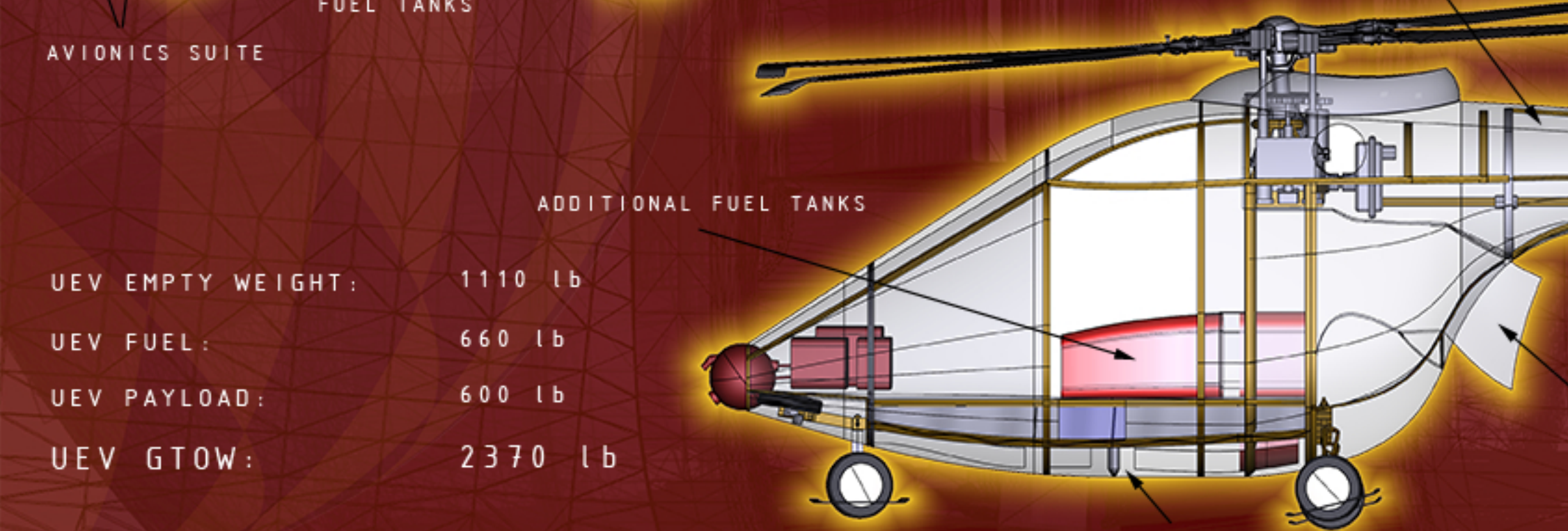
UEV EMPTY WEIGHT: 1110 lb
UEV FUEL: 660 lb
UEV PAYLOAD: 600 lb
UEV GTOW: 2370 lb

LHLRS

UNIVERSITY OF MARYLAND

1   Introduction

The RFP for the 24th Annual AHS Student Design Competition (*Advanced Deployable Compact Rotorcraft in support of Special Operations Forces*), sponsored by Sikorsky Aircraft, requires the design of VTOL aircraft for special operations missions launched via retrofitted *Ohio* class submarine (SSGN). The primary purpose of these Special Operations Forces (SOF) missions is stealthy deployment to maritime littoral regions.

The TRITON Advanced Deployment System proposes a three-part design solution to comprehensively meet the tasks stated in RFP: an Approach and Recovery Vehicle (dubbed TRITON ARV), an Unmanned Escort Vehicle (TRITON UEV), and an innovative launch and recovery system to facilitate deployment from a submersible ship aircraft carrier (SSCN). The TRITON ARV is tasked with the physical transportation of the SOF, while the UEV provides "eye-in-the-sky" support to personnel on the ground, in the air, and underwater.

Each TRITON ARV carries two non-pilot-trained SOF, with a maximum payload of 800 lbs. The mission profile for the ARV is given in Figure 1.1.

The UEV provides necessary aerial surveillance and reconnaissance during the duration of SOF deployment, carrying a payload of 600 lbs. Mission profile for the UEV is provided in Figure 1.2.

The launch and recovery system is stored within the shell of a converted *Ohio* class SSGN. Space previously used for Trident missile storage is converted to provide hangar space for the TRITON deployment system, reclassifying the submarine as an SSCN; all vehicles and launch/recovery hardware are stored in this region. Removal of 20 Trident missile silos—the maximum allowed by RFP—results in a box-like hangar space of length 70 ft, width 14 ft and height 44 ft. Figure 1.3 illustrates the SSGN space available for conversion.

1.1   Design Drivers

Since the primary design goal is to transport as many SOF team members within a fixed time window, and the number of SOF per vehicle has been fixed to two persons, the following primary design objectives become clear:

i (the overall folded dimensions of the vehicles should be minimized in order to maximize the number of vehicles that can be stored in the submarine.

ii the vehicle cruise speed should be maximized to decrease the time duration of each round trip to and from the desired destination.

Additionally, the clandestine nature of Special Operations missions indicates a third primary design driver:

iii visual and acoustic detectability should be minimized to ensure mission integrity.
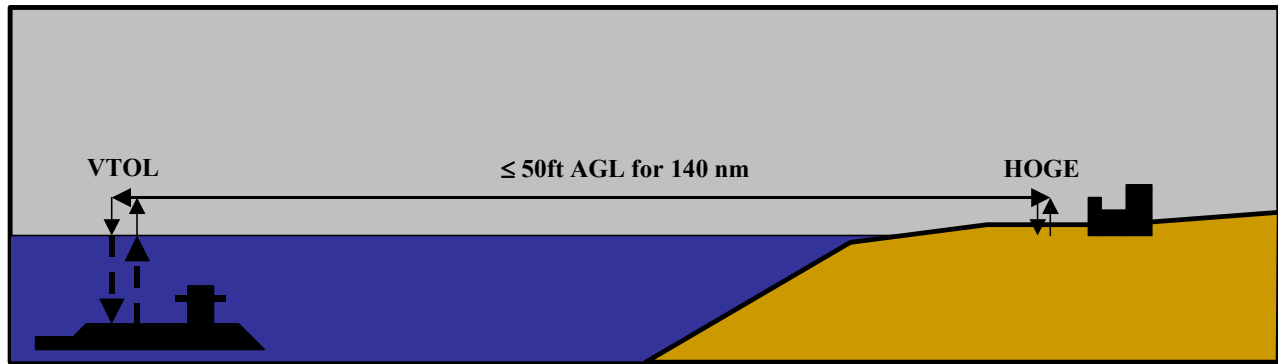
ARV Mission Profile

Segment	1	2	3	4	5	6	7	Units
Type	Idle	HOGE	Cruise	HOGE	Cruise	HOGE	Reserve	-
Speed	0	0	V_{br-99}	0	V_{br-99}	0	V_{be}	ktas
Time	4	2	-	4	-	2	20	min
Range	-	-	140	-	140	-	-	nm
Altitude	0	0	0	0	0	0	0	ft
Temperature	102.92	102.92	102.92	102.92	102.92	102.92	102.92	°F
Engine Rating	IRP	MRP	MCP	MRP	MCP	MRP	MCP	-

Figure 1.1: Mission profile for Approach and Recovery Vehicle

1.2   Configuration Selection

1.2.1 Methodology.

Selection of the optimal VTOL configurations for this mission was aided by use of the Pugh decision matrix. This method provides a means of evaluating many possible solutions based on the degree to which each solution satisfies a number of mission-specific design criteria. The result is a qualitative measure of the overall effectiveness of each possible design solution.

Of the many Pugh method variations, the following selection scheme is used:

1. Identify all relevant design criteria.

2. Identify all feasible vehicle configurations of interest.

3. Choose a baseline configuration against which all other "alternative" configurations are scored.

4. Assign numerical weights—from 1 to 10—to each of the design criteria, where a score of 1 indicates a criterion of little to no importance and a score of 10 indicates a criterion critical to mission success.

5. Assign scores—from -3 to +3—to a particular configuration's ability to meet each of the design criteria.
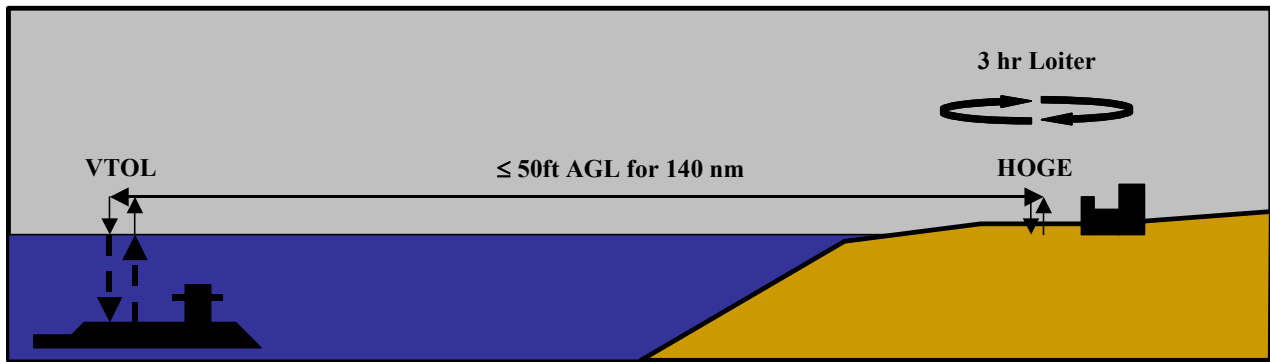
UEV Mission Profile

Segment	1	2	3	4	5	6	7	Units
Type	Idle	HOGE	Cruise	Loiter	Cruise	HOGE	Reserve	-
Speed	0	0	V_{br-99}	V_{be}	V_{br-99}	0	V_{be}	ktas
Time	4	2	-	180	-	2	20	min
Range	-	-	140	-	140	-	-	nm
Altitude	0	0	0	0	0	0	0	ft
Temperature	102.92	102.92	102.92	102.92	102.92	102.92	102.92	°F
Engine Rating	IRP	MRP	MCP	MCP	MCP	MRP	MCP	-

Figure 1.2: Mission profile for Unmanned Escort Vehicle
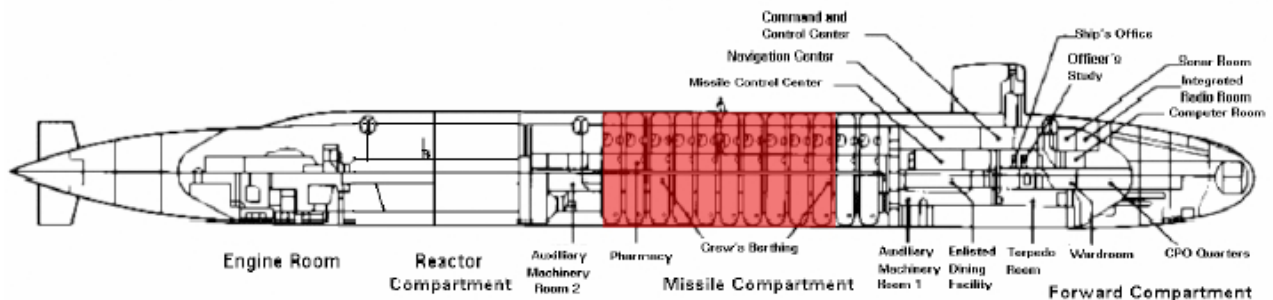
Figure 1.3: Available SSGN space

A score of -3 represents much worse than baseline, 0 represents equivalence to baseline, while +3 is much superior to baseline.

6. Compute a total weighted score for each configuration.

The final weighted scores reflect the relative merit of choosing a particular configuration.

1.2.2 Selection Criteria.   The following criteria are used to evaluate the *relative* merit of each alternative

VTOL configuration:

- **Compactness of folded vehicle dimensions**
- **Maturity of technology**
- **Aerodynamic cleanliness**
- **Low empty weight**
- **High hover efficiency**
- **High endurance**
- **Range**
- **High cruise speed**
- **Agility**
- **Low vibration**
- **Low downwash**

- **Safety**
- **Concealment of critical components**
- **Low IR signature**
- **Low radar signature**
- **Low acoustic signature**
- **Low visual signature**
- **Ease of manufacture**
- **Low manufacturing cost**
- **High maintainability**
- **Low operation and maintenance cost**

1.2.3 Vehicle Configurations.

The conventional single main-rotor/tail-rotor (SMR/TR) configuration was selected as the baseline VTOL configuration. Of the existing known VTOL configurations, the following were identified as alternative configurations:

- **Single Main Rotor with Fenestron**
- **Single Main Rotor with NOTAR**
- **Tip jet (cold)**
- **Tip jet (hot)**
- **Coaxial**
- **Coaxial rigid**

- **Syncropter**
- **Tandem**
- **Lift and thrust compound**
- **Tilt rotor**
- **Tilt wing**

1.2.4 Criteria Weighting.   The weight of each design criterion is driven by the specific mission requirements and operating environment stipulated in RFP. Recognizing that the ARV and UEV have differing mission requirements, different criteria weights are assigned for each vehicle. Table 1.2.4 shows the assigned weights for the ARV and UEV.

Table 1.1: Criteria weights

	Weight	
Criteria	ARV	UEV
Compactness (folded)	10	10
Maturity of technology	7	7
Aerodynamic cleanliness	6	6
Empty weight	5	5
Hover efficiency	5	6
Endurance	6	9
Range	9	6
Max cruise speed	9	8
Agility	8	7
Vibration	7	7
Downwash	9	6
Safety	5	5
Concealment of critical components	6	6
IR signature	9	9
Radar signature	9	9
Acoustic signature	10	10
Visual signature	9	9
Manufacturability	6	6
Manufacturing costs	5	5
Maintainability	7	7
Operation and maintenance costs	5	5

1.2.5 Configuration Ranking.   Table 1.2 provides the scoring of each configuration with respect to design criteria. The following is a brief discussion of the rationale behind each score based on notes compiled from a series of configuration selection meetings.

Table 1.2: Criterion-specific configuration scores

Criteria	SMR w/TR (baseline)	SMR w/Fenestron	SMR w/NOTAR	Tip Jet (cold)	Tip Jet (hot)	Coaxial	Coaxial Rigid	Syncropter	Tandem	Lift Thrust Compound	Tilt Rotor	Tilt Wing
Compactness	0	-1	-2	2	2	2	1	1	-2	-1	-2	-2
Maturity of Tech.	0	0	-1	-2	-2	0	-1	0	0	-1	-1	-2
Aero. Cleanliness	0	1	1	0	0	-2	-1	-2	-2	-2	1	2
Empty Weight	0	-1	-2	-1	-1	-1	-2	-1	-1	-2	-2	-2
Hover Efficiency	0	0	0	-2	-2	0	0	0	1	-2	-2	-2
Endurance	0	1	0	-2	-2	-2	-1	-1	-2	-1	1	1
Range	0	0	0	-1	-1	-2	-1	-1	-1	1	2	2
Max Cruise Speed	0	0	0	-1	-1	0	1	-1	-1	1	3	3
Agility	0	1	-2	-1	-1	1	3	0	-1	1	1	1
Vibration	0	1	2	-1	-1	-1	-2	-1	0	1	2	2
Downwash	0	0	0	0	0	-1	-1	-1	2	-1	-2	-3
Safety	0	1	2	2	0	2	2	1	2	-1	1	1
Concealment of Components	0	1	2	1	1	-1	1	-1	0	-1	0	0
IR Signature	0	0	0	0	-3	0	0	0	0	0	0	0
Radar Signature	0	1	0	0	0	-1	-1	-1	-1	-3	-2	-2
Acoustic Signature	0	0	1	-3	-3	0	0	0	0	-2	-1	-1
Visual Signature	0	0	0	1	1	1	1	1	-1	-1	-2	-2
Manufacturability	0	-1	-1	-3	1	-1	-2	-1	0	-2	-3	-3
Manufacturing Costs	0	-1	-2	-1	-1	-1	-2	-1	0	-2	-3	-3
Maintainability	0	-1	-2	-2	0	-1	-1	-1	-1	-2	-2	-2
O & M Costs	0	0	0	-2	-2	-1	-1	-1	-1	-2	-2	-2

- **Compactness:** The coaxial and tip jet configurations were scored the highest primarily due to absence of an anti-torque system and short tail boom requirement. Tilt rotors and tilt wings were scored lowest due to the space required for wing and rotor systems.

- **Maturity of Technology:** SMR w/ Fenestron was scored equal to the conventional tail rotor configuration. Though the Fenestron concept is "newer," extensive research and usage in existing vehicles has established its maturity. Tip jet and tilt-wing configurations were scored lowest due to limited usage in industry.

- **Aerodynamic Cleanliness:** The tilt-wing concept was scored highest due to optimal alignment of the

wings in hover, and axial flow through the rotor system during forward flight. Tilt-rotor was scored lower due to the poor wing alignment in hover. NOTAR and Fenestron scored higher than SMR/TR due to limited adverse interactions with the main rotor wake and the elimination of tail rotor hub drag. Tip jet configurations were scored equal to the baseline (SMR/TR) despite the drag increase due to thicker blade sections (required for fuel lines and/or air ducts, and structural strength) due to lack of tail rotor wake interaction.

- **Empty Weight:** All alternative configurations were scored lower than the baseline SMR/TR configuration. Fenestron scored lower due to the additional, weight-increasing ductwork required to surround the fan. The compressor system introduces weight penalties to the NOTAR configuration. The tip jet configurations save weight associated with a tail rotor system and drive train; however, the added structural weight of the rotor system induces a weight penalty. Auxiliary lift and propulsion systems associated with compound, tilt rotor and tilt wing configurations were estimated to introduce significant weight penalties.

- **Hover Efficiency:** Hover efficiency was evaluated based on relative disk loading, with the tandem scoring the highest. The lift and thrust compound was penalized for the rotor download on the wing, and tilt rotor and tilt wing were penalized for low rotor solidity.

- **Endurance:** The high fuel consumption of tip jet rotors was the basis for their low endurance score. Dual rotors configurations scored lower for increased hub drag, with an additional penalty for the coaxial configurations due to the large rotor mast.

- **Cruise Speed:** Both tilt rotor and tilt wing configurations were scored the highest. Forward speed of tip jet rotors is limited by the power required by the rotor at high speed.

- **Agility:** The agility of a rotary-wing vehicle is largely dictated by the rotor system. The rigid coaxial configuration was ranked highest due to responsiveness of its rigid rotor system and high yaw rates achieved through differential collective inputs. NOTAR was scored lower because of the slow response of aerodynamic forces generated by the Coanda jet.

- **Vibration:** The tilt rotor/wing concepts were scored highest. Since the rotor system essentially sees only axial flow in high-speed forward flight, there is no significant asymmetry in the aerodynamic loading; therefore, the vibration associated with the rotor system is small. On the other end of the spectrum lies the coaxial rigid rotor concept. The asymmetry of the aerodynamic loading combined with rigid blades could yield a potentially large source of vibration.

- **Downwash:** The downwash from the rotor system is estimated by the rotor disk loading. Hence, the tilt-wing and tilt-rotor configurations were scored lowest. For similar reasons, the tandem was awarded the highest score.

- **Safety:** Exposed tail rotor systems are known for being potential safety hazards; they represent an obvious danger to ground crew, and when in flight can cause catastrophic failure if impacted. Shrouded and tail rotor-free designs were scored higher, while the tip jet (hot) was penalized for the proximity of the hot jet exhaust to ground level. Syncropter was scored lower for the low head clearance due to the angled tip-path-plane.

- **Concealment of Components:** The concealment of components for most configurations was viewed to be on par with the SMR/TR configuration. Exceptions include the NOTAR system, which scored higher for the enclosed nature of its anti-torque system. Coaxial rotor systems scored lower for the exposure of additional rotor control components.

- **IR Signature:** With the exception of the tip jet (hot), all alternative configurations were scored the same. The tip jet exhaust increases IR detectability.

- **Radar Signature:** One major contributor to the radar signature of a vehicle is the rotor system. Since a compound helicopter has wings and engine nacelles in addition to the main rotor system, it scored the lowest. For similar reasons, the tilt rotor/wing configurations were given negative scores; however, penalties were not as severe due to the smaller rotor sizes. Dual rotor configurations were also scored lower for having two large rotors.

- **Acoustic Signature:** The noise associated with the tip jet-driven rotors resulted in their low acoustic score. The lack of a tail rotor or fan results in NOTAR vehicles having favorable acoustic properties.

- **Visual Signature:** Visual signature of each configuration was determined by the relative size of each configuration. With the exception of the tandem, all dual rotor configurations were awarded positive points due to the short tail boom. Negative scores were given to the tilt-rotor/wing vehicles as a result of larger airframes.

- **Manufacturability:** Manufacturability score of tip jet (cold) vehicles was scored lower for complex blade and tip jet design. Also, the rotating mechanism and complex control rigging of tilt rotor/wing configurations resulted in negative manufacturing scores. The tip jet (hot) configuration was awarded positive points since its working components are essentially external to the vehicle and lacks the need of a transmission or tail-rotor system.

- **Manufacturing Costs:** Scoring of manufacturing costs essentially followed the same rationale used to evaluate the manufacturing criteria. NOTAR received a lower score because of the extra cost of the compressor.

- **Maintainability:** Maintainability scores of each configuration were driven by overall complexity. The tilt rotor/wing configurations received negative points for the rotating mechanism required to actuate the

working surfaces. The tip jet (hot) was not scored as low as tip jet (cold) as most of its major components are external to the vehicle and can be easily accessed.

- **Operation and Maintenance Cost:** The Operation and Maintenance (O & M) scores were driven by estimated fuel costs. Therefore, the scores given are the same as those assigned for the endurance criteria.

1.2.6 Total Mission Weighted Scores.

The final configuration scores are provided in Figure 1.4. It is clear that SMR w/ Fenestron configuration is the optimal choice for both ARV and UEV mission profiles. Due to mechanical complexity of coaxial rotor designs, large overall size of tilt rotor or tilt wing configurations and poor performance of tip-jet rotors, neither of these configurations are likely to be optimal for either ARV or UEV missions.
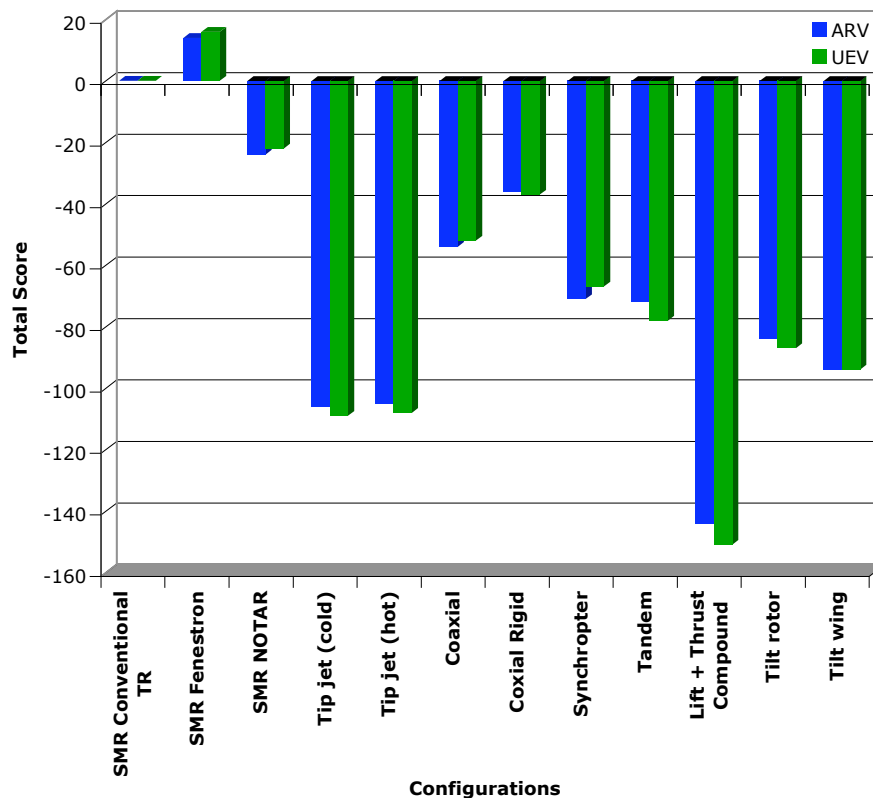
Figure 1.4: Total mission weighted configuration scores

1.2.7 Summary.   As indicated by the results of the Pugh decision matrix, the configuration of choice for both ARV and UEV missions is the SMR w/ Fenestron.

TRITON SUBMERSIBLE LAUNCH AND RECOVERY POD

TELESCOPING
PNEUMATIC PROBE
GUIDES DESCENT

CIRCULAR GRID
PROVIDES
LANDING TARGET

LIGHT HARPOON
LANDING RESTRAINT
SYSTEM (LHLRS)

UCARS TRANSPONDER
PROVIDES LANDING SUPPORT

ELECTRIC MOTORS
DEPLOY SLRP WALLS

MANUAL/EMERGENCY
ESCAPE HATCH

WATERPROOF BAFFLES
PREVENT SEAWATER INTRUSION

INFLATABLE BLADDERS PROVIDE
BUOYANCY, STABILITY

UNIVERSITY OF
MARYLAND
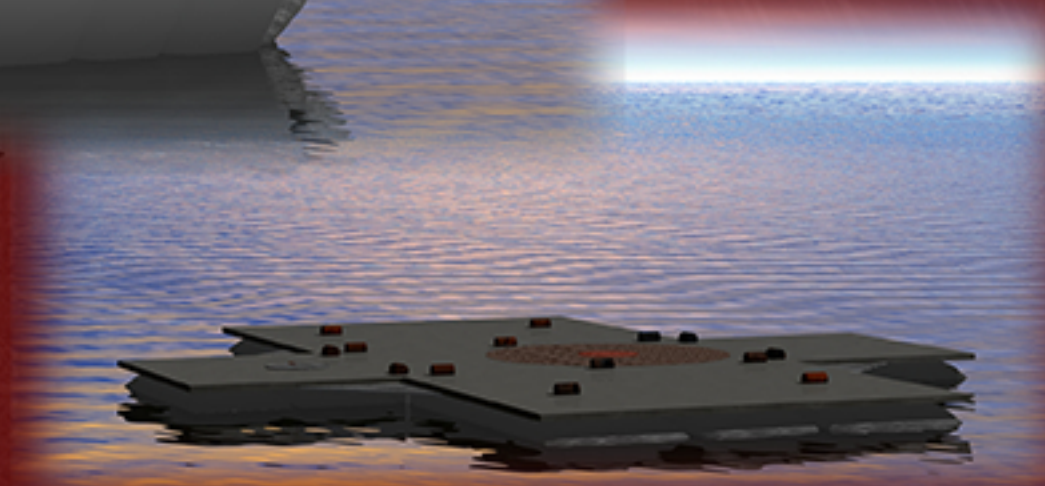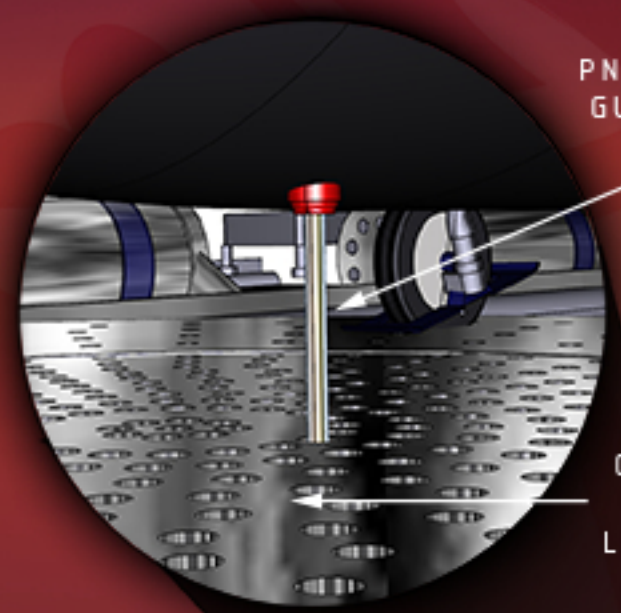
2 Launch/Recovery System and Mission Capability

The TRITON Advanced Deployment System relies on an innovative launch and recovery system to efficiently deploy up to 28 SOF members in the RFP-stipulated time window. This is accomplished through use of the TRITON Submersible Launch and Recovery Pod and appropriate conversion of an SSGN submarine. This chapter describes the launch and recovery procedure in detail to illustrate the effectiveness of this design.

2.1 Submersible Launch and Recovery Pod (SLRP)

2.1.1 SLRP Concept. A custom launch and recovery system is used to facilitate deployment of the ARV and UEV. This system relies on specially designed Submersible Launch and Recovery Pods (SLRP) to transport vehicles to and from the submarine hangar bay. Upon reaching the surface of the water, the pod expands into a floating platform from which the helicopters may take off and land. A pod-like concept was selected for waterborne transport to avoid the difficulties associated with sealing an entire vehicle (as would have been necessary for a fully submersible helicopter design). Additionally, the effect of constant exposure to corrosive seawater could be disastrous[1].

Each Submersible Launch and Recovery Pod (SLRP) contains a single helicopter and is raised and lowered from the submarine hangar bay by a cable winch system. Upon reaching the surface, air bladders surrounding the pod inflate and the walls unfold to provide a stable floating platform for takeoff, landing, troop/equipment loading, and hot refueling. Using the platform as a helipad prevents the need to fully seal the underside of the fuselage for water landing. The SLRP deploys and recovers ARV and UEV helicopters safely and covertly. As opposed to a submersible helicopter, the SLRP is a simple, elegant design that is feasible at the current technology state.

2.1.2 SLRP Design. The SLRP is attached at each corner by a cable connected to a winch system internal to the sub. The winch system is designed with a clutch to take up slack or provide slack as necessary to provide hydrodynamic stability while floating on the water's surface. In the event of an emergency in which the pod cannot be recovered to the sub, hydraulic guillotines on the sub will cut the cables and 'pickle' the pod. Subsystems are connected to the SLRP from the hangar bay via a flexible umbilical cord. These systems include: a hydraulic pump to power pod folding actuators, a pneumatic pump to inflate air bladders and provide an emergency air supply to the pod, an electric generator to power onboard avionics, and a fuel pump for hot refueling (while engine running) of the helicopters. The MacArtney Group specializes in the design of marine launch and recovery systems, including winches, umbilical lines, dynamic cables, and wave compensation systems[2] and would be

Figure 2.1: Unmanned Air Vehicle Common Automatic Recovery System (UCARS)
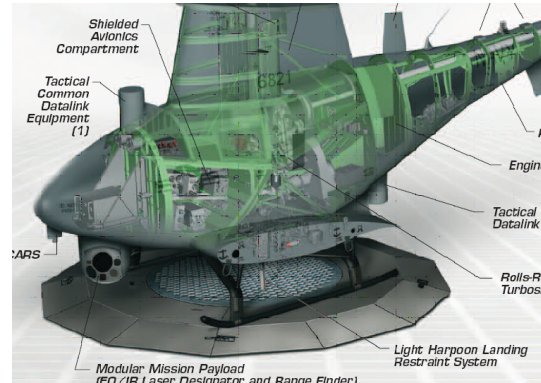
Figure 2.2: Light Harpoon Landing Restraint System (LHLRS)

consulted in full development of the SLRP.

The SLRP's structure is designed to handle the pressures greater than those experienced at periscope depth. Support beams mounted to the outside pod walls are designed to help align the pod as it is recovered into the sub and protect the deflated air bladders from damage. Compression seals between the beveled wall edges prevent any water intrusion while the pod is submerged. The closed pod has strong positive buoyancy that allows it to rise from the sub without needing to inflate the bladders. The bladders inflate as the pod ascends until the pod reaches equilibrium buoyancy with a pod height 6.6 feet (2 m) above the water's surface. At this point the pod walls deploy, raising the platform surface 1.5 feet (0.46 m) above the water. Folding waterproof baffles attached between the side and end walls prevent water intrusion while the SLRP converts back to sealed pod form.

A door on one end of the pod allows SOF to exit or enter the pod while it is stowed in the submarine. Figure (see Foldout 1.2.7) provides an overview of the aforementioned design features.

SLRP Automatic Landing System

The UEV/ARV must be capable of automatic and precise landing in any weather, regardless of wind and sea conditions. To accomplish this, the SLRP uses the Unmanned Air Vehicle Common Automatic Recovery System[3] (UCARS) (Fig. 2.1) to assist in the guided landing of the helicopter to the SLRP. The UCARS system uses K_a band (26.5 to 40 GHz) tracking radar and data from a platform motion sensor to provide precise position of the platform relative to the ARV/UEV. This permits the helicopter to maneuver to a low dispersion landing point on the platform within an area capable of post-recovery restraint and stow prior to the pod closing.

Once the aircraft maneuvers to a point over the computed touchdown point, the Light Harpoon Landing Restraint System[4] (LHLRS) (Fig. 2.2) completes the recovery procedure. The LHLRS consists of a pneumatically fired telescoping probe mounted at the bottom of the ARV/UEV near the aircraft c.g.. The probe extends and attaches to a circular grid, which is integrated into the SLRP deck. The harpoon then retracts and secures the

helicopter to the platform. The harpoon also serves as a deck restraint to stabilize the aircraft when in stow. The LHLRS is currently in use by US Coast Guard, NATO Navies, and the USN Firescout[4].

The combination of UCARS and LHLRS allow the helicopter to land within a narrow dispersion radius of the desired touchdown point over a wide range of platform pitch, roll, and sink rates. The large size and weight of the SLRP help to reduce those deck motions. To assist with correct yaw positioning of the ARV/UEV—with respect to the pod—the LHLRS landing grid is placed at the center of a large turntable that can correct for misalignment to ensure clearance between the aircraft and the closed pod walls. This process is controlled by the sub-based operators at their TCS station (see Chapter 7) via live video from cameras on the SLRP platform.

2.1.3 SLRP Deployment/Recovery Procedure.   The following is the full, automated deployment procedure for the SLRP:

- Seal off launching area from sub hangar, flood chamber. (4 minutes)
- Open sub hull doors, winch out cable lines controlling pod ascent against positive buoyancy. (1 minute)
- Inflate bottom, side, and top bladders during ascent to surface. (5 minutes)
- Open simultaneously side and end walls of SLRP at water surface. (2 minutes)
- Open top wall of pod, lock platform in open position. (1 minute)
- Unfold helicopter blades and tail, release deck mounts and harpoon. (3 minutes)
- Start engines, begin takeoff. (1 minute)

The full deployment procedure requires 10 minutes to reach the water surface and an additional 7 minutes for vehicle takeoff. The following is the full, assisted recovery procedure for the SLRP:

- Land helicopter, shut down engine. (1 minute)
- Slow and index blades, fold blades and tail. (3 minute)
- Make turntable adjustments to ensure pod is not obstructed from folding. (2 minutes)
- Release locking pins, seal pod completely with actuators. (3 minutes)
- Ensure adequate sealing, winch the pod back to sub. (5 minutes)
- Seal sub hull doors, pressurize pod, open SLRP chamber. (5 minutes)

The full recovery procedure requires 9 minutes to fully submerge the pod after helicopter landing, and an additional 10 minutes to recover the pod to the sub and stage it for reloading.

2.2   Submarine Reconfiguration

The largest concern with SSGN-to-SSCN conversion is the ability to implement significant changes to the ship's hull and internal layout while maintaining overall structural integrity [5]. Additionally, logistic considerations—such as portside location of the crew berthing—placed further constraints on possible reconfiguration scenarios. It was decided that the most practical option for SLRP launch is via a hangar door on top of the submarine; this allows the simplest path for launch and recovery, and by minimizing the amount of internal space that needs to be flooded prior to launch, avoids undesirable changes to submarine center of buoyancy (CB).

Silo launch points are removed to accommodate a hangar door on the top surface of the SSCN. To compensate for structural changes, minor strengthening of submarine frames and stringers will be necessary. Furthermore, additional ballasting may prove useful for maintaining the position of the ship's CB while flooding the launch chamber.

2.2.1 Hangar Bay Layout.   Two different hangar bay configurations are possible, allowing freedom to configure the submarine for a variety of missions. The optimal hangar bay layout (Fig 2.3) requires removal of 20 missile silos, accommodating up to 9 helicopters and 2 SLRPs. The hangar door allows the SLRPs to be launched or recovered simultaneously. An alternative configuration (Fig 2.4) requires the removal of only 14 missile silos while storing up to 5 helicopters and a single SLRP. This provides 6 additional missile silos for missions requiring additional ordnance. The hangar bay provides all functions necessary for UEV/ARV operations and is entirely self-sufficient from the rest of the sub.

Storage bays hold one aircraft, handling dollies, pressure washers, hoists, and other fleet level maintenance equipment. One storage bay will also house the entire TCS station, where all aircraft operations are controlled and monitored. The elevator shaft quickly transports helicopters from the storage bays to the pods and vice versa. The elevator platform shifts fore and aft on track rollers to allow for pod door clearance.

2.3   Primary Productivity Metric

The primary productivity metric for this design is given by the RFP as being, "The total number of SOF soldiers transported from a single SSCN in a 6-hour time window, while providing UEV support at the 140 nm range location (one UEV must be in the air providing support to ground forces at all times)." The RFP further states, "Assume that both ARV crew members can be dropped off at the mid-mission point, and that a 4-minute hover is required to unload the crew." In response to this request, the design of the TRITON, SLRP and the SSCN hangar have been optimized to provide rapid deployment capability of up to 28 SOF soldiers in all possible operating environments: desert, arctic, tropical and maritime.
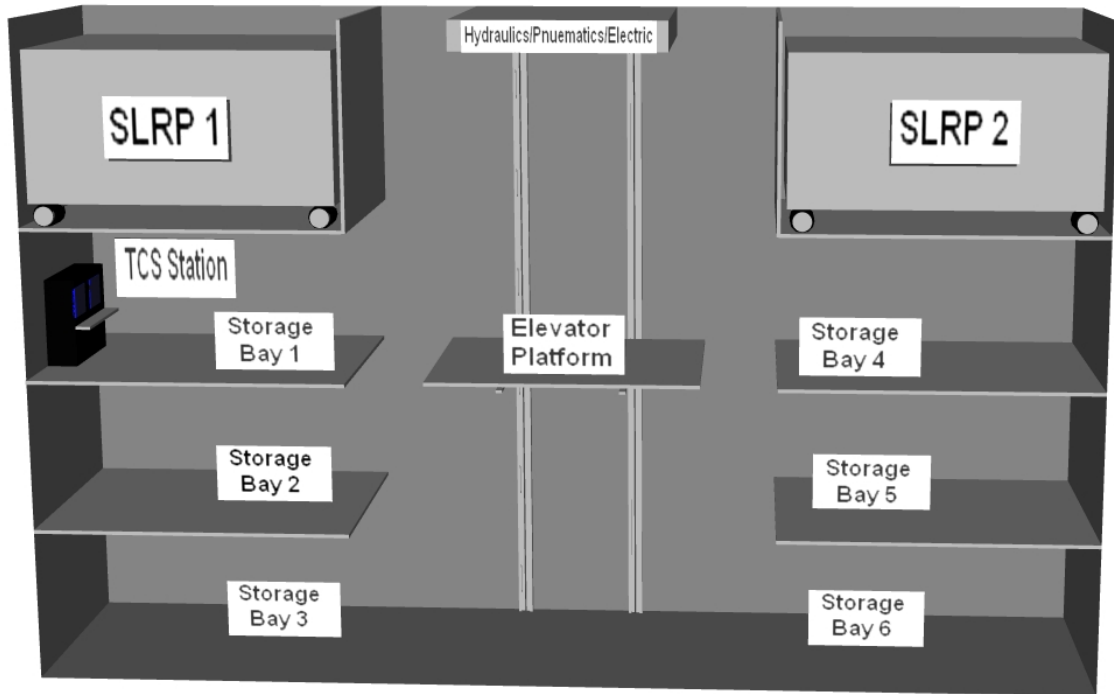
Figure 2.3: Hangar bay configuration
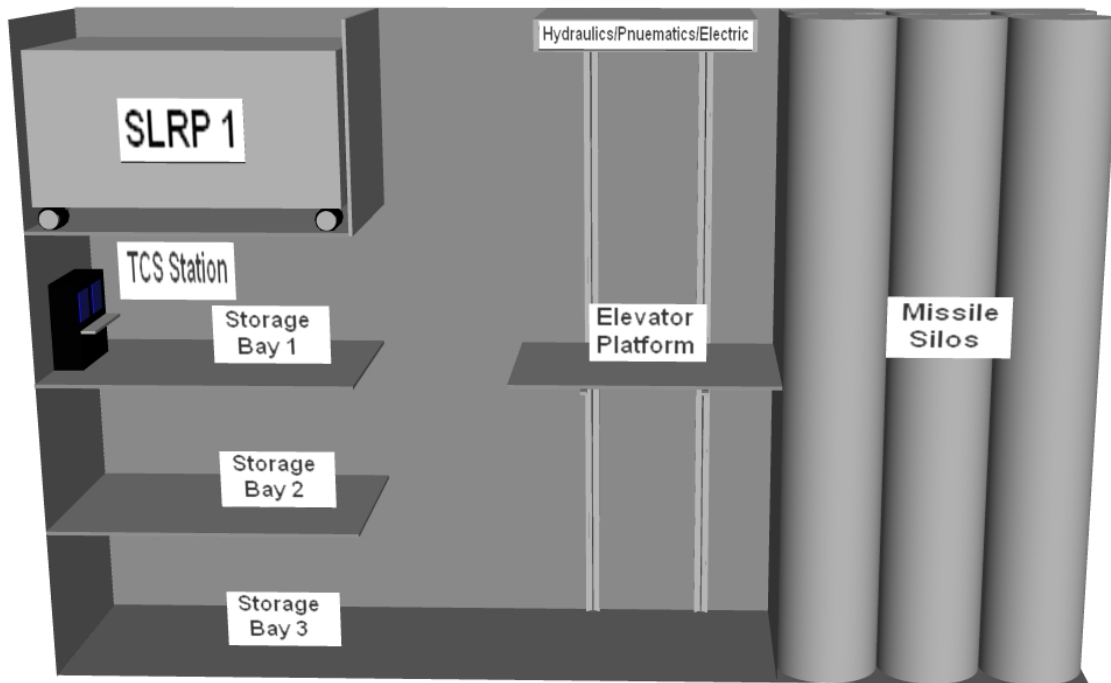
Figure 2.4: Alternate hangar bay configuration

To ensure rapid deployment of the maximum number of SOF-soldiers, thorough analysis of the given mission profile along with SLRP deployment and recovery sequencing was performed. This analysis shows that
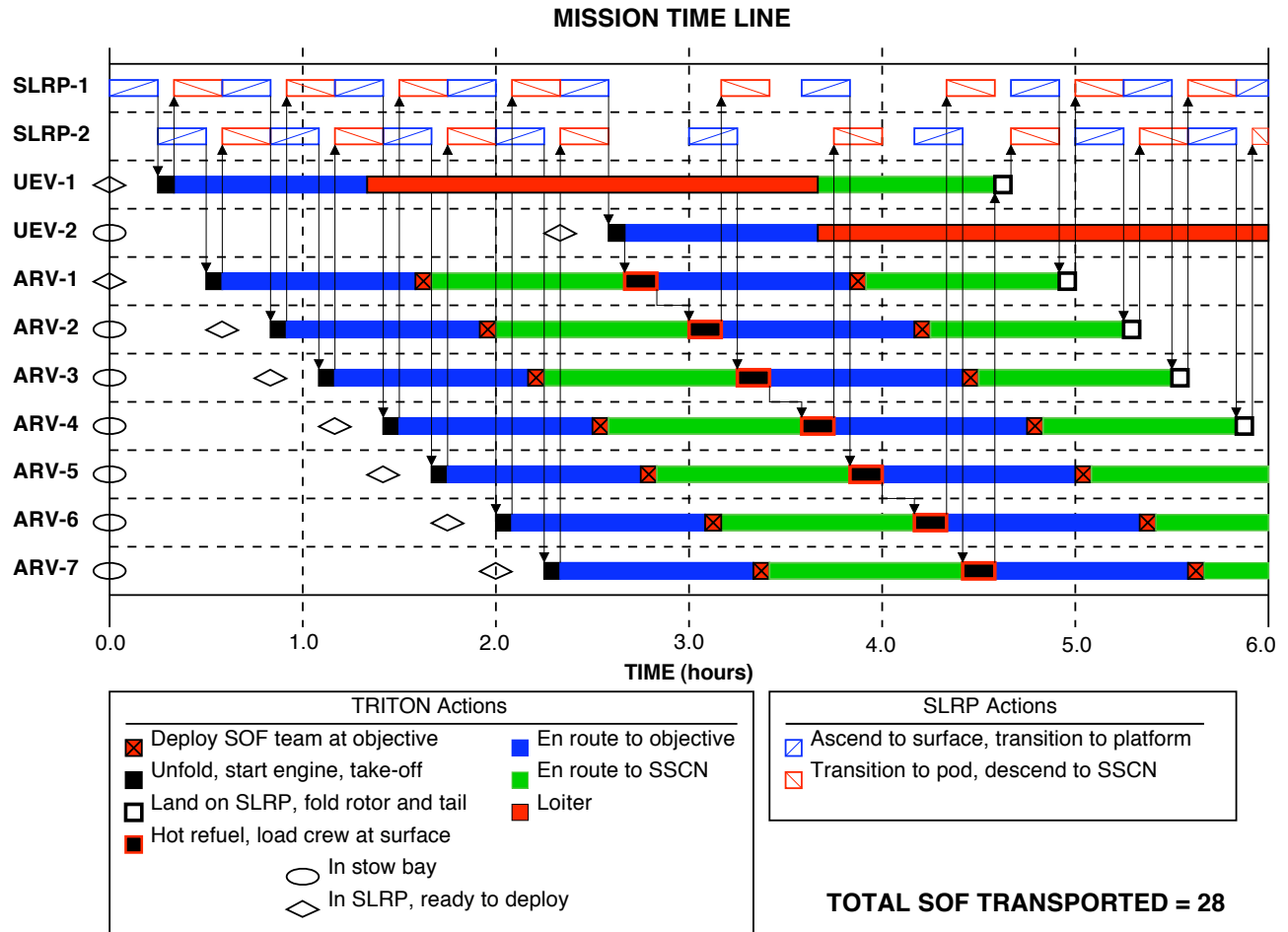
MISSION TIME LINE

the proposed SSCN hangar layout along with the SLRP system are not a significant limitation in the deployment capability of the SSCN.

2.3.1 Mission Time Line.

To assist with choreographing the launch and recovery sequence, the time histories for each element of the mission were generated as shown in Figure 2.3.1. The horizontal axes in Figure 2.3.1 represent time from receipt of mission task in hours. Stacked in the vertical direction are the individual time lines for each element of the SOF mission: two UEVs, two SLRPs and seven ARVs. The colored horizontal bars represent estimated duration for each action required by the mission elements. The open symbols indicate the initial state of each TRITON vehicle. The vertical black arrows represent action dependencies. For example, UEV-1 must wait for SLRP-1 to reach the water's surface and complete the transition process from pod to platform before takeoff. Similarly, SLRP-1 cannot begin its decent back to the SSCN until UEV-1 has completed blade and tail unfolding

and has cleared the SLRP.

Prior to mission tasking, it has been assumed that the full SSCN hangar configuration is used, which has the capacity to store 9-TRITONs, two of which are configured as UEVs and seven of which are configured as ARVs. It is also assumed that one ARV and UEV is already loaded into an SLRP and ready for deployment. Upon receipt of mission task, the first UEV (UEV-1) is immediately deployed and the SOF team are alerted. During its ascent, mission information including flight plans are loading onto the UEV's onboard computer. Once the first SOF team are ready, the first ARV (ARV-1) is deployed. It has been assumed that time required for SOF briefing and preparation of personal gear can be accomplished in 15 minutes; the communication capabilities of TRITON permit additional mission briefing to be conducted en-route to the objective if needed.

As shown in Figure 2.3.1, the initial phase of deployment consists of deployment of ARV vehicles containing SOF crew members. Once an ARV has been deployed, the SLRP returns the the SSCN where it is loaded with the next ARV containing 2 crew members. Since the flight time between SSCN and objective is approximately 1 hour, a total of two trips are made by all seven ARV's. At 2.6 hours into the mission the second UEV (UEV-2) is deployed; the phasing of this deployment is critical to such that a UEV is at the objective throughout the entire duration of the mission, while ensuring that an an SLRP is available to recovery returning ARVs. To facilitate a prompt turn-around time, four SOF crew members are transported per SLRP (no vehicle) to the ocean's surface to prior to the return of an ARV. Once an ARV lands on the SLRP platform, the ARV is refueled and two SOF crew board. The SLRP is then momentarily kept at the surface for the next returning ARV; the maximum wait at the surface is 20 minutes. After approximately 4.5 hours into the mission, returning ARVs no longer have sufficient time to continue relaying SOF crew members. At which time, empty SLRPs are deployed to the surface to recover the returning vehicles.

3   Preliminary Sizing and Weight Estimate

The goal of the preliminary sizing stage was to develop designs that meet the requirements of the RFP and to perform trade studies to select the best design. The trade studies performed at this stage were: the variation of the number of rotor blades, the rotor solidity, and the number of engines. The overall size of each design was determined in terms of gross takeoff weight (GTOW) and rotor diameter. In addition, the component weights and acquisition costs were estimated using a modified version of the sizing code originally developed by Tishchenko [6]. The candidate designs were then compared over various design parameters to select the best configuration.

3.1   Design Requirements

The objective of RFP, primarily, is the design of an advanced manned *Approach and Recovery Vehicle* (ARV) that is capable of meeting the following requirements,

- Payload = 800 lbs (including crew/pilots)
- Hover-out-of-ground-effect (HOGE) at 6k/95($6,000$ ft/$95°$F) (for a maximum duration of 8 minutes)
- Cruise Above Ground Level (AGL) at height $\leq$ 50 ft for 280 nm.

The secondary objective, is the design of an advanced *Unmanned Escort Vehicle* (UEV), whose requirements are similar to ARV described above, differing only in terms of payload (600 lbs) and an added loiter time of three hours. As discussed previously, a decision matrix method (Pugh's method) was used to decide on a single main rotor configuration with a fenestron. This, along with the above RFP requirements, provided the necessary inputs for preliminary sizing and weight analysis.

3.2   Method of Analysis

The analysis, modified specifically for the high cruise performance requirements of the present design, uses an iterative process that begins with input specifications such as the required payload and range of the aircraft. A series of performance and sizing calculations based on these requirements and other user inputs (such as propulsive efficiency, lift-to-drag ratio, transmission efficiency, tip speeds, and figure of merit are performed). Once these calculations are complete, a series of component weight calculations are performed based on correlation equations obtained from historical data. Next, these component weights are used to sum up to the total empty weight and recalculate the weight efficiency. This value is then substituted into the previous calculations and the program runs iteratively until convergence is achieved. After the analysis converges, acquisition and operating costs are evaluated based on empirical equations and factors developed by Tishchenko [6]. The work flow of the design methodology is depicted in Figure 3.1. This entire process is run concurrently for various combinations of number of blades, blade aspect ratio, and number of engines. This allows the direct comparison of various configurations and, ultimately, the selection of the best design. The tail rotor sizing and weight equations were modified to model the fan in fin design of the TRITON .

3.2.1 Initial Sizing.

Figure 3.2 shows the gross take off weight (GTOW) versus disk loading for different numbers of blades and different aspect ratios. The preliminary sizing calculations were carried out assuming a $C_T/\sigma = 0.075$, a value chosen by keeping blade stall into consideration. The figure shows different design points for a given
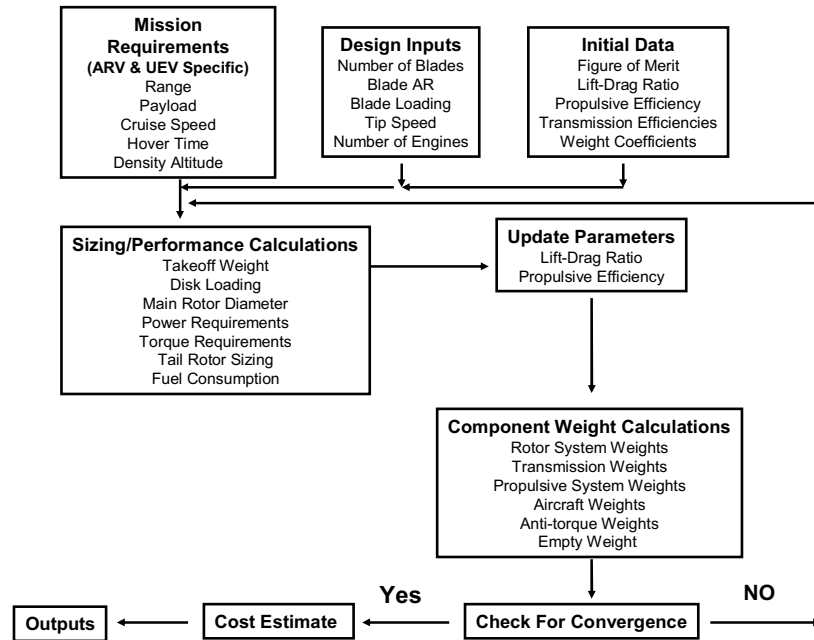
Figure 3.1: Block Diagram for the Design Code

C_T/σ. The design parameters for a particular GTOW in this figure are, aspect ratio, number of blades and disk loading (AR, Nb, and DL, respectively). A combination of these three parameters correspond to a particular value of solidity (σ). Therefore, effectively the design parameters are: σ, Nb, and DL. It is seen that choosing a rotor with a lower number of blades of higher aspect ratio leads to reduction in GTOW. A similar trend can be observed for power requirement (Figure 3.4) and fuel weight estimates (Figure 3.5), though the influence of these parameters is not as significant. A higher aspect ratio than 21 would result in large rotor diameters (Figure 3.3). Similarly, a two-bladed rotor would result in larger rotor diameters again. When it comes to comparing a three-bladed rotor with a four-bladed rotor, their relative gains shown by the Figures 3.2, 3.3 , 3.4 and 3.5 are not sufficient. Therefore, for further analysis the design window was limited to an aspect ratio range from 18 to 21 and to a 3 or 4 bladed rotor (this corresponds to solidity values ranging from $\sigma = 0.046$ to $\sigma = 0.071$).

3.2.2 Performance Considerations. The cruise performance study and overall helicopter sizing study influence each other while finalizing on number of blades and aspect ratio and various other vehicle design parameters. To converge on the final choices and the sizes, the vehicle's performance calculation for cruise (and hover) were performed. For the analysis, the best cruise speed was rated at maximum continuous power (MCP)
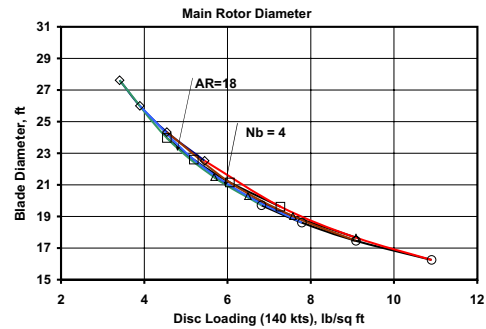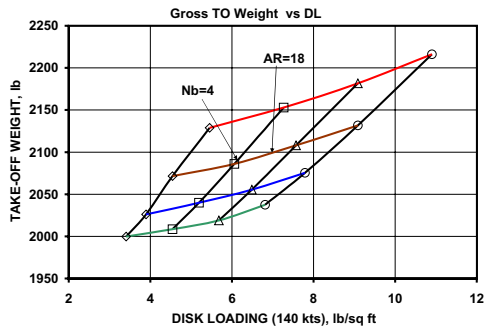
Figure 3.2: Gross Take-off Weight versus Disk Loading   **Figure 3.3:** Main Rotor Diameter versus Disk loading

Figure 3.5: Maximum Fuel Weight versus Disk loading
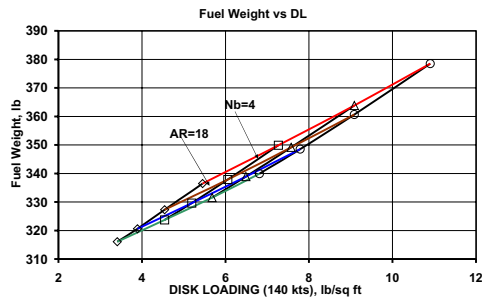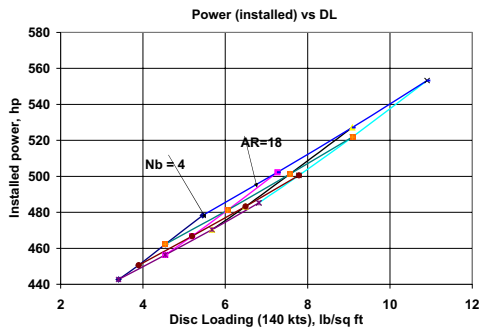
Figure 3.4: Total Installed Power versus Disk Loading

and the maximum attainable speed was rated at maximum rated power (MRP). Figure 3.6 compares different values of aspect ratio (or solidity, σ) for a four-bladed rotor. While each of the curves suggest a best range cruise speed of 140 knots, the blades with higher aspect ratio (lower σ) have better specific ranges. Figures 3.7 and 3.8 show similar trend for power and fuel requirements, respectively.

Figures 3.9, 3.10, 3.11 compare relative performance values (range, power, and fuel required, respectively) of a three-bladed rotor against a four bladed rotor (with aspect ratio of 21). A four-bladed rotor provides better cruise performance than the three-bladed rotor. This analysis helps in deciding on the final choice of number of blades and blade aspect ratio.

Choice of Number of Blades

The relative performance of $N_b = 3$ and 4 can not be judged based entirely on the analysis presented above, because the differences are only marginally. To help decide on the final configuration we consider the following:
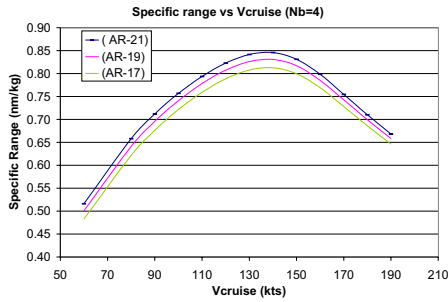
Figure 3.6: Specific Range versus cruise speed for different aspect ratios
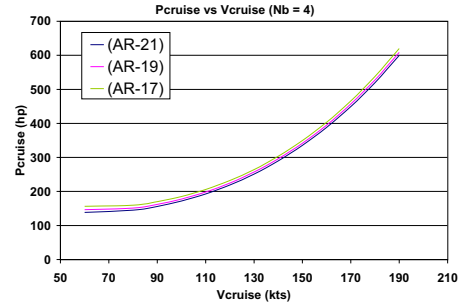
Figure 3.7: Power versus cruise speed for different aspect ratios
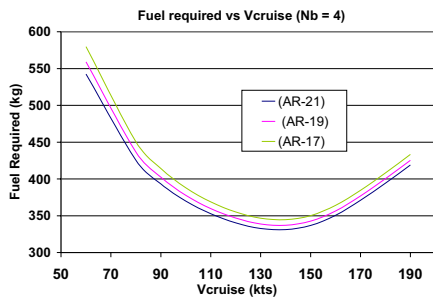
Figure 3.8: Fuel versus cruise speed for different aspect ratios
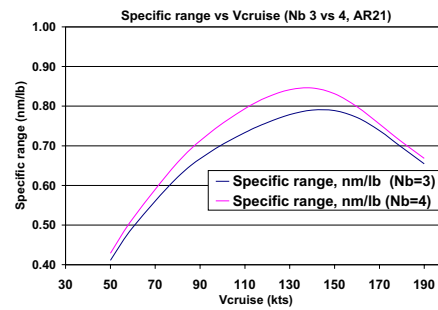
Figure 3.9: Specific Range versus cruise speed for blade numbers = 3 or 4
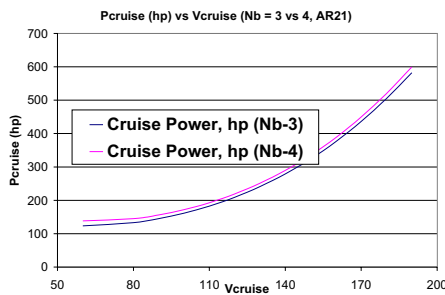
Figure 3.10: Power versus cruise speed for different number of blades = 3 or 4
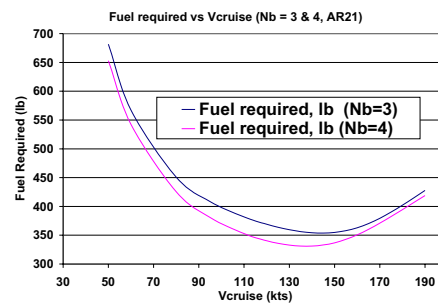
Figure 3.11: Fuel versus cruise speed for different number of blades = 3 or 4

Table 3.1: Trade Study on N_b ($AR = 18$)

Parameters	3	4
DL (lb/ft^2)	4.54	6.05
D_{MR} (ft)	24.3	21.2
Solidity (σ)	0.053	0.071
C_{MR} (ft)	0.67	0.59
P_{inst}(hp)	462	481
M_{TO}(lb)	2071	2130
Total cost ($M)	0.809	0.817
Specific Range (nm/lb)	0.77	0.83
Fuel Required (lb)	338	361

Table 3.2: Trade Study on Aspect Ratio ($N_b = 4$)

Parameters	18	21
DL (lb/ft^2)	6.05	5.1
D_{MR} (ft)	21.2	22.5
Solidity (σ)	0.07	0.06
C_{MR} (ft)	0.58	0.53
P_{inst}(hp)	480	466
M_{TO}(lb)	2230	2190
Total cost ($M)	0.88	0.89
Specific Range (nm/lb)	0.83	0.79
Fuel Required (lb)	339	329

- A four-bladed rotor results in lower vibration than a three-bladed rotor.

- Four-bladed rotor results in a smaller main rotor diameter (21.5 ft) and thus the overall length of the helicopter can be restricted to be within the margin of 20 ft, which fits well into the proposed hangar layout design inside submarine (28 + 21 + 21 ft).

- Both the ARV and UEV need to be transported in C-130J, which has a cabin dimension of 40 ft $\times$ 10.25 ft $\times$ 9 ft (length $\times$ width $\times$ height). An overall length of 20 ft allows transportation of two ARV/UEVs at a time.

- Even though a three-bladed rotor offers less complex hub design and better foldability characteristics, it leads to higher main rotor blade diameters. For example, three bladed rotor main diameter is $\sim$ 3 ft larger than a four bladed main rotor diameter for an aspect ratio of 18.

Analyzing the above trade-off points (Table 3.1), a four-bladed main rotor was chosen. Choosing a four-bladed main rotor over three bladed rotor results not only in higher specific range (Figure 3.12) but also in lower fuel requirement (Figure 3.13).

Aspect Ratio

Figures 3.2,3.3,3.4 and 3.5 show that a higher aspect ratio blade (lower solidity) is more desirable. But a high aspect ratio blade means a slender blade and hence perhaps structurally more demanding. If the blade aspect ratio is decreased from 21 to 18, the penalty associated with GTOW (3.2), power (3.4) or fuel (3.5) is less than 3% in each case. Table 3.2 shows a comparison of results for an aspect ratio $AR = 18$ and $AR = 21$. An aspect ratio of $AR = 18$ was chosen because this leads to:

- A lower main rotor diameter (more favorable from overall size point of view)

- A higher solidity (better hover characteristics, for a constant C_T/σ)

- A blade configuration which is structurally less demanding
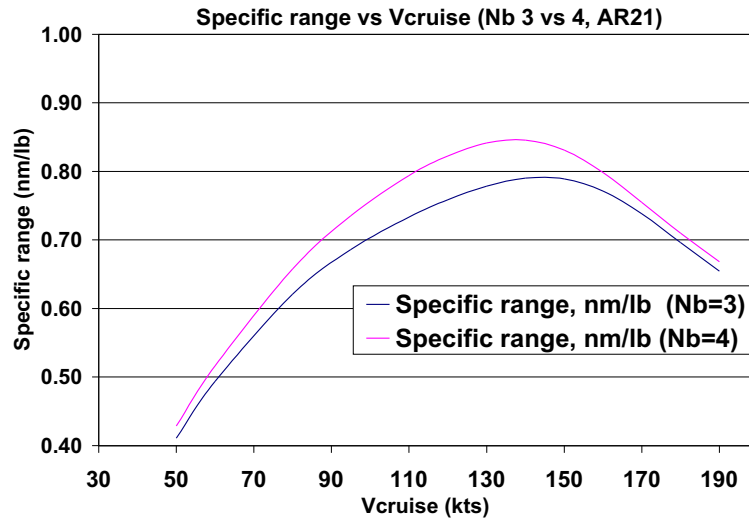
Figure 3.12: Trade Study for number of blades: Specific Range
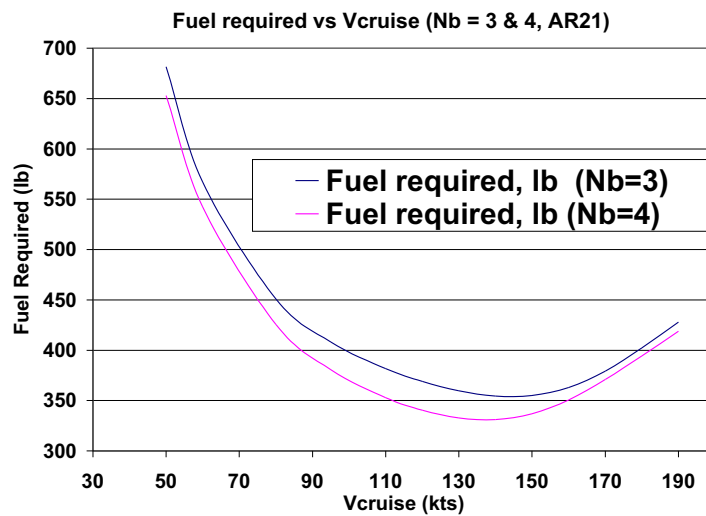
Figure 3.13: Trade Study for number of blades: Fuel Required

Table 3.3: ARV & UEV

Vehicle Type (Payload in lbs)	ARV (800)	UEV (600)
M_{TO} (lb)	2230	2370
P_{inst} (hp)	480	499
M_{fuel} (lb)	320	660
K_{WE}	0.51	0.53
D_{MR} (ft)	21.2	22.1

3.2.3 ARV & UEV: Single Modular Design.

During the design process, two different vehicle concepts were considered for the two distinct mission profiles, one for the ARV and other for the UEV. As discussed earlier, these are two different concept vehicles. Besides differing in mission roles, from vehicle sizing point of view they also differ in their design requirements such as total payload and total fuel required. The design iteration produced two different vehicle sizes for ARV and UEV. Table 3.3 compares the major design features of the two vehicles. The fuel required for the UEV is 97% higher than that required by the ARV. In addition, the UEV is 9% heavier than the ARV. Despite this, the power required for the UEV is only 4% higher. Moreover, the diameter of the rotor for the UEV is 1 ft larger than that of ARV. So, it was proposed that both vehicles to be designed to be as common vehicle. The advantages of having such a simple, common design are the following:

- It can have mission adaptability. For example, during an emergency an UEV can be used as an ARV by adjusting the payloads.
- There can be *commonality in cost* with respect to the following considerations: manufacture, spares, tools, training of ground crew, and interchangeability.
- There can be huge reduction in cost on research and development as well as on testing.
- The current design has new transmission and rotors, which are major factors affecting the cost of the vehicle.
- There can be a reduction in costs of fabrication as well as costs of maintenance (since similar machine tools and machine expertise is used).

In view of the above discussed points, it was decided that the ARV and UEV should have same structural designs. The only difference would be in the fuel weight (the fuel tank being sized according to the UEV fuel requirement) and payload. The trade offs for this were investigated and it was observed that the power and fuel requirements were only marginally higher ($\Delta P_{inst} \sim 5\%$ and $\Delta M_f \sim 2\%$). This gave the confidence to go ahead with the single module design. Thus, the final GTOWs are $2,230$ lbs for ARV and $2,370$ lb for the UEV, and the

fuel weight of 320 lbs for ARV and 660 lbs for UEV. The higher GTOW for the UEV is accounted for by very high fuel requirement, even though the payload is lower. From a mission operation point of view the UEV differs from the ARV with respect to cabin interior arrangements, such as use of crew seats (not required for the UEV), positioning of avionics (more important for the UEV), and other payload for each of these vehicles.

4   Main Rotor/Hub Design

The TRITON features a 4-bladed, swashplateless rotor capable of automatic folding to fit within the constraints of the Submersible Launch and Recovery Pod (SLRP). Individual Blade Control (IBC) is provided by electric actuators for both primary control and vibration reduction using trailing edge flaps; a weighty and mechanically complex hydraulic system is not needed for blade actuation or blade folding, keeping the TRITON a hydraulic-free vehicle. The swashplateless design is a robust, low-drag solution, carefully tailored and optimized to meet the requirements of its mission.

4.1   Design Evolution/Emergence

The primary control of a conventional helicopter involves the transfer of mechanical input, provided by the pilot in the non-rotating frame, to the blade pitch horn in the rotating frame through a chain of mechanical, hydraulic and/or electronic elements. This information is also conditioned using a flight control system before transfer to the rotating frame through the swashplate where the pilot's inputs are resolved and distributed to the individual blades. Using the swashplate as means for primary actuation restricts blade pitch motion to collective control and 1/rev cyclic control. Also, such mechanical assemblies are heavy and contribute significantly to parasitic drag. It has been realized that a helicopter in forward flight can greatly benefit from a more complex pitch control scheme, which also allows for vibration and noise reduction. As a result, significant research has gone into the area of individual blade control through on-blade actuation for vibration and noise reduction as well as improvement in overall performance[7, 8]. Currently, Eurocopter (BK117) and Boeing (MD-900) are exploring trailing edge flap actuation for vibration and noise reduction while primary control is carried out using the conventional swashplate mechanism. Because the inclusion of additional actuation systems in the rotating frame introduces a weight penalty, it is advantageous to have the on-blade actuation serve the purpose of primary control in addition to the vibration and noise control to minimize these penalties[9, 10].

A swashplateless rotor is more desirable than the conventional swashplate-controlled rotor, providing a lighter and aerodynamically cleaner design with reduced susceptibility to ballistic threat. Blade pitching for swashplateless rotors can be obtained using external servo flaps, trailing edge flaps (ailerons) or individual blade

actuation at the blade root[10]. Kaman uses external servo flaps as primary control device, though these flaps introduce additional drag due to exposed linkages. Furthermore, the center of gravity is pushed further aft. A rotor with integrated trailing edge (TE) flap can eliminate some of the aforementioned problems.

The TE flap can work in one of two ways, producing either additional lift or introducing an additional moment. The primary function of the lift flap is to change the lift characteristics of the blades which are torsionally stiff. Moment flaps on the other hand are used to elastically twist the blade and are therefore more effective when the blades are torsionally soft. The TE flap deflections required in the latter case are smaller than those of former case [9], hence trailing edge moment flaps are selected for the TRITON .

4.2   Details of the Trailing Edge Flap Design

The cross-sectional parameters of the flap are shown in Figure (4.1).
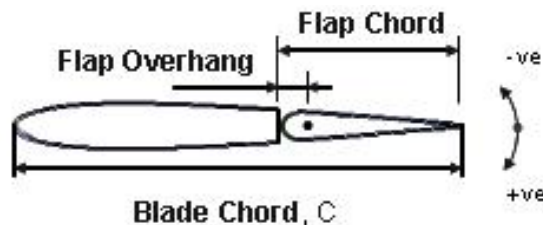
Figure 4.1: Cross-section parameters of the trailing edge flap

To explore the design space for the trailing edge flap, the following design variables were considered:

1. *Blade pitch index angle (pre-pitch)*

   The index angle is the pre-collective applied to the blade to minimize torsional deflection required to trim for a given flight condition resulting in reduced flap deflection. Figure 4.2 shows the effect of blade pitch indexing. An indexed blade not only minimizes actuation requirement, but also improves the net lift.

2. *Flap chord ratio*

   The flap chord ratio refers to the flap chord with respect to main blade chord (c_f/c). A small flap chord can increase the moment arm thus increasing the effectiveness of the moment flap.

3. *Radial Location of Flap*

   Radial location of the flap refers to the location of the midspan of the flap relative to the blade radius. Outboard positioning exposes the flap to a higher dynamic pressure, thus smaller flap deflections are required

to obtain the desired blade deflection.

4. *Flap overhang*

   Flap overhang is the position of the flap hinge relative to the leading edge of the flap, as shown in Figure(4.1). An overhang helps to reduce the actuation requirement.

5. *Blade torsional frequency*

   The blade torsional frequency has to be much lower than that of conventional blades. For effectiveness of flaps for primary control, the rotating torsional frequency has to fall between 1.5/rev to 2.5/rev.

6. *Flap span*

   Flap span is the spanwise length relative to blade radius; a larger flap span reduces the flap deflection requirement.
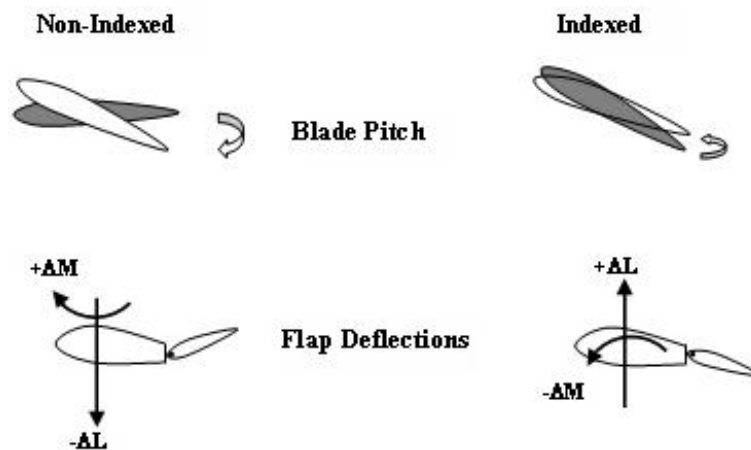
Figure 4.2: Blade Pitch Indexing

To investigate the effect of the above design variables, a simple aeroelastic trim model is used to obtain the required trailing edge flap angles in forward flight by varying the design variables. The trim variables for the swashplateless rotor are: trailing edge flap collective deflection δ_0, flap deflections, δ_{1c} and δ_{1s}, and blade torsional deflection.

$$\delta(\psi) = \delta_0 + \delta_{1c}\cos(\psi) + \delta_{1s}\sin(\psi)$$

The trim targets are thrust and zero hub roll and pitch moments.

In general, it has been observed [11] that the overhang and flap chord ratio influences the hinge moments, while keeping flap deflection constant. On the other hand, modification of the index angle does influence the

flap deflection. The flap span influences both the hinge moments as well as the flap angles. Therefore, based on the previous studies, the baseline configuration parameters selected were: index angle of $15°$, flap chord ratio (c_f/c) of 20%, flap overhang of $0.25c_f(.05c)$ flap overhang, flap span of $40\%R$, flap location at $0.7R$, and first blade torsional frequency of 1.7/rev. These parameters are then varied from the baseline values to obtain an optimized trailing edge flap configuration. The design constraints were: flap deflection (collective and Half Peak-to-Peak (HPP)) and hinge moment. A small positive collective trailing edge flap deflection implies positive lift produced by the TE flap (aileron) and hence a more uniform blade loading and a small hinge-moment—desirable characteristics, as the lower actuation power requirement allow a smaller, lighter actuator.

4.2.1 Optimization of Trailing Edge Flap Configuration. The indexing angle is varied from the baseline configuration to obtain an optimized index angle for the entire flight envelope. Figure 4.3 show the effects of changing index angle. It is desirable to have small positive TE flap deflections with minimum hinge moment requirements. Hence, an index angle of $12°$ is selected, as the hinge-moment requirements are lower than other configurations.

(a) Collective, δ_0 (b) Hinge Moment
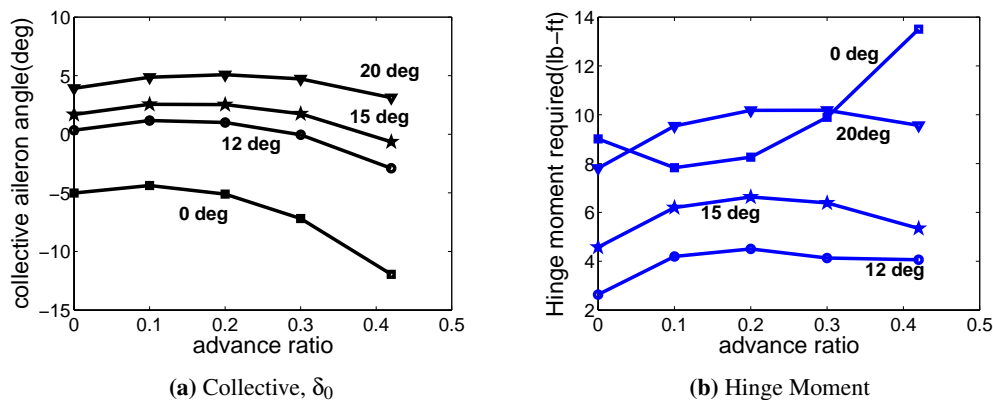
Figure 4.3: Aileron deflection and Hinge Moment Variation with Index angle

The flap chord is varied from 15% to 30% of the blade chord. The change in maximum aileron angle and hinge moment at maximum speed ($\mu = .43$) are shown in Figure 4.4. It is observed that the magnitude of deflection does not vary with the TE flap chord but the hinge moment increases with the TE flap chord ratio. Therefore a TE flap chord ratio of 15% is chosen. It is not reduced further to obtain a reduction in hinge moment as the effectiveness a the small TE flap decreases due to flow separation during maneuver.

The radial location of the TE flap is varied from inboard to outboard $(0.4R - 0.75R)$. The change in

(a) Flap Angle, δ
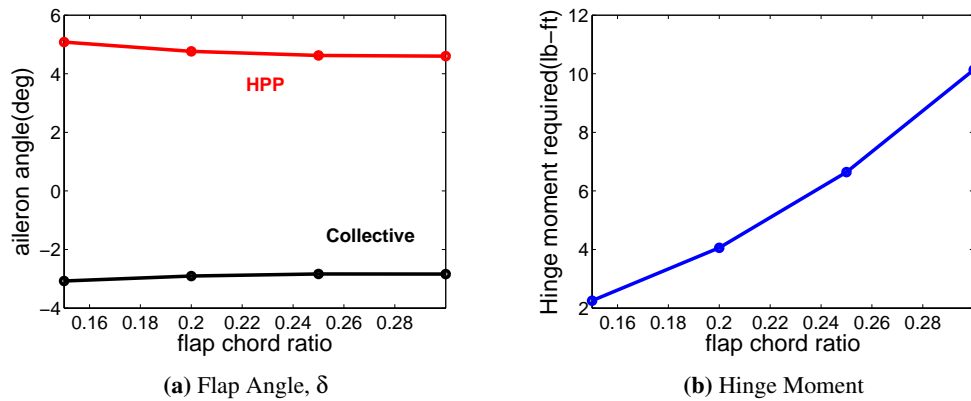
(b) Hinge Moment

Figure 4.4: Aileron deflection and Hinge Moment Variation with flap chord at maximum forward speed, ($\mu = .43$)

deflection and hinge moment are shown in Figure 4.5. The TE flap deflection and hinge moment both show favorable trends with outboard mid-span location. However, the gain obtained by shifting mid-span from $0.7R$ to $0.75R$ is not substantial compared to inboard shifting. Since it is desirable to have a blade sweep for efficient forward flight performance, the mid-span location is restricted to the $0.7R$ location.

(a) Flap Angle, δ
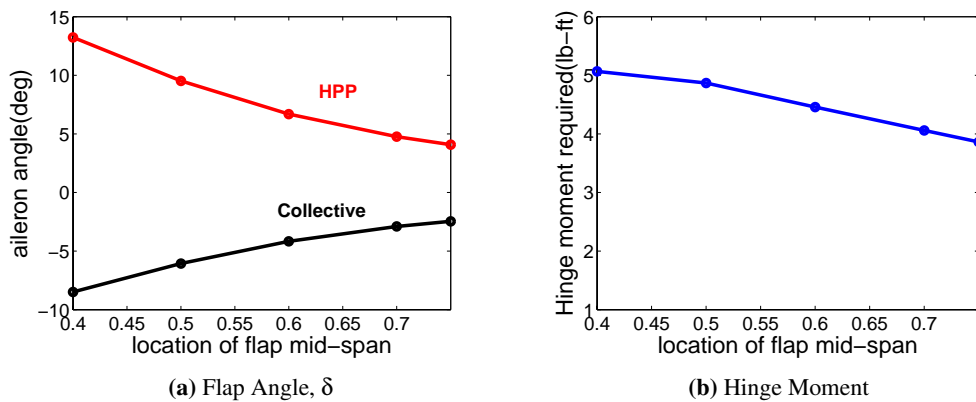
(b) Hinge Moment

Figure 4.5: Aileron deflection and Hinge Moment Variation with Flap Mid- Span Location,($\mu = .43$)

The change in the hinge-moment and flap deflection with variation of flap overhang to beyond 50% c_f are shown in Figure 4.6. It is observed that the flap deflection is not affected by the overhang, yet the hinge-moment is minimized with the $40\% c_f$, i.e, $8\% c$ overhang configuration. $40\% c_f$ is selected as the optimum overhang configuration .

From previous research, comprehensive analysis of flexible rotor blades [11] indicates a reduction in blade pitch change with trailing edge flap deflection as torsional frequency increases. Figure 4.7 shows the changes in

(a) Flap Angle, δ
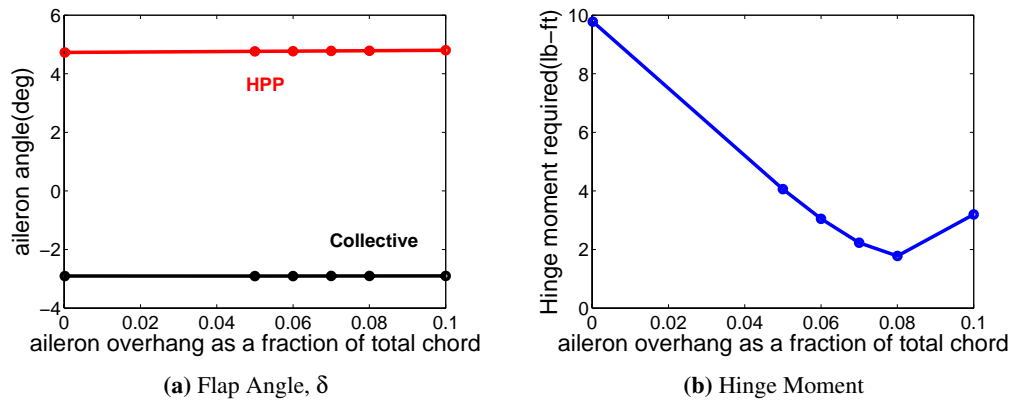
(b) Hinge Moment

Figure 4.6: Aileron deflection and Hinge Moment Variation with Hinge Overhang, ($\mu = .43$)

trailing edge flap angle and hinge requirement for varying torsional frequencies over the entire flight envelope. With torsional frequency below 1.5/rev, the blade can experience static divergence instability, whereas above 2.5/rev, it requires a larger actuation force. Based on this, a torsional frequency of 1.7/rev is selected for the present design.

(a) Flap Angle, δ
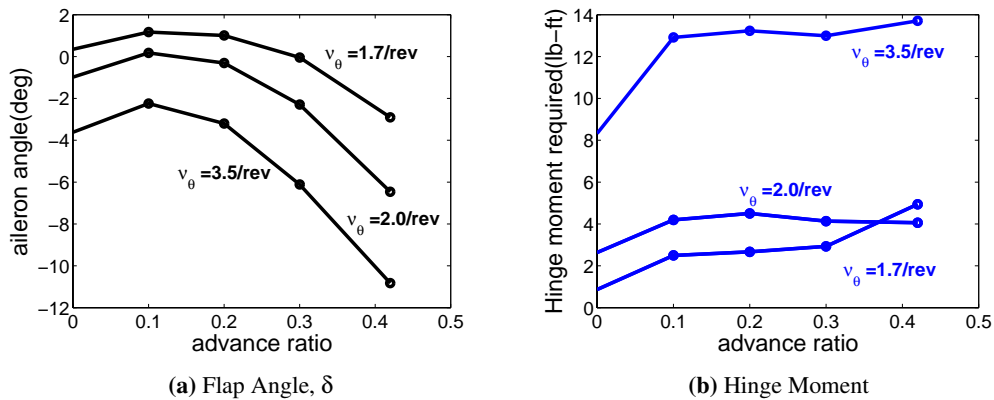
(b) Hinge Moment

Figure 4.7: Aileron deflection and Hinge Moment Variation with torsion frequency

The changes in the flap angle and hinge moment with flap span are shown in Figure 4.8. Aileron angles (especially the cyclic or HPP) decrease with an increase in TE flap span from $15°$ to about $2°$. The hinge-moment increases marginally beyond a span of $0.2R$, but a larger flap span is desirable because of small cyclic flap deflection requirements—as well as the added benefit of increased safety; a larger span can be divided into multiple flaps adding more redundancy. Therefore, the baseline flap span of $40\% R$ is retained.

The optimized TE flap configuration is given in Table 4.1 and the TE flap deflection and hinge-moment

(a) Flap Angle, δ
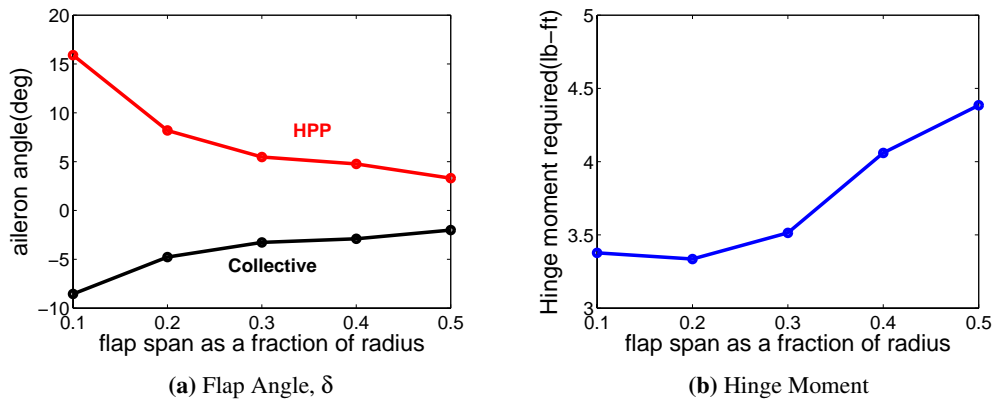
(b) Hinge Moment

Figure 4.8: Aileron deflection and Hinge Moment Variation with Span, ($\mu = .43$)

for the complete flight envelope are shown in Figure 4.9.

(a) Flap Angle, δ
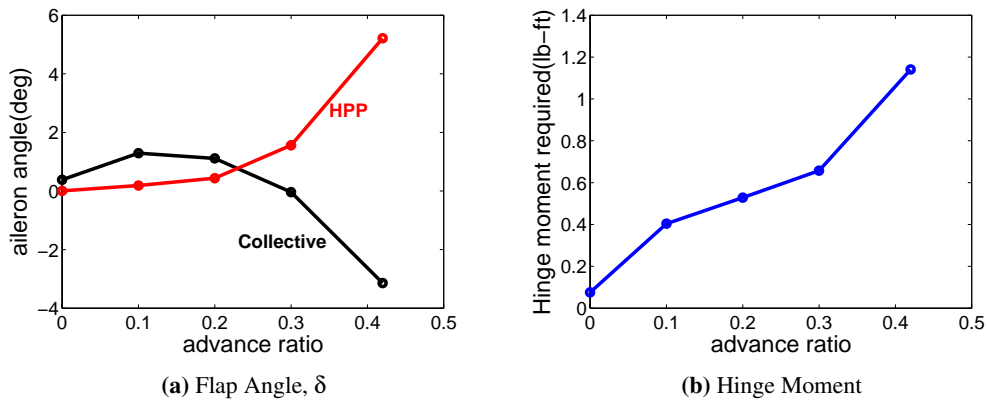
(b) Hinge Moment

Figure 4.9: Flap deflection and Hinge Moment Variation with optimized Trailing Edge Flap Configuration

4.2.2 Trailing Edge Flap Actuator Design.   A compact and effective actuator embedded in the blade is required to provide commanded deflection of the trailing edge flap throughout the flight envelope.

The maximum hinge moment requirement for each blade is 1.2 lb-ft (1.6 Nm) at a frequency of 10 Hz for primary control. A survey of various actuators using smart materials is summarized in Table 4.2. Piezo-hydraulic pump actuators are the state-of-the-art smart actuators, designed primarily for trailing edge flap actuation. The output stroke is generally insufficient even at moderate frequencies, for primary rotor control. The Terfenol-D hydraulic pump has the required high output frequency, but is heavy and bulky. It was concluded that smart actuators could not be used for the present design.

Recent research is focused on use of ultrasonic motors for blade actuation [10]. It appears possible to

Table 4.1: Trailing Edge Flap Design Parameters

Parameter	Value
Blade Pitch Index-Angle	$12°$
Flap Chord Ratio c_f/c	0.15
Flap Radial Location	$0.70R$
Flap Overhang	$0.06c$
Torsion Frequency,ν_θ	1.7/rev
Flap Span	$0.40R$
Flap Span-wise Location	
First Flap	$0.47R - 0.57R$
Second Flap	$0.59R - 0.69R$
Third Flap	$0.71R - 0.81R$
Fourth Flap	$0.83R - 0.93R$

Table 4.2: Comparison of candidate smart actuators for actuation

Smart Actuator	Maximum Strain	Blocked Force	Bandwidth	Evaluation
Shape Memory Alloy	High $4 - 6\%$	High	Low (< 1 Hz)	Suitable for blade tracking but not for primary control
Magnetic Shape Memory Alloy	High $4 - 6\%$	Low	High (1 kHz)	Difficult to accommodate inside blade section, bulky and soft
Electrostrictive	Low 0.1%	Moderate	High (< 100 kHz)	Very temperature sensitive
Magnetostrictive	Low 0.2%	Moderate	High (< 10 kHz)	Bulky and heavy
Piezobimorphs	Moderate	Low	High (< 100 kHz)	Insufficient block force and moderate strain
Piezostack	Low 0.1%	Moderate	High (< 100kHz)	Insufficient strain
Piezo Pump	High	Moderate	Moderate (100Hz)	Heating problems at high input frequency, low output frequency
Terfenol-D Pump	High	Moderate	Moderate (100Hz)	Heavy and bulky

reverse the direction of electric DC brushless motors using a controller and to obtain the flapping motion of the trailing edge flap. Table 4.3 provides data on some electric motors that can perform the required actuation.[12]

One of the primary design constraints is the size of the motor, as it needs to be embedded in the blade section. Therefore, to reduce the size of the motor required, it was decided to divide the TE flap into four smaller spanwise flaps, reducing the torque required to drive each flap section individually. Additionally, use of multiple flaps provides redundancy in case of failure or damage. However, care must be taken to ensure synchronous operation of each flap section motor. The EC-16 motor is selected for the present design with a 16 mm planetary

Table 4.3: Comparison of Candidate Electric Motors for Actuation

Motor	Motor Specifications				Evaluation
	Diameter (φ)mm	Torque mNm	Power W	Weight g	
EC-10	10	1	8	10	Low Torque, Power
EC-16	16	8	40	58	Moderate Torque, Power
EC-32	32	28	80	270	Moderate Torque, Power
EC-Powermax-22	22	50	120	160	High Torque, Power

gearhead to increase the torque output.

Actuator Mounting and Actuation

The actuator housing is placed behind the blade-spar, to which it is attached with bolts. The spar is strengthened locally with an additional six plies [90]. The torque from the motor needs to be transmitted to the trailing edge flap hinge tube with minimum losses. This is achieved by using a pre-stressed (tensile) toothed belt to connect a pulley mounted on the rotating shaft of the motor to the hinge tube of the flap as shown in Figure 4.10. The toothed belts prevents slipping, and pre-stressing ensures minimum loss in the torque transfer. Position and speed control is obtained by attaching an encoder (Type A MR encoder) to the motor along with the planetary gearhead for torque increment. For rotational direction reversal, a controller (available with the motor, EPOS 24/1) is used. A potentiometer mounted on the hinge tube provides an estimate of the flap deflection and acts as a fault detection sensor. The motors are powered by the generator installed in the fuselage. The voltage required is 12 V. A panel is provided above each motor to allow easy access to the motor. The panel is secured using countersunk screws so that the complete assembly fits within the airfoil contour.
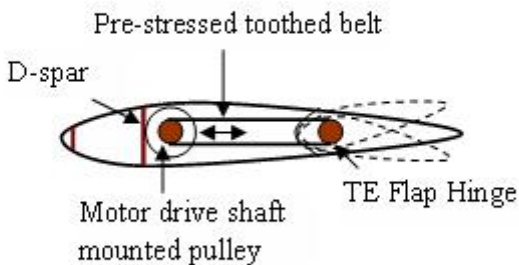
Figure 4.10: Schematic Actuation Mechanism

Safety and Monitoring

The motor chosen for actuating the flaps is a DC brushless motor with long life, as there are no mechanical brushes to wear out. The motor is assembled such that the coils are outside the rotor, providing good heat dissipation and high overload capability. The EC-16 is rated to work in ambient temperatures ranging from $-4°$ to $+275°F$, while electronic commutation minimizes electrical noise. On-blade heating is provided to ensure operation in arctic ($-60°$ F) conditions (see section 4.2.3). The power output of each motor is 40 W; the power requirement for primary blade control of each blade is 58 W, that is, about 15W for each flap, therefore 4 motors are used (one for each of the four flap sections) to ensure enough redundancy. In the event of failure of any one of the motors, the remaining motors have enough authority to execute primary control and trim the helicopter. In case of engine or tail-rotor failure, the TE flap controllers are designed to immediately position the TE flap at the programmed optimum angle to allow rapid entry into autorotation. The motor has the ability to provide mean displacement beyond the normal requirements to allow a higher collective for flare when performing an autorotational landing. In case of generator failure, the motors are powered using emergency storage batteries to land safely.

Slip Ring

The power supplied to the motors needs to be transferred from the non-rotating frame of the fuselage to the rotating frame of the rotor system. This is achieved by use of an electrical contact slip ring. Special long-life rotor brushes and specially-finished stator surfaces allow extended operation by minimizing debris build-up. The slip ring is hermetically sealed against dust, sand and water intrusion to ensure proper operation even under harsh environmental conditions. The slip ring components are easily replaced; all maintenance can be performed by personnel aboard the SSCN.

4.2.3 Blade Structural Design.   The blade structure is designed to meet the following design requirements:

- Adequate stiffness to support the centrifugal force and the steady and oscillatory stresses due to flap, lead/lag and torsional moments.
- Accommodation of flap actuators and related hardware
- Adequate mass to provide the inertia required for autorotation

Material Selection

Composite materials are used for the present design because of their resistance to corrosion, superior fatigue characteristics, high specific strength and stiffness and safe failure modes. Mechanical properties of the materials

Table 4.4: Comparison Properties of Candidate Composite Materials

Material	Density	Young's Modulus	Cost
	$\frac{Mg}{m^3}$	E_{11}, GPa	$\$/kg$
Glass	1.95	43	9
Graphite	1.60	177	60
Kevlar	1.38	87	140

considered are provided in Table 4.4[13]. The glass-fiber composite is most affordable and has shown good impact tolerance, but has low specific strength compared to Kevlar and Graphite-fiber composites. Kevlar is the lightest and has very good damage tolerance capabilities, but it is very expensive and susceptible to ultra-violet damage; therefore, for the present design IM7 Graphite fiber composite is selected.

Blade Structure

The blade structure consists of three main components: (a) the blade spar to support bending and axial stresses,(b) the skin to support the shear stress and (c) the core filling to preserve shape of the airfoil. A D-spar is selected for the blade spar cross-section as it provides higher torsional stiffness compared to open cross-sections like the I-section or C-section. The D-spar is comprised primarily of prepreg unidirectional plies running span-wise. At the blade root, these plies are wound around a bushing for the two index-splice attachment bolts. The skin consists of four plies of woven graphite epoxy composite, and Nomex Honeycomb is selected as the core material since it bonds well with the skin and has low moisture absorbtion. To determine the dimensions of the constitutive components, the design parameters are defined as follows: the number of plies in the D-spar, orientation of the plies of the skin, and the chordwise dimension of the D-spar. Based on the study of design space by varying the design parameters and determining sectional properties and natural frequencies, an appropriate ply layup was chosen for the present design. Another consideration in deciding the ply layup for the D-spar is the possibility of vibration reduction. Wind tunnel studies on composite-tailored, Mach-scaled rotors have demonstrated significant reduction in the 4/rev vibratory loads (reduction of 14% vertical shear, 12% in-plane shear and 18% head moment) through use of dual, spanwise segmented pitch-flap coupling[14]. The blades in the present design make use of this technology to minimize inherent vibratory loads. The blade spar is designed to have negative pitch-flap coupling up to 75% of the span and positive pitch-flap coupling beyond that as shown in Figure 4.11.

A typical section has a spar with ten unidirectional sub-laminates for axial and bending stiffness, four balanced $[+45/-45]$ sub-laminates for shear stiffness, and six layers of unbalanced $[20_6]$ plies to introduce the coupling. The layup of the D-spar is $[+45_2/0_{10}/-20_6/-45_2]$ inboard and $[+45_2/0_{10}/+20_6/-45_2]$ outboard.
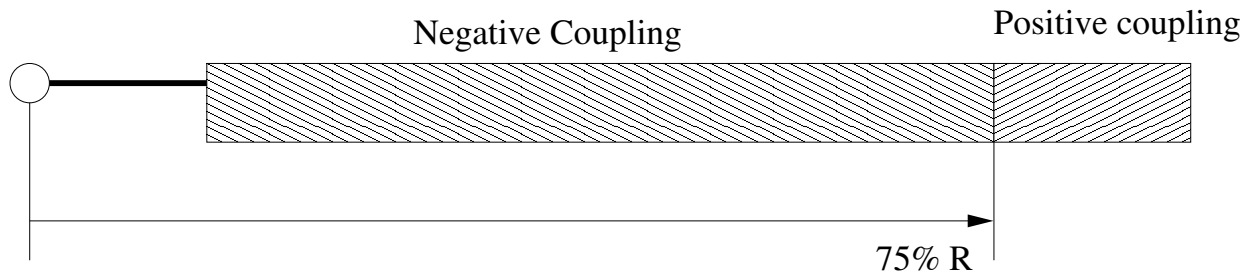
Figure 4.11: Composite Tailoring for Vibration Reduction

The D-spar itself extends from 2% to 28% chord-wise. The skin lay-up is 4 plies of woven $[0/90]$ cut at $45°$ to give maximum torsional stiffness. Leading edge mass of 0.75 lb (0.35 kg) is placed ahead of the D-spar to bring the center of gravity of the blade section ahead of the quarter chord (aerodynamic center). The leading edge is a shaped tungsten rod bonded to the spar and held tightly in place with the skin wrapped around it. Aft CG movement results from the placement of actuators and related hardware in the blade section, therefore a distributed mass of 3.5 lb (1.6 kg) is placed from 50% to 90% radius to serve the dual purpose of moving the CG to 23% of the chord and to improve to blade autorotative inertia. This mass is a tungsten rod inserted into and bolted to the D-spar. The D-spar is locally strengthened by adding $[90_6]$ plies. The blades have a static droop of less than $5°$. Titanium strips are mounted over the blade leading edge to prevent erosion. The total mass of each blade including the leading edge masses and actuators is computed to be approximately 15.4 lb (7 kg).

Electromagnetic Shielding and De-icing

Lightning protection is very important for this design, as the blades are built out of composite and the heating caused by lightning can delaminate the composites. The design requirements are that the helicopter blades should be capable of withstanding 200 kA lightnings strike while still permitting safe landing[15]. To protect the blade, the skin is covered with aluminum mesh screens to conduct current to the titanium abrasion strip and into the blade root. A titanium strip connects the abrasion guard to a hub lightning ground cable to avoid any electrostatic charge build up in the blade. The blade mounted motor housing is wrapped in a nickel/iron alloy foil to shield it from low frequency electromagnetic signals.

De-icing is provided through an electrically insulated heating element placed underneath the leading edge erosion strip. This "de-icing" blanket is distributed such that it can also provide heating to the flap actuators to ensure operability in extremely low temperatures. See Figure 4.12 for a detailed blade cross-section.

4.2.4 Hub Design.   The main focus of the hub design was to minimize aerodynamic drag at the high cruise

(a) Typical Blade Section **(b)** Blade Section With Flap
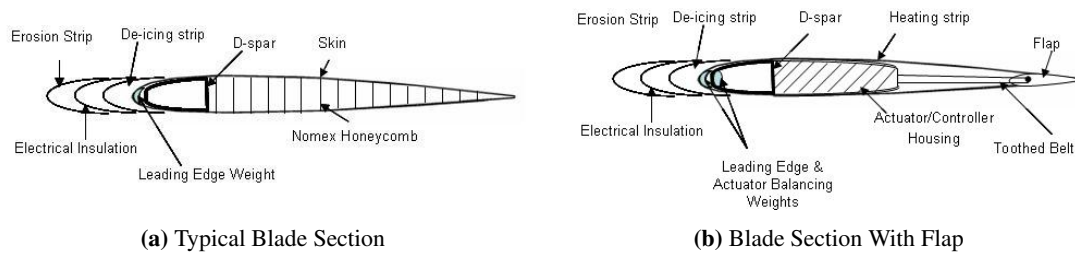
Figure 4.12: Blade Cross-sections

speed and reduce mechanical complexity for high reliability during extended deployments in a maritime environment. Since trailing edge flaps are used for flight control, a low torsional blade stiffness was required. For these reasons, a bearingless hub was designed. The hub is designed to be soft in-plane ensuring lower in-plane loads. A detailed dynamic analysis is carried out to ensure the stability of the soft in-plane rotor for aeromechanical/aeroelastic problems. Bearingless rotor hubs command more control authority than articulated designs, resulting in improved handling qualities. These hubs also eliminate many wear surfaces that often fail early due to the corrosion and dust or sand intrusion common to U.S. Navy operating environments. This greatly reduces the maintenance time typically required to inspect and replace the many dynamic components on a fully articulated design. The TRITON hub (see Foldout 4.6.3) has four primary elements: a flexbeam that accommodates pitch flap and lag motions, a pitch case, an elastomeric damper to provide lead-lag damping, and the droop stop to prevent the blades from hitting the airframe at low rotor speeds.

For the four-bladed TRITON hub, two flexbeams are overlapped and bolted at 90° (see Foldout 4.6.3). By extending the two opposing flexbeams into a single piece attached directly to the rotor shaft, the critical joint between the hub and flexbeam is eliminated, further reducing failure modes and increasing fatigue life. Each flexbeam is manufactured as a single piece composite laminate with titanium bushings inserted into the lay-up. The two flexbeams are joined to the rotor shaft by circular titanium plates, bolted together. All bolts are secured with lock wire. The rotor shaft passes through the center of each flexbeam and transmits torque through a splined bushing. The spline has a missing a tooth to ensure that the hub is always assembled in the assigned sequence. Due to the maritime operating environment, every effort was made to reduce corrosion sensitive components. Smooth radius corners are incorporated where possible to reduce high stress concentrations.

Flexbeam

The design considerations for the flexbeam are:

- Attachment joints to the hub must be structurally rigid to transmit the blade loads to the hub.

Table 4.5: Flexbeam Dimensions and Properties

End Dimensions (mm)	Lay-up	Mid Dimensions (mm)	Lay-up
$L = 100$ $W = 96$ $D = 34$	$[+45_{50}/0_{120}/-45_{50}]$	$L = 300$ W=35 $D = 14$	$[0_{80}]$

- Central tapered part to provide bending and pitching flexibility.

- Flap, lead-lag, torsion stiffness of each crossection is tailored to obtain the required rotor frequencies.

- The cross-section is designed to support the centrifugal force at each section along with the shear forces, bending moments due to flap, lag and torsion motions.

- Rectangular cross-section is selected for flexbeam since manufacturing procedure is simple compared to that of hollow ribbed sections.

For the material, fiberglass and graphite-fiber composites were considered. Fiberglass composites have good impact tolerances but low stiffness to weight ratio, whereas graphite-fiber composites have poor impact tolerances but better stiffness to weight ratio. Therefore, unidirectional fiberglass is used along with $\pm45°$ graphite-fiber composite to provide the necessary stiffness. Fiberglass is used in the central portion to facilitate better bending and torsion, while the graphite-fiber provides the torsional stiffness required at the splice attachment. Based on these considerations, the cross-section of the flexbeam is presented in Table 4.5. The maximum strain in the flexbeam is designed to be less than 0.3%.

Pitch Case

The pitch case is stiff in pitch, lag and flap and reacts against a spherical elastomeric damper to provide lag damping and required torsional frequency. The pitch case is connected to the flexbeam index-splice attachment at the outboard end and to the lag damper at the inboard end. It is constructed of $[\pm45_{26}]$ graphite-fiber composite plies. Unidirectional tape is added to increase chordwise stiffness. The pitch case lag damper attachment is designed such that the flapping of the blade is not restricted—for this, a pin attached to the damper cases passes through a hole drilled through the top and bottom surfaces of the pitch case.

Elastomeric Damper

An elastomeric lead-lag damper is provided to augment lead-lag stability of the soft in-plane TRITON hub. In order to avoid the maintenance problems associated with hydraulic dampers and additional power requirement with magneto-rheological dampers, an elastomeric damper is used. These dampers have long service life, high

reliability and are effective over a wide range of temperatures ($-65°$ F to $+200°$ F). The damper chosen for this design has horizontal and spherical layers of metal shims and elastomers to provide leag-lag damping and tune the torsional frequency to 1.7/rev, thus eliminating the need for a pitch spring[16]. The damper is located at the hub end of the flexbeam, bolted to the flexbeam on both top and bottom surfaces. The pitch case is connected to the damper at the inboard end through a pin attached to the upper and lower casing of the damper, thus enabling the movement of the pitch case during blade flapping.

Droop Stop

The inboard, lower portion of the pitch case rests on the droop stop, which is attached to the rotor shaft via a spherical bearing-mounted steel ring (see Foldout 4.6.3). This ensures that the pitch case is supported—preventing flexbeam bending—when the blades tend to droop at low speeds without restricting flapping freedom in flight.

4.2.5 Autorotational Characteristics.

All helicopters are required to demonstrate autorotational capabilities that allow recovery of the vehicle in the event of engine failure, loss of tail rotor or transmission problems. For single-engine manned helicopters, autorotation is not feasible at the high speed and low altitude flight demonstrated by the TRITON mission profile due to the required pilot reaction time. However, as the present design features autonomous capabilities. In the event of a failure, the vehicle can compensate by initiating climb prior to autorotation with quicker reaction time than that of a human pilot. An estimate of the autorotational capability of TRITON is obtained by computing the Sikorsky autorotation index (AI)—the ratio of stored kinetic energy of the rotor to the product of gross weight and disk loading of the rotor. The computed AI of 21 ft^3/lb, satisfies the minimum required index for single-engine helicopters of 20 ft^3/lb[17].

4.2.6 Primary Control.

The primary control scheme is shown in Figure 4.13(a). The flight control system (FCS) commands are given as input to the actuator controller computer (ACC). The ACC computes the required TE flap deflections for the desired control angles and relays the information to the controller/motor assembly on each blade. The actuator controller processes the information and feeds the required signal to the motor, which actuates the TE flaps to achieve deflection of the blade. The helicopter states are measured using: an inertial navigation system (INS) for pitch, roll and yaw attitude; a global positioning system (GPS) for velocities; and a differential global positioning system (DGPS) for position and FCS feedback.

4.2.7 Active Vibration Control.

The main rotor is the primary contributer to helicopter vibration; the complex and highly unsteady aerodynamic environment in which the rotor operates, and the dynamic response of the long, flexible rotor blades results in large vibratory forces transferred to the fuselage by way of the rotor

(a) Primary Control Scheme   **(b)** Vibration Reduction Scheme
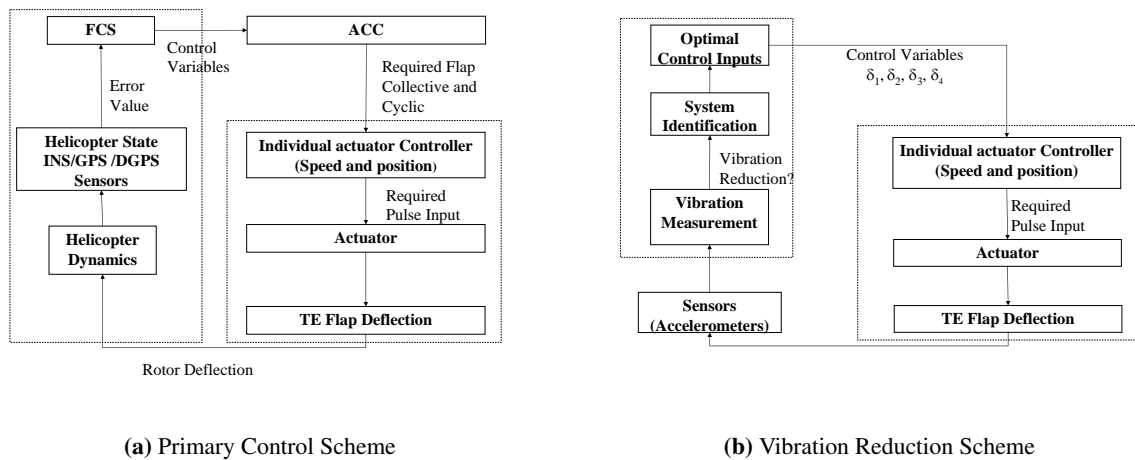
Figure 4.13: TE Flap Deflection Control Scheme for Primary and Vibration Control

hub. In theory, vibration reduction can be achieved by some control input to all the blades provided there is appropriate phasing. However, some degree of rotor dissimilarity is always present and thus individual blade control (IBC) is desired. In the present design, tight manufacturing tolerances are imposed to minimize blade dissimilarity, and the TRITON rotor blades were tailored using pitch-flap coupling to minimize kN_b/rev loads. However, to completely minimize vibrations and suppress non-kN_b (where k is an integer and N_b is the number of blades) vibratory loads, IBC is employed.

IBC requires the derivation of an optimal control input for each blade in order to generate the unsteady airload required for vibration reduction. To achieve this, the vibratory hub loads are measured in the fixed frame and system identification is performed. The system identification process calculates the uncontrolled hub loads and then evaluates the transfer matrix relating each component of hub load to the flap deflection of each blade. Because the transfer matrix varies with vehicle fight condition, system identification is performed in real time. Once state estimates are made, the optimal control inputs ($\delta_1, \delta_2, \delta_3, \delta_4$ in this case) are determined by minimizing an objective function involving the TE flap angles and vibratory hub loads. The vibration control scheme is shown in Figure 4.13(b). A robust and computationally efficient Kalman filter-based adaptive control scheme is employed in the present design[8].

This controller has successfully demonstrated the minimization of overall hub harmonic loads in Mach-scale wind tunnel rotor testing[8]. It has also shown the ability to minimize non-harmonic vibrations, e.g., rotor tracking errors.

Table 4.6: Power Requirements

Component	Power Required (kW)
Flap Actuation	1.0
De-icing	0.1
Avionics	2.5
Computers	0.2
Door hinges (Landing Gear)	1.0

4.2.8 Electrical Power Systems. The basic electrical system design and layout are determined based on total electrical power consumption, availability of space, and the weight penalty imposed by the selected system. The TRITON electrical system consists of a power generation subsystem and a power distribution subsystem. The power generation system provides power to drive all electrically powered equipment, while the power distribution system channels power from the generator to the essential power bus and battery bus. All components vital for safe operation of the helicopter are connected to the essential power bus. This provides a layer of redundancy, as power is available to TRITON through two sources, battery and generator. All the electrical/electronic systems on TRITON operate on DC power, hence a DC starter/generator is installed for all the electrical/electronic needs of the vehicle including powering the actuators. The starter/generator unit is mounted on the side of the engine gearbox. The power requirements for the various components are listed in Table 4.6.

Based on the power required (about 5kW during flight), a *Unison (formerly Aircraft Parts Corp.)* APC 200SGL series [18] starter/generator with long life brushes, rated at 200A/28Vdc is chosen. The generator is controlled by a generator controller unit that incorporates all the normal control and protective functions required for 28V DC electrical power system. The battery provides power for ground start, and in case of emergency, it provides power to the battery bus and essential bus for 30 minutes to actuate the flaps for safe landing of the vehicle. The battery is located on the fuselage and is a vented cell 30-ampere-hour, 28V dc nickel/cadmium battery, weighing about 26.4lbs. The battery is recharged by the generator during flight. The generator powers the blade and tail folding actuators after landing. The dimensions and specifications of the power generator subsystem is provided in Table 4.7.

4.2.9 Rotor Dynamics. The TRITON rotor is bearingless and soft in-plane; to ensure proper frequency placement and verify aeromechanical stability, the dynamic characteristics are studied extensively.

Table 4.7: Generator Specification

Specification	Value
Rated Output	6.0kW
Continuous Load	200A
Speed range	$7000 - 12500$ RPM
Starter Output	5.8HP
Dimensions	Length = 8.80in
	Diameter=5.3in
Weight	22.5lbs

Table 4.8: Rotor Frequencies

Mode	Flap	Lag	Torsion
First	1.05	0.42	1.70
Second	2.84	4.72	-
Third	5.31	-	-

Dynamic Analysis

The blade frequencies are obtained by using the University of Maryland Advanced Rotorcraft Code (UMARC). The blade was modeled using 16 finite elements for the blade and 4 elements for flexbeam. The blade stiffness and mass distributions are shown in Figure 4.14. The flexbeam stiffness was changed to appropriately place the blade frequencies away from multiples of rotor harmonics, as shown in Figure 4.15(a). The rotor frequencies are given in Table 4.8.
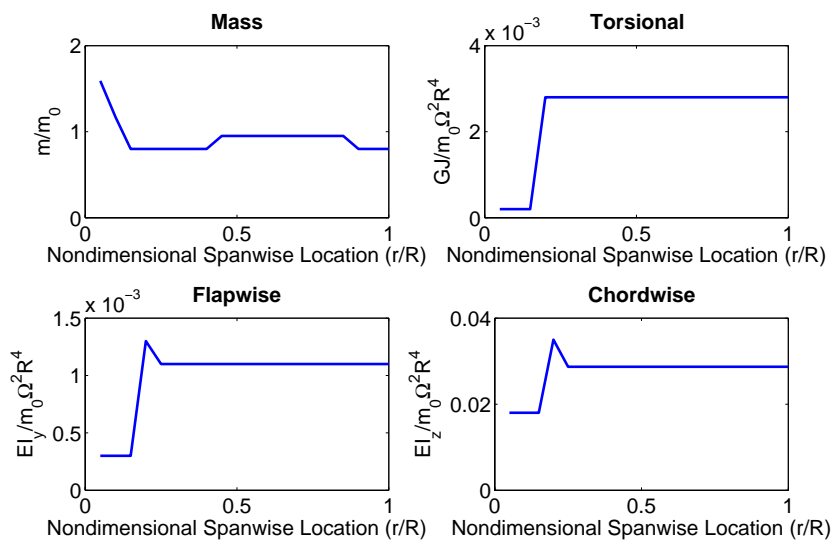
Figure 4.14: Blade Mass and Stiffness Properties

(a) Rotor Fan Plot   **(b)** Flutter/Divergence Stability Boundary
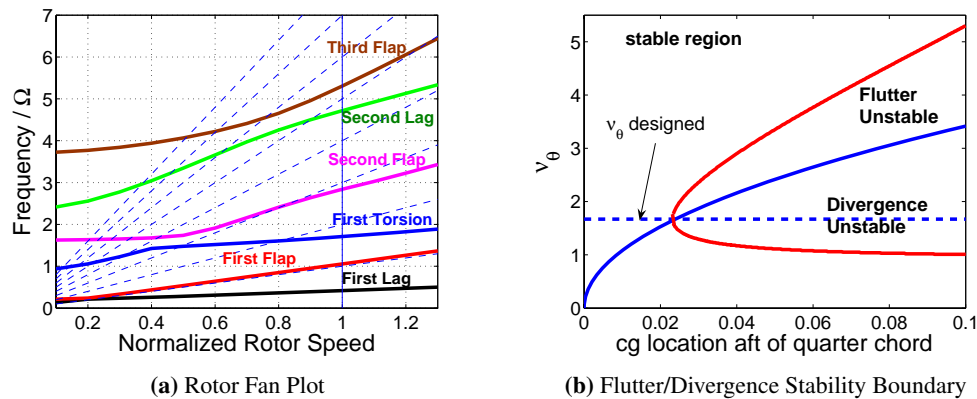
Figure 4.15: Rotor Dynamic and Aeroelastic Analysis

Aeroelastic Analysis

The blades are soft in torsion to provide efficient swashplateless primary control, and thus are susceptible to pitch-flap flutter and divergence problems. To evaluate the extent of these problems, a pitch-flap flutter and divergence analysis is performed. The analysis results, shown in Figure 4.15(b), suggest that for pitch-flap stability, the blade section center of gravity should not be more than .02C aft of the aerodynamic center (quarter chord). The cg in the present design was placed at 0.23C from the leading edge (0.02c ahead of aerodynamic center) by adding leading edge weights to ensure sufficient aeroelastic stability margins.

Ground/Air/Water Resonance

Ground resonance occurs in soft in-plane rotors when regressive lag couples with airframe modes. Since it is an explosive instability, ground resonance analysis[19] is performed systematically to ensure stability of the rotor at all operating conditions. Figure 4.16(a) shows that near operating RPM, the regressive lag frequency and airframe frequencies are well separated. Figure 4.16(b) shows that all the modes are stable and adequately damped, hence the in-plane modes are stable.

  Air resonance occurs in hingeless soft in-plane rotors with high flap frequencies ($\nu_\beta > 1.08$). The regressive flap couples with airframe pitch/roll motion to produce a low frequency nutation mode while the regressive lag couples with this nutation to cause air resonance. It is a mild instability giving rise to limit cycle oscillations. In the present design, the flap frequency is low; however, a comprehensive air resonance analysis is also performed using UMARC to ensure stability throughout the entire flight envelope. Figure 4.17 shows that the rotor lag modes remain stable at all advance ratios, while the inclusion of the elastomeric lag damper further augments the stability in forward flight.

  The vehicle lands on a floating platform and the pitching, rolling, heaving and lateral motion of the floating

(a) Frequency Variation

(b) Damping Coefficient Variation
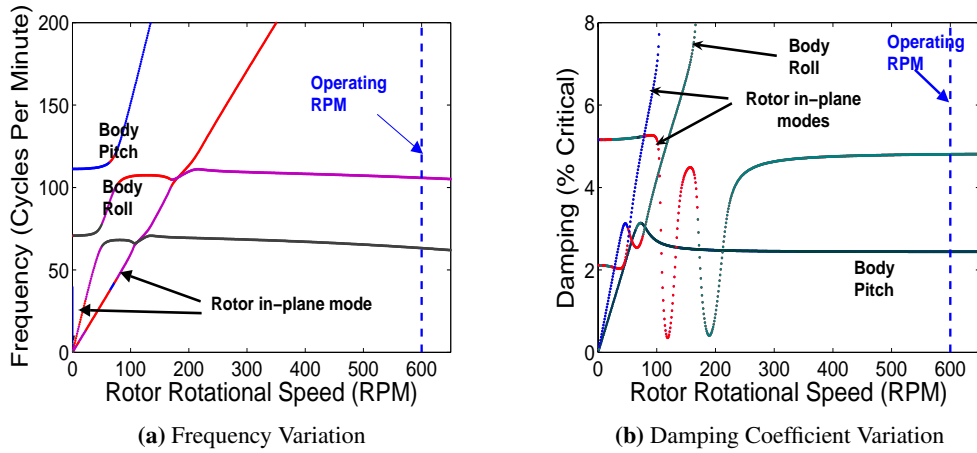
Figure 4.16: Ground Resonance Analysis

(a) Flap/Lag/Torion Damping

(b) Lag Damping
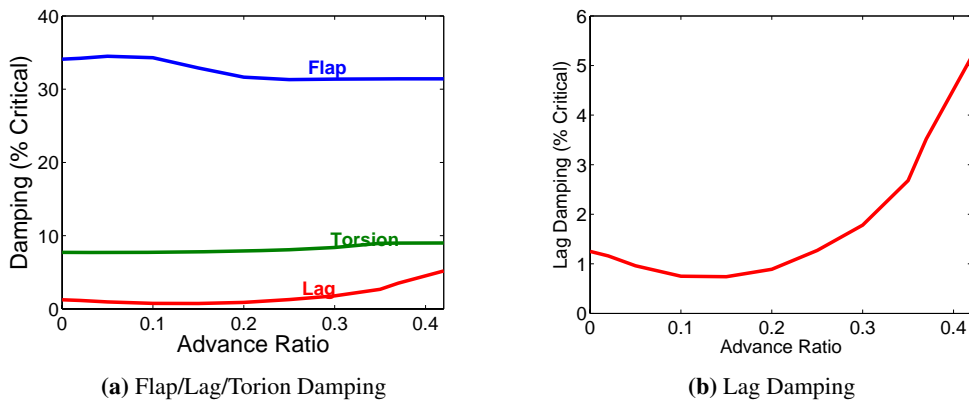
Figure 4.17: Air Resonance Analysis

platform can give rise to water resonance problem. A detailed analysis of the floating platform is required to conclusively determine the stability of the vehicle-floating platform stability. Any instability in the in-plane modes can be avoided with the addition of appropriate lag damping by tailoring the properties of the elastomeric layers of the lag damper. A detailed analysis would require the properties of the platform and floats, and a measure viscous damping provided by the sea-water. For a preliminary design stability estimate, it is assumed that the lateral motion of the platform due to wind (15kts) or waves is negligible. A qualitative analysis of the present design suggested that the heaving of the platform in sea state 3 is not a major concern, the pitching and rolling can however couple with the regressive lag mode and give rise to instabilities. A simple analysis is performed to verify if the floating platform (pod) frequencies could coalesce with regressive lag to produce an instability similar to ground resonance. The frequencies for the pod were computed assuming small displacements in still water. The frequencies of pod and wave excitation are shown in Figure 4.18. It is observed that the regressive lag
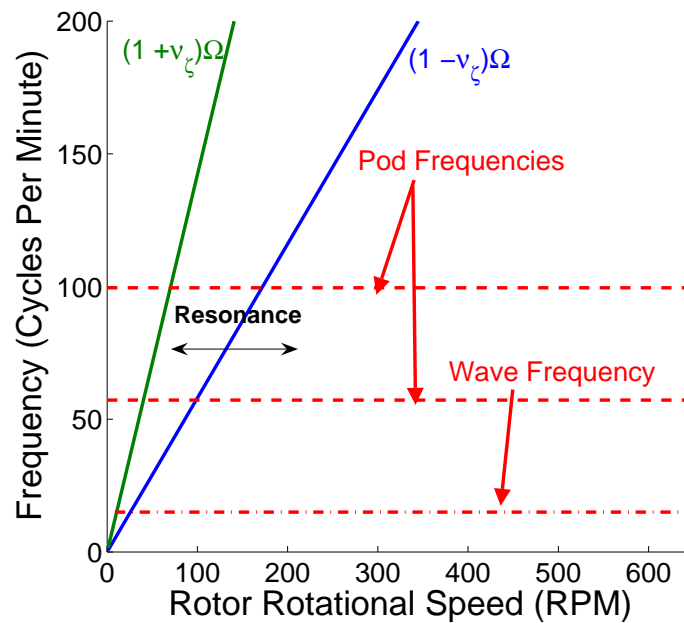
Figure 4.18: Water Resonance Analysis

frequency is well separated near the operating RPM. Overall, from this simple analysis it can be concluded that the vehicle is stable on the floating platform.

4.3   Airfoil Selection

Airfoil selection for TRITON was primarily driven by aerodynamic considerations; however, since a trailing edge flap actuation system is also being employed, it was necessary to consider the space available for both the internal blade structure and the flap actuation mechanisms.

In general, airfoil selection for a rotary-wing requires a compromise to be drawn between the conflicting requirements for good transonic performance on the advancing side of the rotor disk while also providing lift in the low, subsonic region on the retreating side. Therefore, airfoils with the following characteristics were sought[20, 21, 22]:

- High maximum lift coefficient to provide sufficient lifting capability on retreating side of the disk, and enough lift margin for maneuvers and stability in wind gusts.
- High drag divergence Mach numbers to allow operation at high forward flight speed without excessive power losses on the advancing side of the disk.
- Good lift-to-drag ratios over a wide range of operating Mach numbers to ensure low power consumption over the operating range and slow autorotative rate of descent.
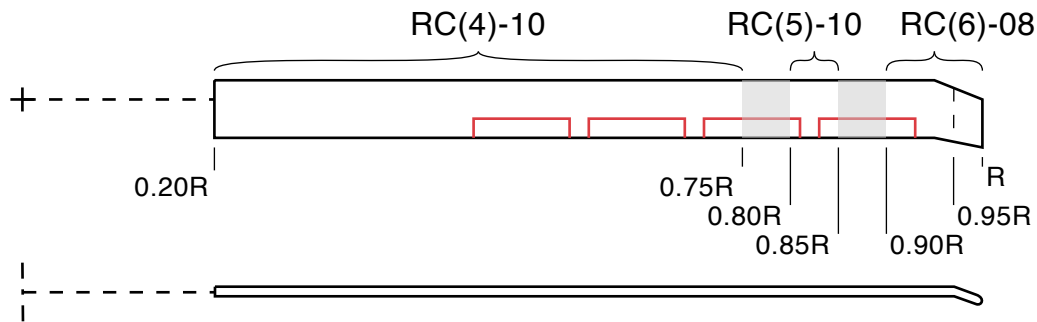
Figure 4.19: Airfoil distribution

- Low pitching moments to minimize control loads, torsional deformation, and vibration.
- Gentle stall characteristics to provide safe, predictable control of the vehicle.

A survey of available airfoil data in the public domain indicates that NASA RC-series airfoils are the optimal choice for the TRITON . It is recognized that other airfoil families exist which may be more optimized for rotary wing applications; however, much of this information is proprietary and thus unavailable for detailed study. As such, the airfoil selection for TRITON was limited to families in which detailed aerodynamic information was available.

For the inboard regions of the blade, spanning $0 < r < 0.75R$ and $0.80 < r < 0.85R$, respectively RC(4)-10 and RC(5)-10 airfoils are used [23]. Both airfoils offer near-zero pitching moments for Mach numbers less than 0.75. Beyond a Mach number of 0.75, a monotonic negative increase in pitching moment occurs. This behavior is characteristic of most airfoils when approaching transonic Mach numbers; however, in comparison with the VR-7 airfoil, this increase in negative pitching moment is less severe. The RC(4)-10 airfoil is capable of operating at higher lift coefficients than the RC(5)-10, however, the RC(5)-10 airfoil offers improved performance at higher Mach numbers. Hence the usage of both RC(4)-10 and RC(5)-10 airfoil for the inboard and midspan sections of the blade is incorporated.

For blade stations outboard of $0.90R$, the RC(6)-08 airfoil is used[24]. This airfoil has been specifically designed for the tip region of a main rotor blade. More specifically, the RC(6)-08 offers a high Mach drag divergence of 0.86 for lift coefficients between -0.1 and 0.1, and near-zero pitching moments for Mach numbers less than 0.8. Beyond a Mach number of 0.8, a gentle negative increase in the pitching moment occurs, thereby reducing the severity of increase in pitching moment commonly encountered on the advancing side of the rotor in high-speed flight.

4.4   Twist and Taper Distribution

Both twist and taper are geometrical means in which the airload distribution along the blade span is controlled. An optimal combination of twist and taper will allow each blade station to operate at its optimal lift-to-drag ratio and encourage uniform inflow. However, with the high aspect ratio of TRITON , and the need to contain trailing flap actuation mechanisms within the blade envelope, it does not appear plausible for significant use of taper for the inboard sections; therefore, the use of taper to optimize rotor performance is restricted to the blade tip. This restricted use of taper will not have a significant effect on rotor performance, as it has been shown that rotor performance is more sensitive to taper near the blade tips than inboard sections[21].

Identification of the optimal twist distribution requires a compromise to be made between both hover and forward flight performance. As can be shown with simple momentum theory, a highly twisted blade with hyperbolic distribution is optimal for hover performance. However, in forward flight, highly twisted blades will result in negative tip loading on the advancing side of the rotor disk. In addition, highly twisted blades limit the ideal thrust operating range of the rotor. Since the primary operating condition for TRITON is in forward flight, a low twist value of $-8°$ was chosen to provide good forward flight performance while providing a good figure of merit in hover.

4.5   Tip Geometry

Proper selection of tip geometry is crucial in the design of high performance rotors. Recognizing that each blade is exposed to both high-speed transonic and low-speed subsonic flows, a compromise must be made between reducing transonic effects on the advancing blade while ensuring sufficient lift capability of the retreating blade. In addition, careful consideration must also be given to inherent aerodynamic/inertial couplings that may be introduced through changes in the blade structure and planform. Lastly, choice of tip geometry may have a strong influence on the strength and placement of trailed tip vortices[25]. Therefore, selection of tip geometry also plays a role in determining induced power losses and acoustic signature of the rotor; e.g. contributions from blade-vortex-interactions (BVI) and vortex-vortex-interactions (VVI)[26].

To reduce transonic effects, sweep is typically introduced to lower the effective free-stream Mach number normal to surface pressure gradients. Though this approach is proven to be effective, excessive sweep may lead to premature stalling of the retreating blade[21]. In addition, the offset of blade mass from the pitch axis serves to increase the effective polar moment of inertia and strengthen the propeller moment acting on the swept elements[27]. Thus, introducing sweep has the effect of increasing the torsional frequency of the blade. This may have the negative consequence of increasing cyclic control forces. Also, torsional deflections due to aerodynamic

center offset may impact the response to collective and cyclic control inputs.

Incorporating anhedral in the tip design aides in reducing the strength of tip vortices and displacing them further from the tip-path-plane. Thus, anhedral can be effective in reducing induced power losses. However, the offset of blade mass from the pitch axis affects torsional frequency and introduces flap-torsion coupling[27].

Tapering of the tip has the effect of biasing the airload distribution further inboard, thereby reducing tip vortex strength and providing a more uniform inflow distribution. Therefore, a reduction of induced power losses may be achieved as well as a reduction in the severity of BVI noise. However, excessive taper may result in high drag penalties due to low-Reynolds number flow encountered by the retreating blade.

Experimental investigations by Desopper[28] have shown that the proper combination of of sweep, taper and anhedral can be used to improve the overall performance of the rotor. Therefore a combination of sweep, taper and anhedral is used to achieve an optimal compromise between both aerodynamic and dynamic considerations. The proposed tip geometry incorporates a constant sweep angle of $20°$, with an constant droop angle of $20°$. The acoustic characteristics of tip geometry similar to this have been investigated experimentally and revealed that reduction in BVI noise is possible during the approach to landing[29].
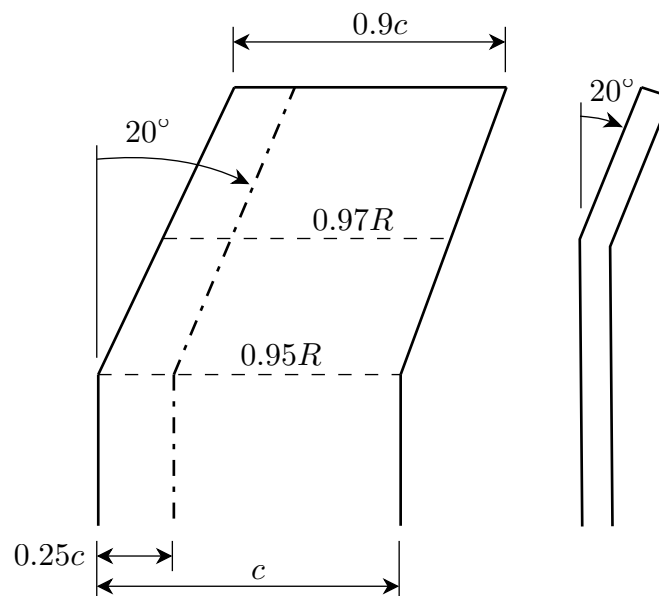
Figure 4.20: Tip geometry

4.6   Automatic Blade Folding and Securing

4.6.1 Automatic Blade Fold System.

The TRITON is required to stow within the confines of the SLRP. To accomplish this, a fully automatic blade fold (ABF) system is required. This system consists of an actuator to remove one of the blade retention bolts and an actuator to rotate the blade about the other retention bolt. All blades are folded aft along the tail section, requiring that the front blades exhibit some cyclic pitch in order to allow them to clear the rotor hub and rear blades when folded. ABF functions are typically reserved for very large helicopters like the H-53, which uses heavy hydraulic actuators located directly on the rotor hub. The addition of hydraulics to the TRITON was deemed unacceptable. Current Navy regulations require the ability to fold the blades in a 45 knot horizontal wind from any azimuth, and secure them in up to 70 knot wind speed.

In the effort to achieve a low-drag, mechanically simple rotor, a very unique system needed to be developed. Additionally, due to the swashplateless rotor design, there is no simple way to set the cyclic pitch of the front blades prior to folding; there is only a pre-collective pitch of $12°$, encompassed entirely within the small index splice between the flex beam and the blade. This requires that the blades are folded using a joint of defined pitch, located outboard of the flexbeam and inboard of the index splice. The dimensional constraints at this section of the rotor are very limiting. Both electric actuators and shape memory alloys were looked at, but the size of actuators required to handle bolt extraction and ABF would require a larger blade root, introducing higher drag and increased mechanical complexity, resulting in reduced reliability.

Therefore, instead of placing the fold system on the rotor, a unique, but simple onboard design was developed. An actuator extends from the rotor mast fairing (see Foldout 4.6.3), engages the fold joint retention bolts, and performs both the bolt extraction and ABF functions.

4.6.2 Automatic Blade Fold Process.   The ABF process begins with engine shutdown after landing. Once the rotor has slowed to approximately 300 rpm, the rotor brake is applied. Feedback from position and speed sensors stop the rotor such that the blades are indexed at $45°$ from the longitudinal and horizontal axis of the fuselage. The rotor parking brake is then engaged to prevent windmilling of the rotor. In the indexed position, the precise locations of the fold joints are always known. Encapsulated in the rotor mast fairing is a mechanical arm, much like existing arms used in a CNC machine, which extends radially from the main rotor mast. The arm can rotate about the rotor mast and precisely align itself with each fold joint retention bolt. Part of the arm then extends upward, engaging with the end of the retention bolt to be removed with a small bit. This bolt is a special adjustable diameter self-retaining bolt produced by Avibank Mfg[30], with a slight $2°$ taper to ensure the blade properly seats and there is no play in the joint when inserted. The bit locks to the end of the bolt, disengages the self-retaining mechanism, and pushes the bolt out of the blade. The bit re-engages the self-retaining mechanism, locking the bolt end into the index splice clevis clear of the blade. The bit retracts from the bolt hole, allowing

free rotation of the blade.

A bevel gear at the end of the arm meshes with a gear attached to the other retention bolt about which the blade is rotated. This bolt is supported on bearings to reduce friction and is locked to the blade bushing through a similar expansion mechanism as supplied by Avibank. Upon rotation of the gear mesh, the blade will rotate about the axis of the bolt. This process is performed sequentially, folding the aft blades 45° back, followed by the forward blades 135° back such that all blades are aligned parallel to the longitudinal axis of the airframe. When unfolding the blades, a chamfered end of the index splice and a slight tapered end of the fold joint ensure the index splice aligns properly into the joint without binding. The port-side blades rotate about the front bolt and the starboard blades fold about the rear bolt. Both retention bolts will be of equal weight to balance the rotor. The complete folding process is estimated to take approximately 3 minutes. If at any point during the fold/unfold process, a step cannot be completed, the procedure halts and the submarine crew is informed of the issue.

The ABF system can be powered from the onboard power supply or from the SLRP or ground cart power supply if necessary. The blades can also be manually folded/unfolded in the event of mechanical failure, and both retention bolts can be manually extracted for blade removal. In addition, this unique ABF design can easily be scaled and retrofitted onto existing and future rotorcraft as a mechanically simple, reliable, low drag solution to blade fold.

4.6.3 Automatic Blade Securing Process.   It is extremely important to secure the rotor blades to protect them from damage due to wind loads and deck motion. As part of the ABF system, mechanical arms located along the top of the tail boom (see Foldout 4.6.3) rise into position prior to blade folding. Each arm features an electromagnet piece that is positioned such that the forward blade folds directly under it and the aft blade folds directly above. Once the blades are folded back into position, the magnet is activated, attracting a small metallic strip in each blade, and firmly securing the blades to the arm . These blade clamps serve both to secure the blades from moving as well as to unload the damper and flexbeam from moments imposed by the folded blade.

LIGHTWEIGHT EPOXY-CARBON COMPOSITE BLADES

ADVANCED TIP GEOMETRY

DROOP STOP

ELASTOMERIC DAMPER

SWASHPLATELESS ROTOR DESIGN

ELECTRIC MOTOR-ACTUATED TRAILING EDGE FLAPS
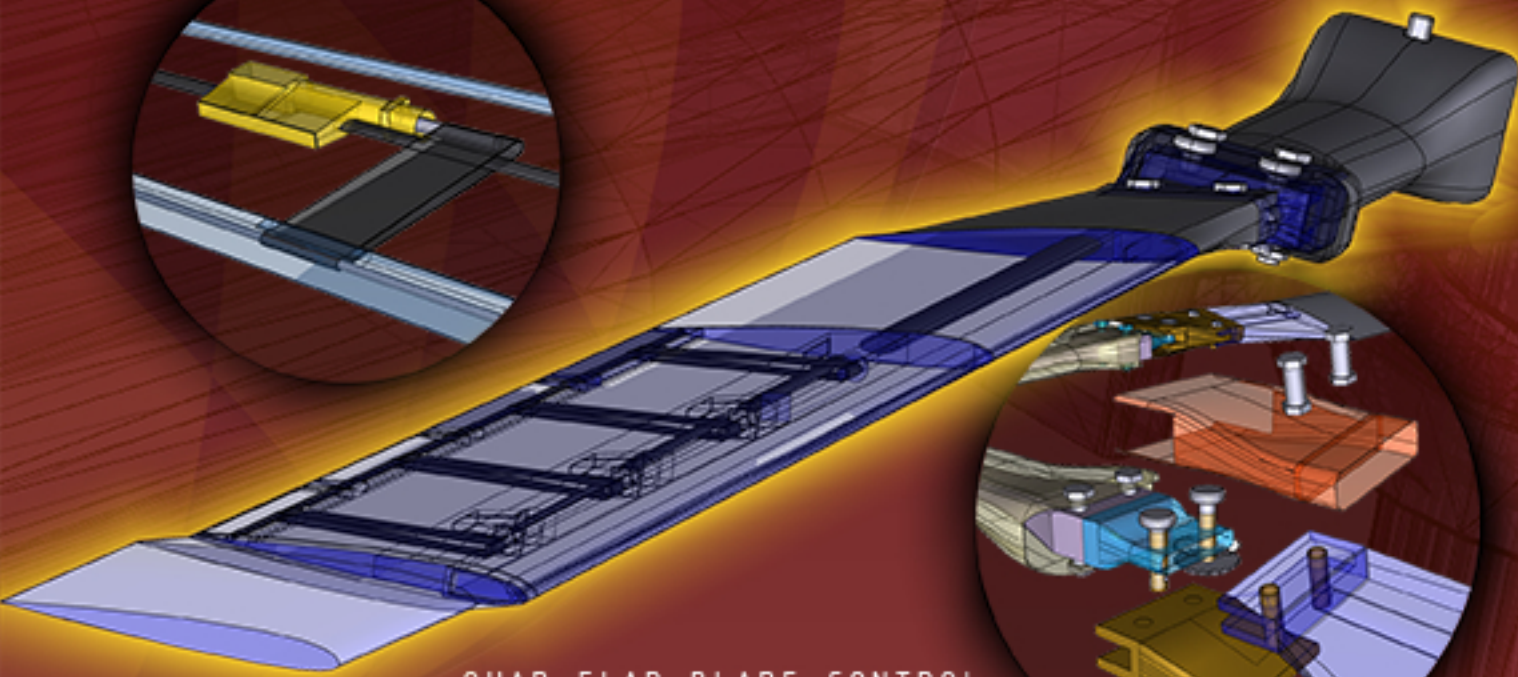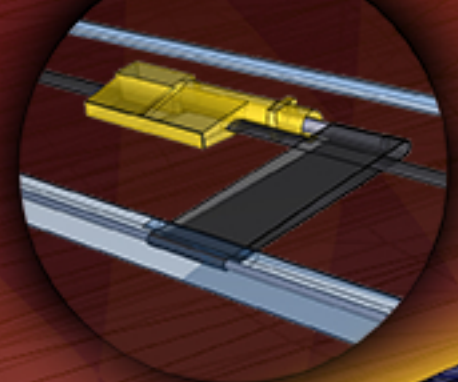
QUAD-FLAP BLADE CONTROL

UNIVERSITY OF
MARYLAND

RETENTION PIN
REMOVAL

ACTUATOR
COWLINGS

BLADE FOLDING
ACTUATOR

AUTOMATIC BLADE AND TAIL FOLDING

BLADE CLAMPING
MECHANISM
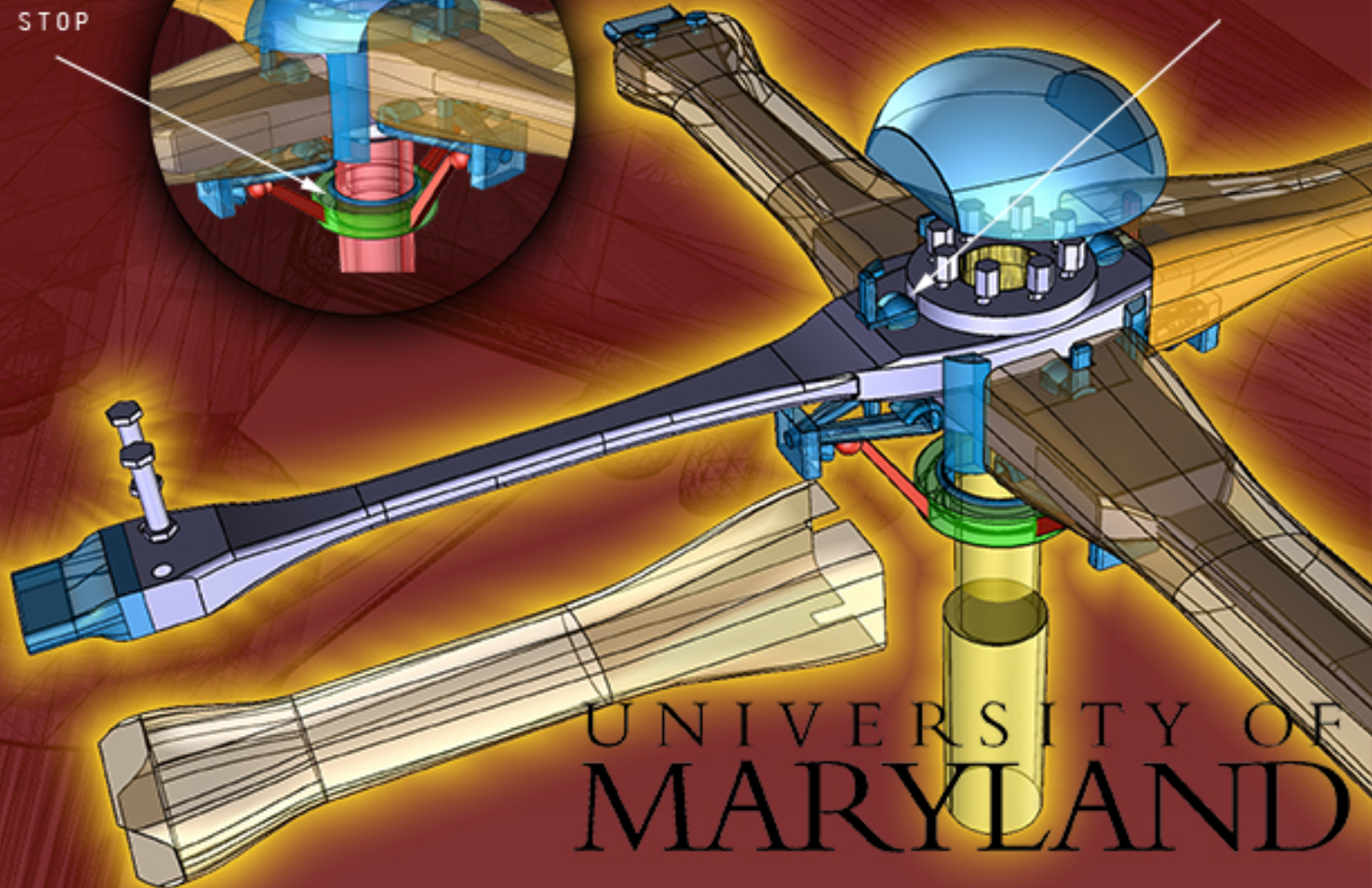
UNIVERSITY OF
MARYLAND
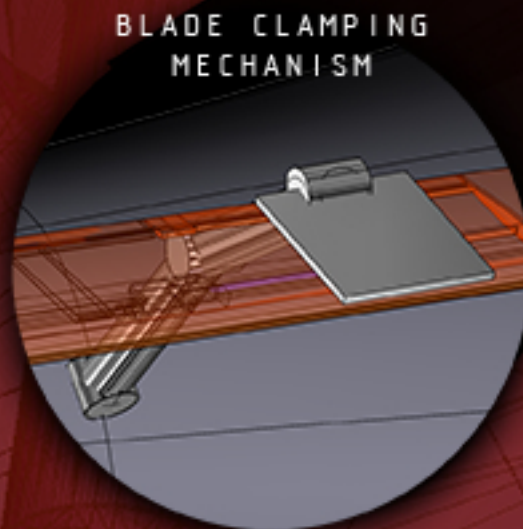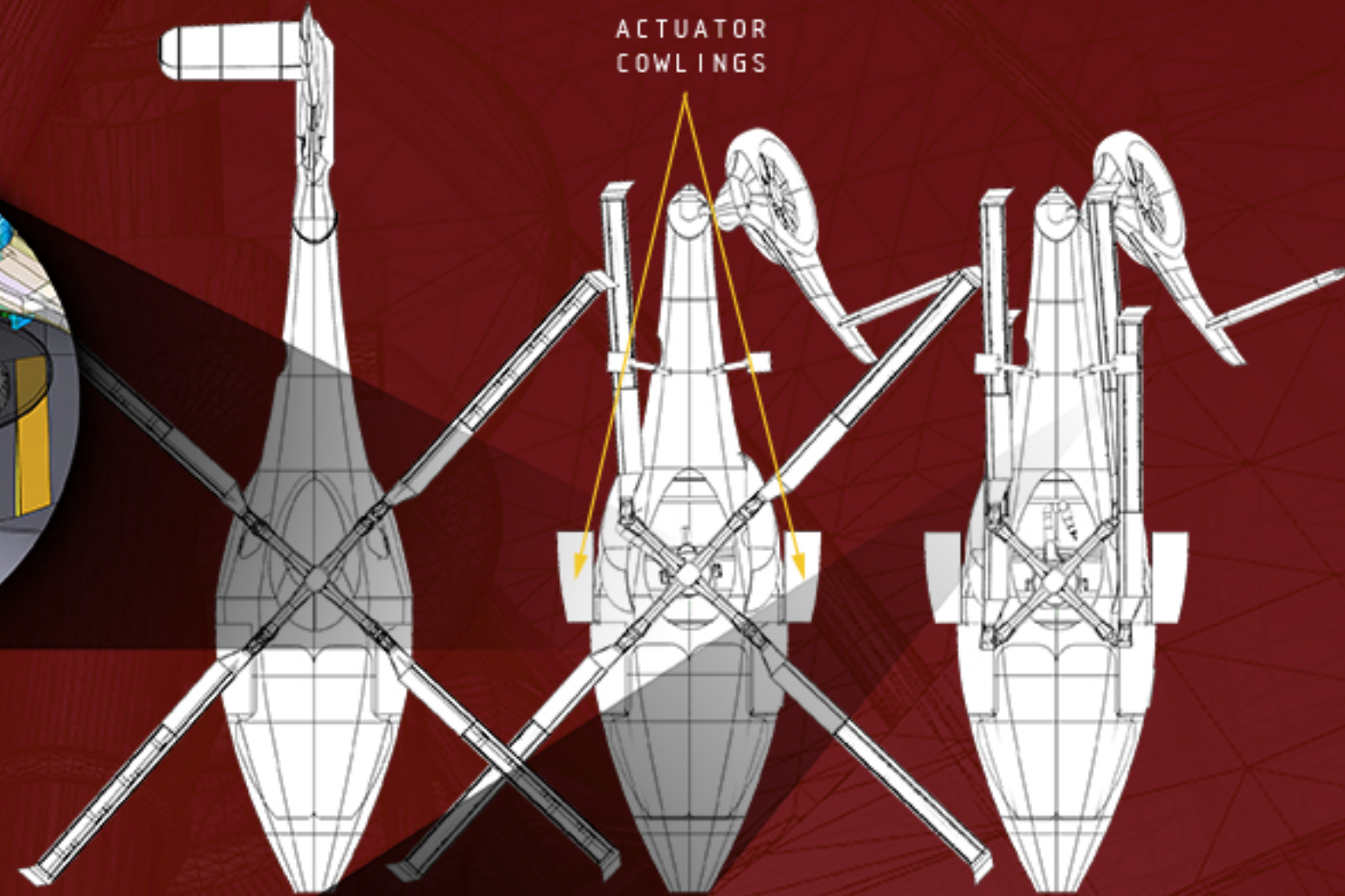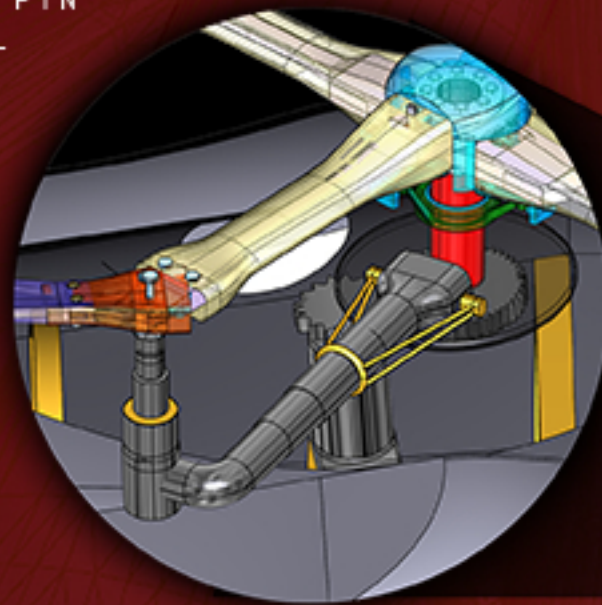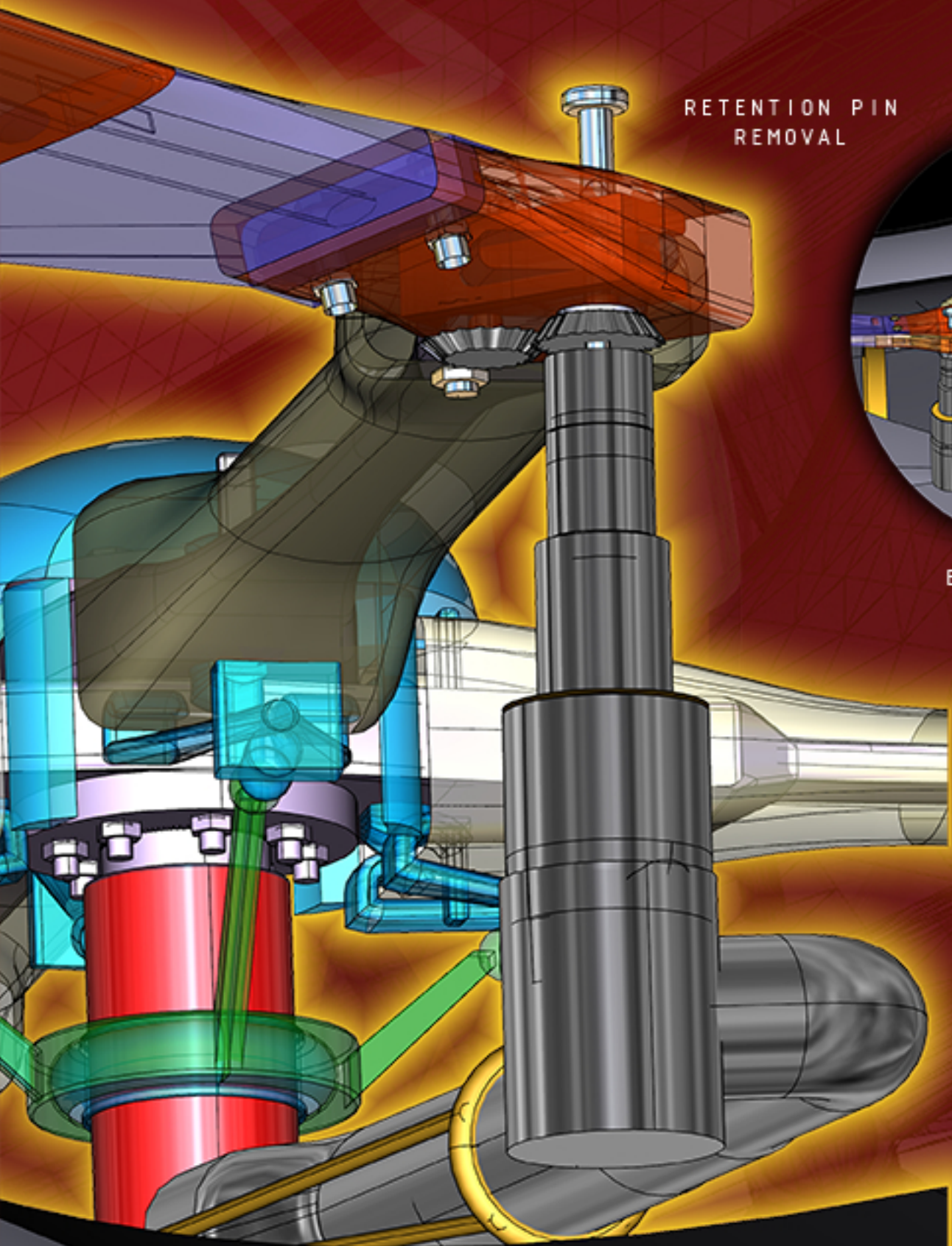
5 Tail Rotor: Fan-in-Fin

5.1 Fenestron versus Conventional

As discussed in Chapter 1, a fan-in-fin (fenestron) configuration was selected for the tail rotor system. The following were key points influencing this decision:

- **Better overall safety:** As the primary use of the TRITON is for military operations, operational safety is a major concern. A fenestron design ensures there are no exposed tail rotor blades which can cause catastrophic failure in the event of blade strike (water, powerlines, trees, etc.). Additionally, the shrouded rotor protects ground personnel from coming into contact with the high-RPM blades.

- **Enhanced maneuverability:** The RFP requires operation in extreme weather conditions; high sidewinds, for example. If the ratio of cross wind to induced velocity of the tail rotor becomes high enough, flow recirculation can occur, creating conditions for vortex ring state. Because the fan-in-fin design produces a higher induced velocity compared to a conventional tail rotor designed for the same thrust, the design is less susceptible to these recirculation effects[31]. Additionally, the fan-in-fin design has sufficient yaw stability and handling qualities required for negotiating through tight spaces.

- **Greater hover efficiency:** Momentum theory shows that a fan-in-fin produces thrust equivalent to that produced by a conventional tail rotor with twice the disk area; the conventional tail rotor loses 10% thrust due to vertical fin blockage, while the fan-in-fin produces additional thrust by way of negative static pressure at the duct inlet. This allows the fenestron to achieve equal thrust to a conventional tail rotor at roughly half the size, providing better hover capability.

- **Better forward flight performance:** In a fenestron configuration, the vertical fin can be made larger without corrupting flow through the tail rotor. This allows for the design of a larger vertical fin to offload the tail rotor during forward flight without inducing further losses. This effectively decreases tail rotor power requirement with increasing flight speed.

- **Reduced acoustic signature:** A fenestron configuration ensures lower noise levels than a conventional tail rotor. While higher frequencies produced by the increased operational RPM of the fenestron are generally considered to be subjectively noisier, the rotor shroud blocks some of the the in-plane sound propagation. Furthermore, these higher frequency sounds are more apt to an atmospheric attenuation affect and thus are objectively less noisy out-of-plane, particularly over large distances. The acoustic signature of the fenestron can be further reduced through introduction of unequal tail rotor blade spacing; by introducing an effective phase lag between propagation of sound pressure, a noise canceling effect can be achieved.

Table 5.1: Duct Geometry

Lip Radius	Duct Length	Diffuser Angle	Supporting Strut Section
$0.14R$	$0.5R$	5.0^o	elliptic

- **Decrease weight and cost:** A conventional tail rotor on a helicopter the size of the TRITON generally requires the addition of a tail pylon to prevent the tail rotor from striking the ground in takeoff or landing. This introduces an additional gearbox stage with a $90°$ change of direction to accommodate relocation of the tail rotor shaft. The fan-in-fin, with a smaller, shrouded rotor does not require the pylon, hence saving the extra weight and cost associated with the additional gearbox requirement (about 20% savings[31]).

5.2   Fenestron Detailed Design

In a fenestron configuration, the fan and the duct produce about the same amount of thrust. The following provides a brief overview of the method used for its design.

5.2.1 Methodology.   The methodology makes use of momentum theory approach[32]. The method provides an estimate of fan blade diameter and chord. The direct effect of duct shape parameters (such as inlet/outlet lip radius, duct closure shaping) are not considered in this simple analysis. The contraction ratio from duct center to freestream was assumed to be 0.95. The fenestron structure is composed of: duct/shroud (inlet lip, fan, hub, stator, diffuser); fan blades; empennage (vertical and horizontal fin).

5.2.2 Duct/Shroud Design.   Because the duct generates about the same amount of thrust as the fan itself, its design is critical. The duct consist of three main sections: inlet lip, fan hub and the diffuser.

Inlet: The inlet lip consists of a round section that creates the suction force from the inflow of the tail rotor. Experimental results performed by United Technology Research Center (UTRC) show that a lip radius of $5-7\%$ of fan diameter results in a duct producing same thrust as fan itself[33, 34]. For the current configuration, the lip radius selected was 7% of the fan diameter.

Fan Hub: Hub consists of fan blades and stator vanes (or guide vanes/flow straighteners). The hub also contains the control linkages used to alter blade collective (*no hydraulics*). The stator vanes help reduce the swirl component of the flow downstream of the fan, improving its efficiency. The number of stator vanes chosen was 10, a typical value for the fenestron as suggested by Marze et al.[35].

Diffuser: The role of the diffuser is to avoid the wake contraction typical of conventional tail rotors while simultaneously preventing flow separation. The diffusion angle was selected based upon those values suggested in literature (Mouille et al.[31], Yoerkie, Jr. et al.). The value selected is $5°$.

Table 5.2: Fan Geometry

Radius (ft)	Nb_{fan}	Solidity (σ_{TR})	Twist (deg)
1.12	9	0.45	-7
RPM	Airfoil	Chord	Rotation Direction
5500	NACA63A312	0.16	BBF (Bottom Blade Forward)

The detailed duct geometry is tabulated in Table 5.1 (*R* being the duct radius) and a sketch is shown in Figure 5.1.
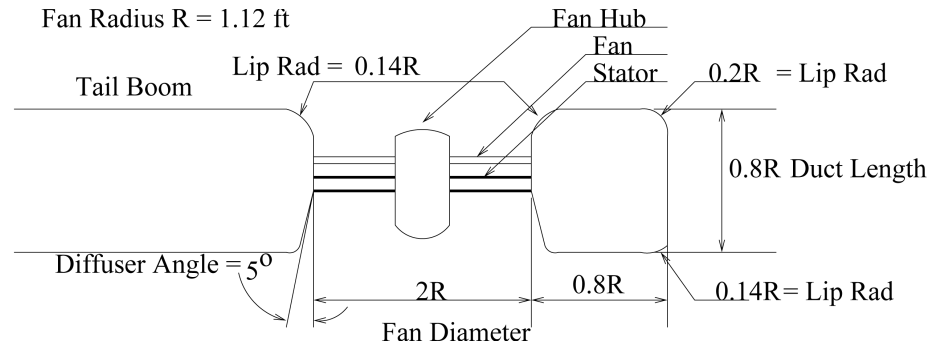
Figure 5.1: Sketch of Duct/Shroud Structure

5.2.3 Fan Design.

The fenestron fan is optimized for high aerodynamic efficiency.

Fan Diameter: The fan is designed such that it produces same thrust as the duct; in other words, half the thrust of the total tail rotor system. Analysis based on this assumption led to the fan geometry as shown in Table 5.2. The analysis also takes into account the contraction ratio, the ratio of duct midsection area to the area of the downwash in the freestream. The main rotor to tail rotor ratio is 9.5, which is a typical value for fenestron tail rotors. The fan diameter is 2.2 ft. while chosen number of fan blades is 9.

Fan Tip Mach Number: The fan tip speed was restricted to 200 m/s to avoid the negative effects of compressibility.

Blade Spacing: The blade spacing is a crucial design issue since it affects the tail rotor noise. From previous research it is known that asymmetrical fan blade arrangements result in reduced noise[36, 35]. Marza et al. suggested the following blade spacing:

$$\theta_n = n \times \frac{360°}{b} + \Delta\theta sin\left(m \times n \times \frac{360°}{b}\right) \tag{5.1}$$

where θ_n is the angular position of the *n*th blade, $b = 9$ is the number of blades. The values of *m* and $\Delta\theta$ are

Table 5.3: Fan Blade Angles

Blade Number	$n=1$	$n=2$	$n=3$	$n=4$	$n=5$	$n=6$	$n=7$	$n=8$	$n=9$
θ_n	45.5	89.1	129.2	165.9	200.4	234.8	27.1	310.7	353.8
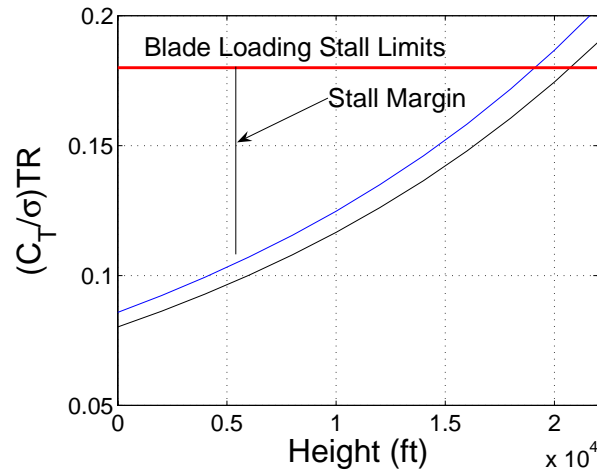
Figure 5.2: Blade Loading Coefficient vs Altitude

dependent upon b, the number of fan blades, and are chosen so as to provide dynamic balancing of the rotor and maintain optimum distribution of the energy over the frequency spectrum. The values chosen also guarantee a minimal inter-blade angular separation imposed by the conditions of angular excursions of the blades in terms of pitch and structural adherence of the blades to the hub. The values corresponding to $b=9$ are, $m=3, \Delta\theta = 9.55°$ [35] and the angle are shown in Table 5.3.

Airfoil: Since fans are small and have high torsional stiffness, in order to achieve high aerodynamic efficiency it is desired to have a highly cambered airfoil. The chosen airfoil was NACA63A312, a 6-series airfoil.

Blade Solidity: The RFP requires that the helicopter be operable at 6000 ft at 95° F. The high altitude consideration led to the choice of a high value of $C_T/\sigma = 0.09$ for the fan blades. The resulting solidity of the tail rotor is 0.45 and the blade chord is 1.12 ft.

Blade Stall Margin: During very high side wind conditions, the fan stall limit becomes a critical issue. Sidewinds influence the tail rotor by increasing the torque generated from fuselage side force, and also by altering the inflow to the duct. The side force is mainly due to the aerodynamic forces generated by the vertical fin. Figure 5.2 shows the variation in blade loading with altitude and indicates that there is sufficient stall margin even during the most adverse cross wind of 40 knots. This demonstrates that the design has very good tail rotor authority in extreme cross winds even at an altitude of 6000 ft (at 95° F). Table 5.2 summarizes various fan geometry sizes.

Table 5.4: Fin Geometry

Area (ft^2)	Span (ft)	Mean Chord (ft)	Aspect Ratio
6.2	3.0	2.1	1.42
Sweep @LE (deg)	Incidence Angle (deg)	Airfoil Section	
30	4	NACA63$_3$A618	

5.3 Vertical Fin Detailed Design

The vertical fin is sized so as to provide the entire anti-torque moment required in forward flight, thus completely offloading the fan, allowing increased life span. The cruise drag penalty due to trim can be reduced by as much as 30%, provided a vertical fin with very high lift-to-drag ratio is used. In addition to increasing the lifespan of the tail rotor, offloading the fan during forward flight also has the following advantages: reduced dynamic strain on rotating parts results in higher fatigue life and low maintenance cost; lower instabilities even in very high forward speeds; and safe return to the submarine with an inoperative fan (see: Dauphin [31]).

Keeping the above discussion in mind, a cambered airfoil with high thickness-to-chord ratio was chosen for the fin. High camber value ensures high lift while minimizing the drag penalty. The chosen fin airfoil is $NASA63_3A618$ and is placed with an incidence angle of 4° to the flow. The fin geometry was obtained using simple airfoil theory and was sized at an altitude of 6000 ft, 95°F. The area of the fin is 6.2 sq-ft. Figure 5.3 shows the fan and fin thrust components relative to the total thrust of the tail rotor, indicating the ability to completely offload the fan during cruise (140 knots). Figure 5.4 illustrates the effect of increased cruise speed on tail rotor power consumption.
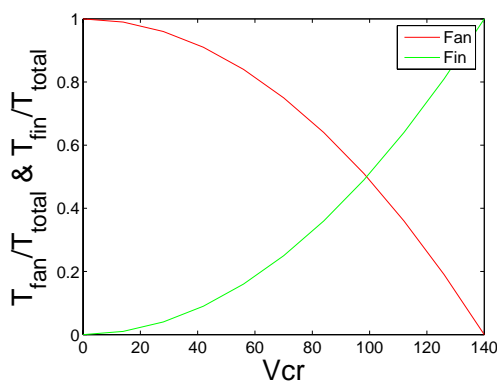
Figure 5.3: Thrust to Total Thrust Ratio vs. Cruise Speed
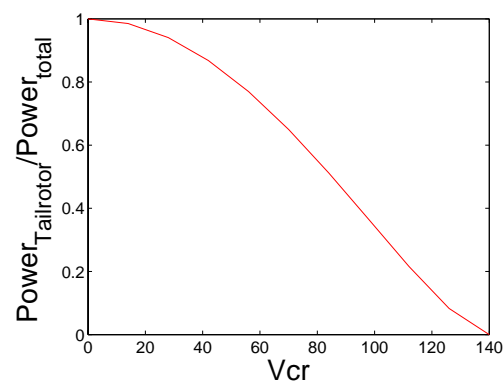
Figure 5.4: Fan Power vs Cruise Speed

5.4 Tail Folding

To meet fuselage dimension constraints, it was found to be necessary to fold the tail rotor. The tail was folded about a hinge inclined to ensure proper length and height reduction. The tail shaft at the fold joint is connected by a set of face gears (see Folding 4.6.3).

6 Airframe Structural Design

The TRITON showcases a compact, crashworthy airframe designed to meet the rigors of military operation. Its unique design features include special CRYSTALOY skin for ballistic protection, a retractable and versatile landing gear system, and is completely modular to support both ARV and UEV missions. Considerable attention was paid to the disposition of the crew, equipment, fuel tanks, engines and transmission, in order to minimize the CG travel between the empty condition and fully loaded condition. This enables the helicopter to be flown under all load flight conditions with the fuselage at almost level attitude.

6.1 Design Evolution

A common airframe design is used for both ARV and UEV vehicles. This provides two distinct advantages: manufacturing logistics is simplified, thereby reducing acquisition costs, and improves the mission capability of a single SSCN by permitting each vehicle in stow to be configured as either an ARV or UEV as dictated by mission requirements. All structural properties and allowable load factors for the TRITON are dictated by U.S. Navy Aeronautical Requirements 56 (AR56): Helicopter Structural Design Requirements[37].

6.2 Structural Sections

The structural layout consists of two primary modules: central fuselage and tail boom. Four bulkheads serve to interconnect modules, to support loads and bending moments, and to support the engine and transmission deck. In addition, secondary bulkheads are used to maintain fuselage shape and frame openings [38]. Two sinewave keelbeams provide structural integrity and support to the cockpit and cabin floor.

The airframe consists of four primary bulkheads. The first bulkhead attaches the nose to the main body of the airframe and serves as the attachment point for the nose landing gear. The second and third primary bulkheads serve as fore and aft support of the transmission deck. In addition, the third primary bulkhead serves as the primary attachment point for the aft landing gear. The fourth primary bulkhead provides load connectivity between main fuselage and tail boom. External shape continuity of the fuselage and support for door openings is provided by secondary bulkheads located between the first and second primary bulkheads. Within the tail

boom section are two secondary bulkheads and four longitudinal stringers. Sinewave keelbeams located between the first and third primary bulkheads provide the crashworthy structure and house the fuel tanks. The semi-monocoque construction of the lower airframe ensures no water ingress during an emergency water landing.

The external shape of the fuselage is selected from a compromise between usable interior space and aerodynamic cleanliness. The cross-section of the fuselage has a box-like envelope to provide maximum usable interior shape while the slight vertical taper and rounded lower body ensures a smooth flow path for rotor down-wash. The steep aft upsweep permits usage of clam-shell doors for improved access to fuselage interior, while a progressive aft taper mitigates the effects of flow separation.

Each of the primary bulkheads has been designed to provide proper load paths for the loads arising from landing, flight, take off, ground handling, and rotor operations. Landing loads received careful scrutiny due to the unsteady motion of the floating platform, the need to land on semiprepared/unprepared surfaces, and potentially aggressive ground handling during loading/unloading into the SSCN hangar bay and C130J cargo bay (see Foldout 6.7).

6.3   Crashworthiness

Special operations missions may require maneuverability through crowded urban environments at low altitudes, often through unfriendly airspace. As such, the airframe is robust and designed to protect human occupants during high load events such as rollover and obstacle strike. Throughout the airframe, structural members have been sized and arranged to maximize energy absorption and dissipation. The sinewave geometry of the two keelbeam webs has have been designed such that they collapse in a higher buckling mode; this pattern increases the amount of energy which is absorbed during an emergency landing. The bulkheads and stringers are arranged to collapse progressively when subjected to high inertial loads such that those loads are substantially reduced before reaching crew seats. Aluminum foam is contained within the seat rails to provide additional force-lessening energy absorption, a simple and inexpensive addition to the airframe structure. Self-sealing, crashworthy fuel tanks are used to prevent disastrous combustion in the event of a crash or hard landing. The fuel tanks are oversized by 10% in order to provide an aircushion for impact when the aircraft is fully loaded. An estimation of buoyant force on the vehicle indicates that, in the event of an emergency water landing, the vehicle can stay afloat 30 minutes in sea state 3.

Heavy mass items such as the rotor, transmission and engines can intrude into the cabin under a high-load crash, presenting danger to the aircraft's occupants. Such intrusion is prevented by restraining the aforementioned components under the following inertial loads as specified in AR56 Section 3.6.8[37]: forward, 20g; upward, 20g; downward, 20g; lateral, 10g.
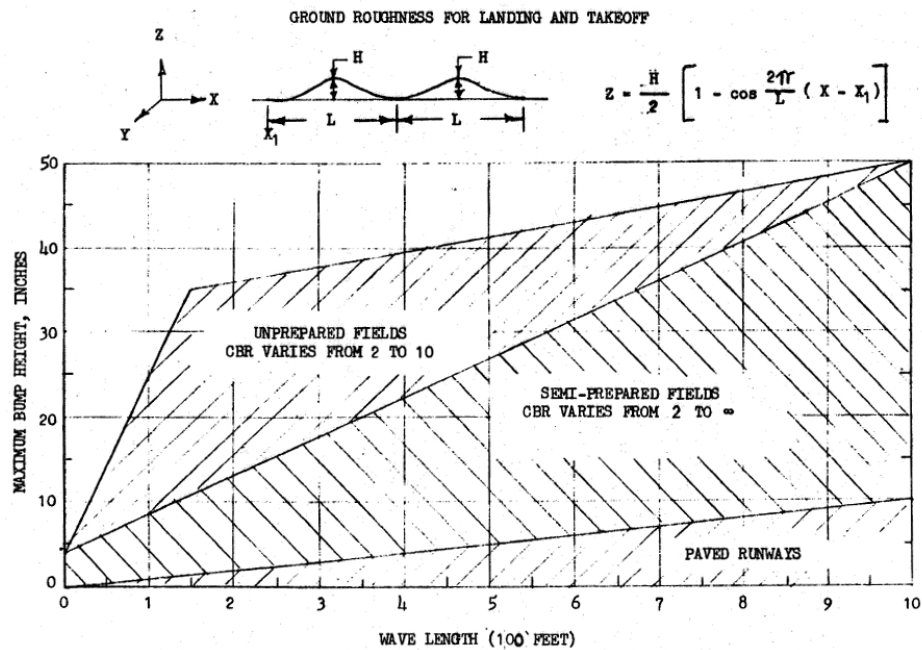
Figure 6.1: AR56-dictated landing surface requirements

To ensure rapid exit from the vehicle, all doors have been designed to remain operable after a high load event.

6.3.1 Landing Gear.

The selection of landing gear configuration was driven by several factors:

- minimal flat plate area in forward flight to reduce drag
- ability to land on a variety of surfaces, including a floating platform, sand dunes, and snowy or icy terrain
- compact size for optimal submarine stowage

After an extensive study of traditional landing gear configurations, a retractable tricycle gearing system was selected. The main wheels and struts are completely stowed in the rear of the fuselage, while the nose gear is fully stowed in the fuselage forebody during forward flight to reduce drag. Tricycle-type landing gear—as opposed to a skid-type landing gear—allows the helicopter to land on a the semi-prepared surfaces dictated by U.S. Navy Aeronautical Requirements 56 (AR56): Helicopter Structural Design Requirements [37]. The wheels are outfitted with snow/sand shoes for adaptability to a variety of terrain conditions. An automatic wheel-braking system prevents sliding when resting on the landing platform or other uneven surfaces, while a claw-like locking mechanism can 'grab' the gridded Submersible Launch and Recovery Pod (see 2) landing platform for redundant support. Electric motors within the bulkhead supply the necessary retraction mechanism.

Sizing Details

Wheel/Tire Sizing

In an effort to provide robust landing capability for dynamic platform conditions, Type III 5.00-4 tires were selected for both the main gear and nose gear. Each tire has 12 plies and can independently support a maximum static load of 2,200 lbs. This overdesign allows for freedom in landing orientation, regardless of SLRP heaving or rolling motion. Additionally, the selection of 12 plies, rather than 6, allows the ability to land on the unprepared and semi-prepared surfaces expected at remote locations. The tires can be inflated to a maximum internal pressure of 90 psi; typically, for unprepared and semi-prepared surfaces, a lower pressure is desired. Tire pressure can be adjusted accordingly in the SSCN hangar bay.

Polyurethane spokes provide support between landing gear struts to allow for effective change in both lateral and longitudinal stiffness. This manufacturing procedure allows the TRITON design to be adapted to alternative mission profiles.

Shock Absorber Sizing

Single oleo-pneumatic shock absorbers are used on each gear, sized to satisfy the landing conditions described in Section 3.4.2.4 of AR56. Raymer[39] provides the following formula for shock absorber sizing:

$$S = \frac{V_{vertical}^2}{2g\eta N_{gear}} - \frac{\eta_T}{\eta}S_T \tag{6.1}$$

Where S is the oleo stroke length, V is the descent velocity (20 ft/s as per AR56), η is oleo efficiency, η_T is tire efficiency, and S_T is tire stroke length. This results in an oleo stroke of 2.25 in, length of 5 in, and diameter of 2 in.

6.4   Small-Arms Ballistic Protection

To ensure survivability of the crew and mission critical equipment during flight through hostile areas, the composite skin of TRITON contains the ceramic matrix composite CRYSTALOY[40]. CRYSTALOY consists of SiC whiskers embedded in the ceramic matrix. The presence of these SiC whiskers serves to constrain grain boundaries of the ceramic matrix during processing to mitigate formation of micro-cracks. In addition, the SiC whiskers have a strain redistributing effect, thereby reducing localized stresses. Should damage causing stresses be induced, the loads transfered by the SiC whiskers results in numerous non-catastrophic cracks as opposed to a single catastrophic failure. Upon ballistic impact, the CRYSTALOY serves to blunt the projectile and induce destructive shock waves within the projectile. The carbon fiber layers surrounding the CRYSTALOY plate absorb

the kinetic energy of the projectile through deformation and failure of the fibers.

6.5   Materials, Manufacturing, Construction

The bulkheads, stringers and keelbeams of the airframe are aluminum-lithium alloy. Lithium being the lightest metallic element, it can reduce the weight of an aluminum alloy by approximately 3% for every 1% of lithium added. Most commercially available Al-Li alloys contain about 2% lithium, offering 7-10% reduction in density, and a 10-15% increase in elastic modulus. This type of alloy also has good resistance to the growth of fatigue cracks, making it advantageous for rotorcraft frames. These elements are overlaid by a woven-graphic/epoxy skin. An aluminum mesh is overlaid to provide protection from lightning strikes.

The engine/transmission deck is made from titanium alloy plate. Titanium was selected over aluminum-lithium and composite sandwich construction for its resistance to heat and fire, as well as oil corrosion. In addition, the usage of a full titanium plate provides crew protection from separated turbine or compressor blades.

The two modules of the vehicle airframe are manufactured separately, and fitted with required subsystems. Final assembly is made easier by the consistency of the cross section and simplicity of interior structure.

6.6   Doors

Primary crew egress is through a pair of sliding doors. Use of sliding doors is required to allow the crew to enter and exit the vehicle and also permit safe crew deployment via fast-lining. In addition, rear clam-shell doors are provided to give easy access to internal cargo and facilitate reconfiguration of the vehicle to either ARV or UEV. All doors frames are strengthened to prevent distortion and can be jettisoned in an emergency.

6.7   Survivability

Susceptibility reduction is achieved in the TRITON by having a fuselage with small frontal area, which provides low visual and radar detectibility. Smooth contours and the use of low glint, composite materials for the fuselage skin helps in further reduction in the visual detection. The engine exhaust is placed in the rotor wake to reduce infrared (IR) signature. IR suppressant paint [41] is used for the fuselage. IR suppressors can also be fit in the engine to obtain greater reduction in IR signature.

TRITON AIRFRAME/LANDING GEAR ASSEMBLY
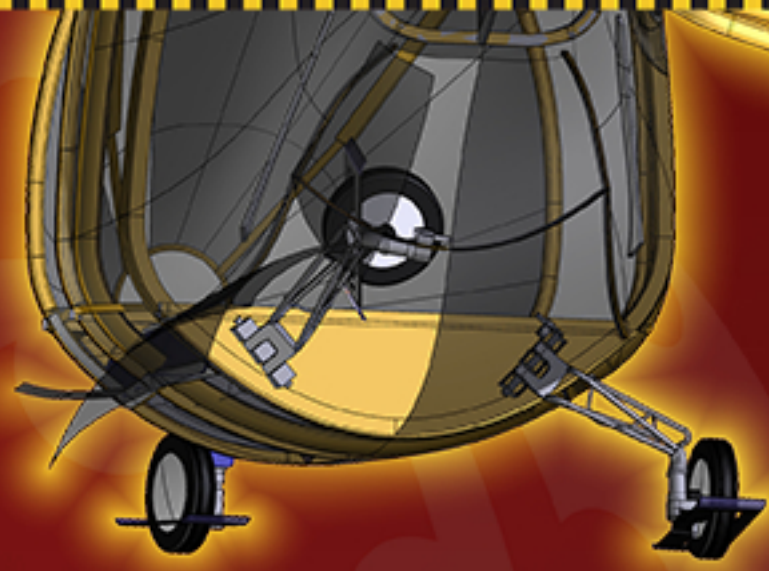
OLEO-PNEUMATIC
SHOCK ABSORBER

TYPE III
5.00-4 TIRES

FULLY RETRACTABLE LANDING GEAR

SNOW/SAND SHOES
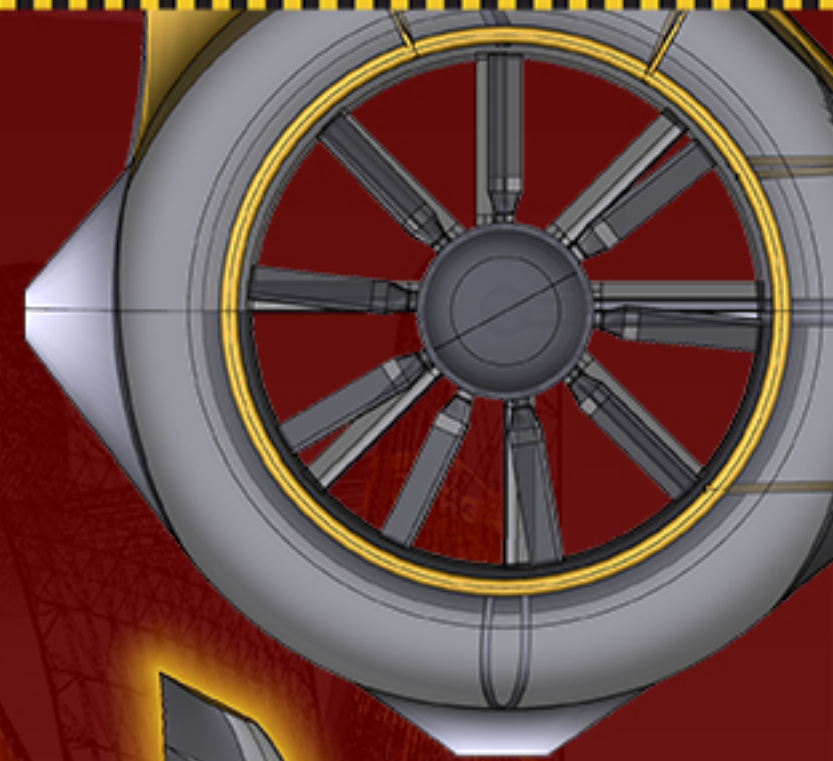
NOISE-REDUCING
BLADE SPACING

ROTOR MAST SUPPORT
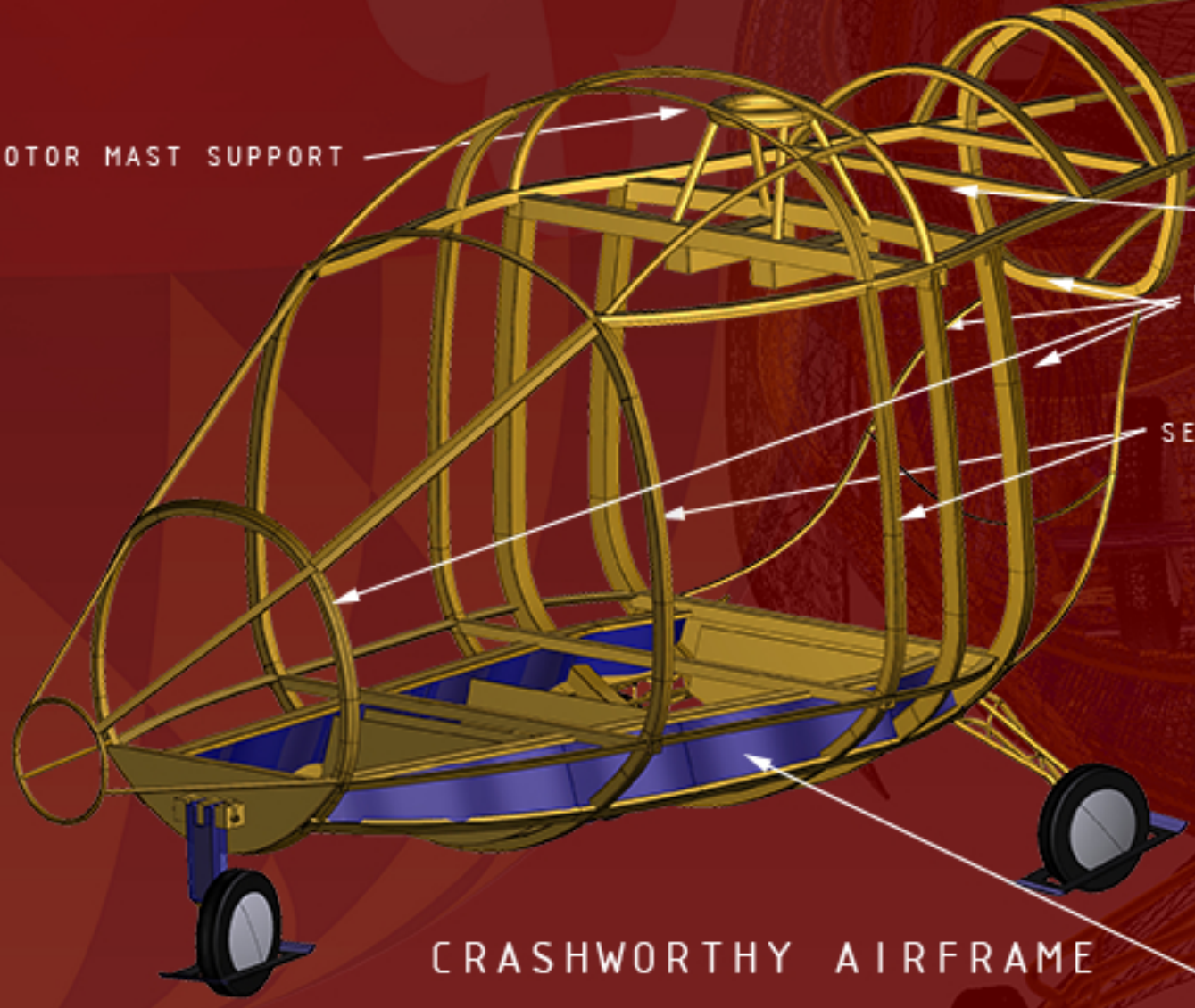
ENGINE/TRANSMISSION DECK

PRIMARY BULKHEADS

SECONDARY BULKHEADS

FAN-IN-FIN
ANTITORQUE

CRASHWORTHY AIRFRAME
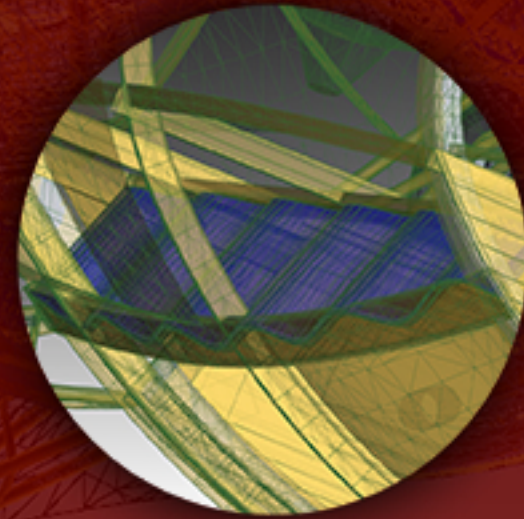
SINEWAVE KEELBEAMS

UNIVERSITY OF
MARYLAND

7 Avionics and Cabin Configuration

7.1 Autonomous Control System

Both the ARV and UEV will be operated autonomously by the Tactical Control System (TCS) software package, developed by Raytheon[42]. This system was designed for seamless automatic flight control of Unmanned Aerial Vehicles (UAV) and is used on several military UAVs. The TCS software provides a standard graphical user interface for operators and full control of data dissemination to the command, control, communications, computers, and intelligence architecture (C4I). The system is scalable for different levels of interactivity and is capable of being made modular. In addition, the basic system is common to all United States Navy UAVs and can be set up, operated and maintained by Navy personnel.

The TCS and its elements are the operational focal point for the ARV/UEV system. The TCS functional capabilities are mission planning, mission control and monitoring, payload data processing, targeting, C4I interfaces and operator interface[43]. TCS is capable of seamlessly transferring command and control between controlling stations, whether they are shipboard-based, helicopter-based, or soldier-based operations. The TCS provides robust and secure command, control, status, and voice relay communication capability between the operators and the AV. The primary data link is through the Tactical Common Data Link (TCDL) while a secondary Ultra-High Frequency/Very-High Frequency (UHF/VHF) data link provides a backup for command and control input to the TRITON .

7.1.1 Sub-based Control System. The U.S. Navy Sea-based TCS, with the command and control functions, is integrated with the ship's internal systems. The operator consoles are integrated into the Combat Information Center (CIC) of the submarine. A TCS station (Fig 7.1), which consists of two redundant, interchangeable workstations, each providing a single user interface that combines computer-generated graphics with payload sensor data[44] will be installed in the modified submarine hangar bay. The workstations provide the operators with access to a variety of sensors, digital computers, and communications with other individuals. The TCS provides the principal Human Computer Interface for commanding, monitoring and controlling all aspects of flight operations.

The TCS station has two operators: the Air Vehicle Operator (AVO) and Mission Payload Operator (MPO). The AVO has the primary task of monitoring aircraft status and controlling launch, flight, and recovery operations. The AVO is also responsible for conducting flight operations including preflight mission planning and post flight data recovery, which includes communications. The MPO has the primary tasks of (1) monitoring the health, status and operation of the aircraft, (2) evaluating aircraft data, and (3) performing real-time operation

Figure 7.1: TCS Station

Figure 7.2: Portable TCS

Figure   7.3:   BriteStar   II
EO/IR/LDRF

of the helicopter as required during the mission.

The capability of Multi-aircraft control (MAC) will be added to the system. MAC is currently in use by the U.S. Air Force, and allows up to 4 vehicles to be operated simultaneously by 5 operators from one station. One AVO dynamically selects which aircraft is under direct control, while four MPOs maintain continuous control of sensors and aircraft with point-and-click commands. Two stations would allow up to 8 ARV/UEVs to be deployed together. Substantial strides are being made in the field of multiple UAV control; it is anticipated that by 2020, more UAVs can be flown autonomously by a smaller system[42].

While its primary mission is recon support for Special Operations Forces, through the TCS control consoles the UEV data will be linked through the existing C4I network to an extended group of users. The UEV will be an integrated component of the battle space and can provide real-time targeting for naval guns and missiles as well as a full range of air-delivered weapons.

7.1.2 ARV-based Control System.   Onboard flight control of the ARV will be accomplished through a modified TCS powered portable system (Fig 7.2)[44]. This system fits into a suitcase, includes full flight controls, and currently weighs less than 100 lbs. The ARV will feature a docking station in front of each crew member that will accommodate the portable TCS system, which can then be removed and deployed in field with the SOF team if desired. This allows the ARV to be fully configurable to suit the mission needs. If full ARV/UEV control is desired in the field, the system can be removed from the ARV when the team extracts and the control is no longer necessary in the now unmanned vehicle. If the ARV needs to be launched without a crew and extra TGOW is desired, both systems can be removed from their docking stations to save nearly 200 lbs. The portable TCS will feature two multi-function displays that can be configured to display varying levels of information, depending on ARV/crew interaction. The displays will also be Night Vision Goggle compatible.

7.1.3 SOF-based Control System.   The Future Combat System (FCS) is a family of manned and unmanned

systems connected by a common network that is to be fielded by 2008[45]. The FCS soldier is provided superior situational awareness through network connectivity allowing remote control of and real time imaging from a UAV. In a similar way, the ARV SOF crew, once deployed, will be directly linked to the ARV/UEV through the TCS software. From a heads up display (HUD) on a helmet-mounted visor, the SOF team can remotely control the waypoint positions and basic operations (i.e. extract, land, recon, return to sub) of the ARV/UEV through simple point-and-click or voice commands. Through the same HUD they can then receive a real time electro-optic and infra-red feed from the UEV. The sub, ARV, and soldier mounted TCS systems provide multiple levels of redundancy and control can be seamlessly transferred from one system to another.

7.2 Avionics Details

The TRITON 's avionics suite also includes BAE systems Identification Friend or Foe (IFF) transponder, Dukane Underwater Locator Beacon, Honeywell radar altimeter, H. Koch Emergency Egress Lighting System (EELS), Ethernet Local Area Network (LAN), electrically heated pitot/static probes, IR lights, and a ground control panel for power hook up, maintenance checks, etc[46, 47, 48, 49]. The avionics bay will be housed in a Faraday cage for EMI protection. All AV electrical power is 28 VDC, compatible with current naval shipboard and aircraft electrical systems and DOD mobile electric generators. The Environmental Control System (ECS) uses forced ambient air. Temperature sensors control cooling fans that vent outside ambient air through intake barrier and EMI filters, through the avionics bay and then onto the engine bay. A basic diagram of the avionics interface is shown in Figure 7.4.

7.2.1 Imaging Payload.   The UEV will feature the FLIR Systems BriteStar II, 3-axis, gimbaled assembly, which provides electro-optic and infra-red imaging and a Laser Designation Range Finder (LDRF) (Fig 7.3)[50]. The unit includes a gyrostabilized platform with 360-degree coverage, a thermal imaging sensor for day/night operations with 5 fields of view, a TV camera for enhanced daytime operation with 3 fields of view, a LDRF, and a laser pointer for spotlighting targets. BriteStar I is currently in service on the UH-1N, and BriteStar II, which features enhanced target location and tracking, is used by the Firescout. Future iterations of advanced FLIR systems can easily be retrofit into the airframe.

7.2.2 Vehicle Management System.   Dual redundant Vehicle Management Computers (VMC) form the core of the system and manage all vehicle and flight critical processes. Dual-redundant buses are used to support flight critical items and ensure data timing constraints. The VMC is the controller for each bus. The VMC and buses operate in a master-slave configuration where only the master issues commands and the slave listens to ensure the master is operating properly.
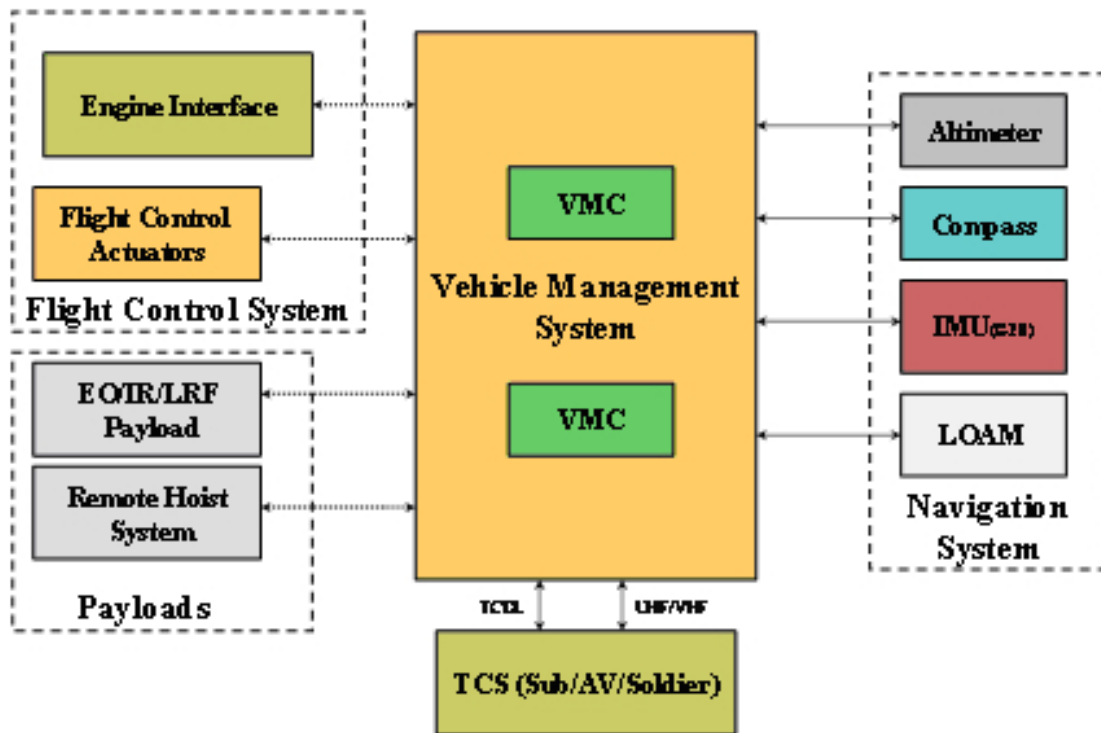
Figure 7.4: Avionics System Interface

7.2.3 Sensor Suite. The navigation subsystem uses dual Kearfott KN-4073 GPS/INS navigators that feature 3-axis monolithic ring laser gyros[51]. GPS position, velocity and acceleration data are provided to a Kalman filter which also accepts data from the Differential GPS (DGPS). A navigation processor integrates this data to provide navigation of positional accuracy to within 2 feet. Position and velocity data are then supplied to the VMC.

7.2.4 Automatic Terrain Following and Avoidance. The mission profile requires the TRITON to fly below 50 ft AGL for the entirety of the mission in order to remain hidden from enemy radar. At a cruise speed of 140 knots, an extremely robust terrain avoidance system is necessary. Nap-of-the-Earth guidance begins with far-field mission planning. A mission flight plan is generated using a high resolution digital map, along with mission requirements and threat information. The greater the detail of these inputs, the more optimized the flight path becomes. A dedicated laser obstacle avoidance monitoring (LOAM) system, produced by Selex Communications will be used for near field flight guidance[52]. This award winning system has been selected for use on the NH90, EH101, and the UH-60. The LOAM system uses laser radar to scan the area around the flight path and identifies possible obstacles on the basis of the returned echo. The system software can identify obstacles ranging from bridges and hills, to 5 mm wires. Sensed obstacle data is fed to the VMC, which then compares it with the far-field mission inputs. If a conflict exists, the VMC then picks from a set of evasive

maneuvers that will successfully avoid the obstacle. If it determines that no combination of evasive maneuvers will resolve the conflict, the helicopter is commanded to hover and await operator input. This obstacle avoidance thought process proved highly acceptable in NASA simulations[53].

7.3 Cabin Configuration
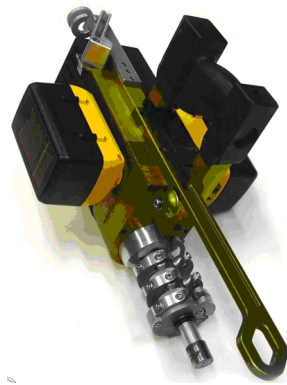
Figure 7.5: Atlas ascender system
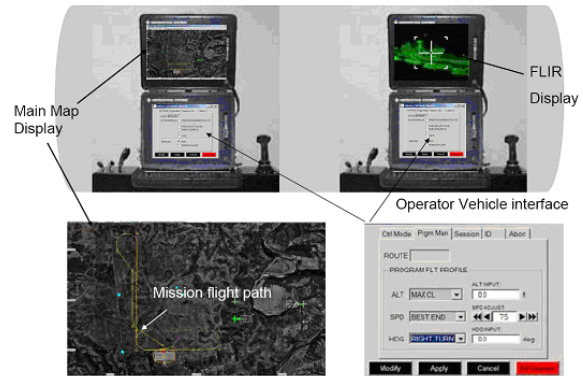
Figure 7.6: Pilot/passenger TCS interface

7.3.1 Internal Configuration.   The primary design driver for the internal layout of the ARV was allowing sufficient space for two fully-equipped SOF soldiers (270 lbs each) and 260 lbs of mission equipment. Because both crew members exit the TRITON at the mid-mission point, it was important they be located near the vehicle's CG. Martin-Baker Armoured Crew seats provide crash attenuation and increased protection from ballistic threats[54]. Space for the typical 260 lb SOF load-out is provided behind the seats such that it is easily accessible. A clam-shell door is incorporated into the aft section of the main fuselage for easy loading of mission equipment (see Foldout). The SOCOM group at NAVAIR was extremely helpful in providing typical SOF missions, equipment load-outs, and other general requirements.

7.3.2 Airborne Insertion/Extraction.   A fast and stealthy insertion/extraction scheme is critical to the success of a SOF mission. For this reason, it is desirable to allow both passengers to simultaneously ingress/egress while in a 50 ft hover. This is safely and easily accounted for electrically actuated sliding doors located on either side of the fuselage. The doors can also be manually opened and jettisoned in case of an emergency. Incorporated into the door frame are a lowered step and a rope attachment hook that automatically deploy with the door. The powered rope ascender from Atlas Devices[55] is used for rappelling and hoisting functions (Fig. 7.5). The Atlas ascender was selected over a standard hoist system because it is lightweight (15 vs. 100 lbs), has a fast ascent rate (10 vs. 4 ft/s), and can be remotely operated by the SOF soldier with only one hand, freeing the other hand

for weapon use. It can handle loads up to 1000 lbs and can be used with various forms of rescue equipment. For insertion, once the crew has rappelled to the ground, they can remotely send the power ascender back up to the AV. A small spool attached to the bottom of the ascender can collect the rope as it ascends. The rope attachment, step, and door then close automatically. The rope can be automatically ditched in the event of an emergency.

7.3.3 Cockpit Display.   The cockpit provides two docking stations for portable TCS laptops. Each laptop features two touch-screen multi-function displays. The Air Vehicle Operator's TCS features a mission map with flight path data, aircraft status (speed, altitude, heading, etc.), and mission/maneuver options (extract, land, recon, return to sub). The Mission Payload Operator's TCS features command and full screen live feed from the EO/IR/LRDF payload on either the ARV or UEV (Fig. 7.6). Both TCS laptops are identical and can be quickly configured for either profile. The TCS offers various levels of interaction from full pilot control of the aircraft (including cyclic stick, collective, and pedals) to completely autonomous flight.

7.3.4 UEV/ARV Conversion.   The interior of the airframe is designed such that the ARV can be converted to the UEV configuration with minimal time and effort. The crew seats, TCS laptops, and rope ascender can all be removed to provide space and provisions for extra fuel. A modular fuel tank can be installed in the cabin and attached using the same hard points as the seats. A fitting in the floor connects the modular fuel tank into the existing fuel system located directly below it. This whole process can be accomplished on the submarine to the meet desired mission requirements on the fly.

FACE GEAR
STAGE (2.52:1)

PINION TEETH: 21
GEAR TEETH: 53
INPUT: 5500 RPM
OUTPUT: 2179 RPM
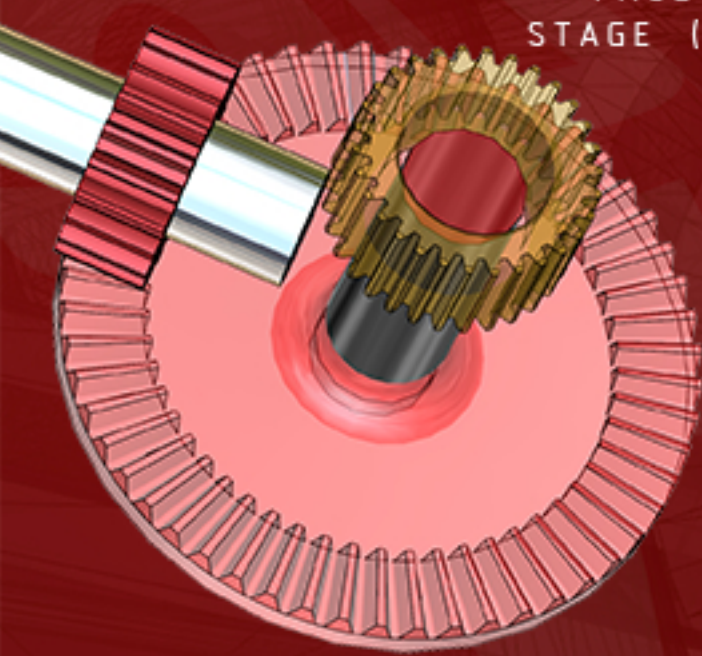
PLANETARY
STAGE (3.65:1)

RING TEETH: 77
SUN TEETH: 29
PLANET TEETH: 24
INPUT: 2179 RPM
OUTPUT: 600 RPM
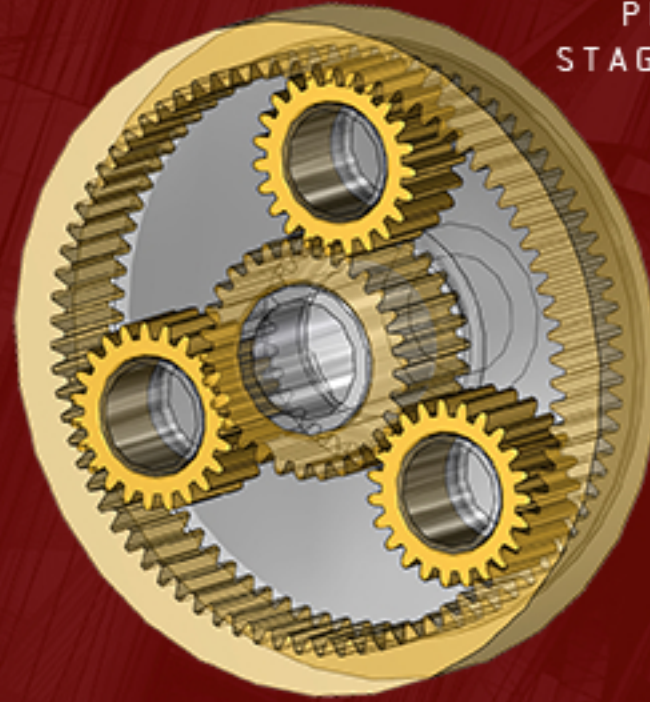
SHAFT RPM:
600

RTM COMPOSITE
GEARBOX CASING

TAIL ROTOR SHAFT

TURBINE ENGINE
18,000 RPM
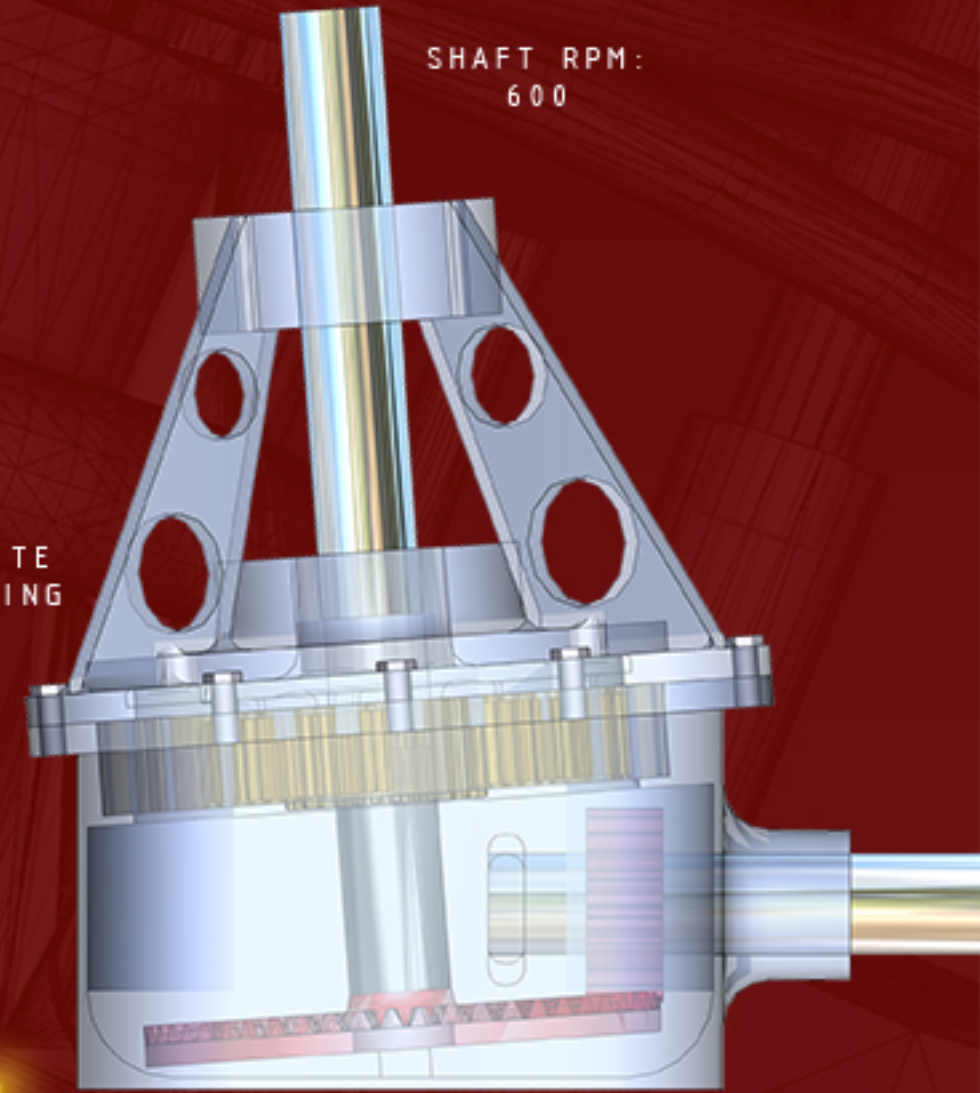
SPRAG
CLUTCH

COMPACT CUSTOM TRANSMISSION

OEM NOSE
GEARBOX
(3:3:1)

ABF MOTOR

ACC.
GEARBOX

MAIN
GEARBOX

GENERATOR

XMSN/AIRFRAME
INTEGRATION

UNIVERSITY OF
MARYLAND
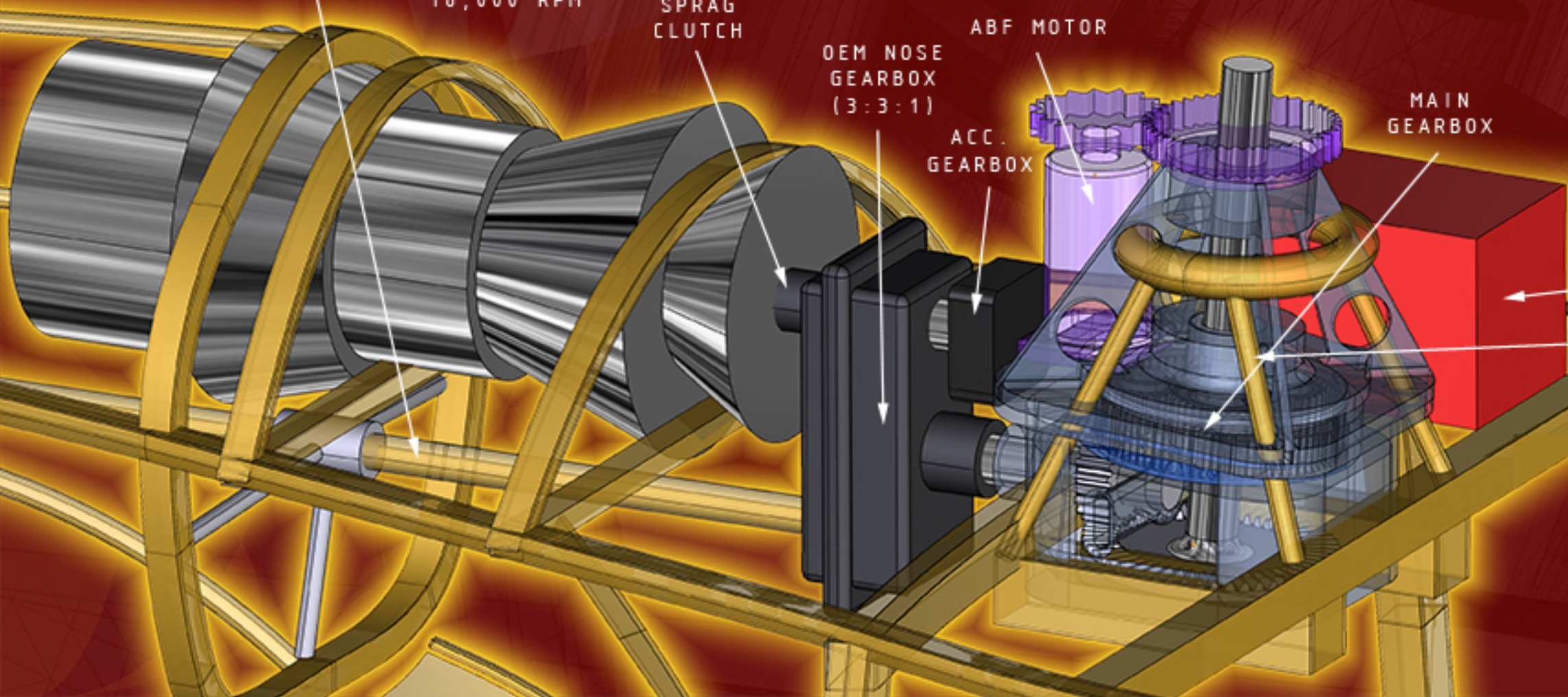
8 Mechanical Subsystems

8.1 Engine Sizing

To reduce mechanical complexity and support the compact design of the TRITON , a single, common engine is used for both ARV and UEV. Scalable turbine engine sizing formulae are recommended in the RFP for the technology levels expected in the year 2020. Parameters for the engine are provided in Table 8.1.

8.2 Transmission

The TRITON custom transmission is a compact drive solution with a 5000 hour mean time between failures (MTBF). The common and off-the shelf components decrease both acquisition and maintenance cost, while innovative material solutions provide protection from harsh environmental operating conditions.

8.2.1 Design Criteria. The factors driving the design of the transmission are similar to the key goals of the overall design. Protection from the harsh marine environment is deemed critical, while compactness helps to minimize the TRITON external dimensions. Additionally, as several TRITON models will be based on a single submarine, it is also desirable from a maintenance perspective to minimize complexity and the number of parts.

A common drivetrain design—made possible by the similarities in mission profile and vehicle size—is used for the ARV and UEV to reduce both cost and overall complexity. Table 8.2 summarizes the basic parameters of the transmission as specified by preliminary sizing.

8.2.2 Transmission Configuration. The drive system for the TRITON is a two-tiered design, featuring an OEM nose gearbox for the initial reduction stage, and a small, two-stage main gearbox to drive the rotor shaft (see foldout 7.3.4). The nose gearbox serves three purposes:

- to reduce the pitchline velocity entering the main gearbox
- cost reduction associated with an off-the-shelf, common part
- provide a takeoff point for the tail rotor without increasing the size of the main gearbox

The nose gearbox provides a nominal reduction ratio of 3.3: 1 to accommodate the speed requirement for the fan-in-fin (5500 RPM), thus eliminating the need for an additional reduction stage in the tail boom. The tail rotor shaft connects the fan-in-fin via a flexible coupling underneath the engine.

The output of the nose gearbox is connected via flexible coupling to the first stage of the main gearbox. The initial reduction in the main gearbox is provided by a face gear stage (2.52: 1), selected for its compact nature. Though unused in existing helicopters for lack of available stress testing data, recent face gear studies

Table 8.1: Engine Sizing Parameters

MRP	499 hp (372 kW)
MCP	380 hp (283 kW)
Diameter	21.1 in (537 mm)
Length	34.5 in (876 mm)
Weight	115 lb (52.1 kg)

Table 8.2: Drive System Design Parameters

Rated Power	499 HP (372 kW)
Engine Output Shaft Speed	18000 RPM
Main Rotor Shaft Speed	600 RPM
Tail Rotor Shaft Speed	5500 RPM

Table 8.3: Gear Sizing

	Main Stage 1		Main Stage 1		
	Pinion	Face	Sun	Planet	Ring
# of teeth	21	53	29	24	77
ratio	2.52: 1		3.65: 1		
RPM	5500	2179	2179	N/A	600
pitch	6	6	8	8	8
pitch diameter (in)	3.500	8.833	3.625	3.000	9.625
face width (in)	1.50	1.35	2.00	1.60	1.85

have demonstrated the feasibility of the face gear as a versatile and weight-saving alternative to spiral bevel stages[56]. The face gear output is coupled to the input to the final, planetary stage (3.51: 1). This reduces the speed to the designed rotor speed of 600 RPM.

The rotor mast bending moment is supported by bearings near the top of the gearbox and also braced by bearings near the fuselage provided by the standpipe.

8.2.3 Gear Sizing.   The gears are sized to provide 5000 hours life at the bending and Hertz stresses encountered at MCP. Dudley[57] provides a sizing method based on AGMA formulae. To reduce manufacturing cost, standard diametral pitches are used for cutting gear teeth. Complete sizing information is provided in Table 8.3.

Carburized and ground AISI 9310 steel gears are used in both stages. After grinding, a super-finish process is employed to provide aerospace-quality gears. This technique has been used by NASA to increase the surface quality of gears by a factor of 6[56]. The face gear is shimmed to avoid edge loading. Gear aspect ratio, as suggested by Dudley[57], is selected to avoid undercutting.

8.2.4 Weight Estimation.

Schmidt[58] provides a useful method for estimating gearbox weight based on the input to the drive system and the gearing configuration. The total weight for each gearing stage is approximated as: $W = 150 \left(\frac{QPUAB}{S_a N} \right)^{0.8}$

The values of U, A, and B are empirically-determined constants. The remaining factors—P, N, Sa, and Q—are the transmitted power, pinion RPM, average Hertz index, and non-dimensional weight factor, respec-

Table 8.4: Subassembly Weights

Subassembly	lb	(kg)
Nose gearbox	45.7	(20.8)
Face gear stage	64.6	(29.4)
Planetary stage	71.5	(32.5)
Dry weight	**181.8**	**(82.6)**
Lubrication	34.9	(15.9)
Composite Savings	-24.4	(-11.1)
Service weight	**192.2**	**(87.4)**

tively. Using this method, the total gearbox weight is estimated to be 192.2 lb (Table 8.4).

8.2.5 Composite Casing. Traditional gearbox casing materials, such as magnesium and aluminum, are highly susceptible to the effects of corrosion in a marine environment. Composite materials represent an appealing alternative for their corrosion resistance, weight savings, and increased ballistic tolerance. Recent advances have indicated the feasibility of composite casings[59] for rotorcraft applications.

The TRITON incorporates a composite gearbox casing to take advantage of these proven features. To avoid the formation of voids during the construction of the composite shell, a low pressure resin injection technique called Resin Transfer Molding (RTM) is used. This allows the gearbox to avoid the potentially disastrous consequences of delamination caused by the voids, which can happen in a carbon fiber-prepreg type of layup.

The non-homogeneous nature of composites traditionally poses a problem when attempting to thread the material for inclusion of a fastening apparatus. Mechanical inserts can be used, yet over time can provide a leak path for fluid contained within the gearbox. Additionally, failures have been shown to propagate faster through metallic inserts than through a purely composite thread[59]. Recent work indicates that purely composite threads can achieve up to 70% of the strengh of those in a homogenous aluminum body when the fiber direction in an RTM-type process is optimized[59]. The TRITON design team is confident that the rapidly advancing field of composite structures will ensure the success of a fully composite gearbox by year 2020.

Perhaps most importantly, the selection of composites over aluminum allows a casing weight savings of 45%. Based on the estimate provided by Schmidt, this represents a savings of 24.4 lb, greater than 10% reduction in total drivetrain weight.

8.2.6 Gearbox Protection. The integrity of the gearbox is essential to mission success; significant damage to the gearbox can ground a helicopter and cost crew their lives. As such, the transmission is fully guarded against a number of failure modes with a comprehensive lubrication system and advanced health and usage monitoring techniques, in addition to the added protection against small-arms fire provided by the composite

casing. Furthermore, the gearbox is fully sealed to prevent water ingress due to environmental conditions.

Lubrication System

Lubrication of the main and nose gearboxes is provided by a pressurized oil pump powered by the accessory gearbox. The lubrication system supplies oil to the bearings and meshing surfaces to prevent the spalling or pitting that can occur with metal-on-metal contact. Because the engine inlet runs directly over the gearbox, a heat exchanger is not needed due to the convection provided by mass flow over the gearbox and oil pump. The oil pump also features a magnetic particulate trap (MPT) and filter to remove any debris present in the system. Blockage of the MPT forces a bypass valve open to ensure oil continues to run through the system.

Health and Usage Monitoring System (HUMS)

The gearbox is fully outfitted with sensing mechanisms to provide real-time diagnostic and prognostic measurements of gearbox health. Embedded sensors provide a variety of information to HUMS, including: oil temperature, oil pressure, MPT status, exterior gearbox local strain measurements, standpipe local strain measurements, and gearbox vibration data provided by tri-axial accelerometers. HUMS provides to the TRITON crew and TCS operators the current status of each gearbox component and its next required date of maintenance using the cutting-edge CAMEO package created by NAVAIR, currently used by the U.S. Marine Corps for maintenance cataloging of the V-22 [60]. Gearbox parts are easily identified and replaced though RFID technology that allows maintenance personnel to identify components without using hard-to-read and easily-obscured barcodes.

9 Flight Mechanics

9.1 Flight Control System

Flight control on TRITON is achieved using quad trailing edge flaps on each rotor blade. Actuation of these flaps produces the collective and cyclic pitch required for vehicle control. The fan-in-fin uses conventional controls. Since TRITON is an autonomous vehicle, the operator interacts with the flight control system (FCS) via the Tactical Control System (TCS) by selecting from a set of pre-programmed flight plans or hold functions. The FCS has been designed for high-speed nap-of-earth flight. Signals to the actuators and servos of the main rotor and fan-in-fin blades are generated by the FCS. A Neural Network Hardware Processor is provided to perform onboard fault diagnostics for the rotor flaps. Any predicted system failures are reported to the vehicle operator via the TCS. If no response is given by the operator, the guidance system aborts the mission and lands the vehicle at the nearest pre-programmed recovery site. If a system failure is detected, an emergency landing is immediately performed.

9.1.1 Design of FCS.

Details of Flight Control System

At the core of the FCS are triplex Flight Control Computers (FCCs), which provide control law processing and perform redundancy management for the FCS. Dual CPUs are provided for each FCC. Actuator Control Computers (ACC) drive the actuators to deflect trailing edge flaps and drive fan-in-fin servos in accordance to the guidance commands from the FCC. The high-level description of the FCS architecture is given in Figure 9.1.

Inner loop vehicle control is governed by four flight control laws: Rate Damping (RD), Rate Command Attitude Hold (RCAH), Attitude Command Attitude Hold (ACAH), and Translational Rate Command (TRC). RD is a stability augmentation system (SAS) that minimizes any overshoots or undershoots of the vehicles response to control inputs. RCAH maintains a one to one correspondence between commanded angular rate and actual vehicle response. This ensures stable vehicle response in the presence of perturbations from sources such as wind. Similarly, ACAH maintains a stabilized vehicle attitude. TRC supplements the guidance functions by providing automated precision hovering over a point.

Neural Network Based Fault Protection

A Neural Network Hardware Processor (NNHP) is used to monitor the performance of trailing edge flaps, and provides subsystem modeling functions in support of fault diagnostics, and aircraft parameter modeling that is used in controller algorithm optimization. Through modeling of normal flap operation and failure modes, the neural network processor is capable of predicting potential failure of the flap system. Training of the neural network under both normal operation and failure modes is required. This may be accomplished either by using data generated during simulation or test operation of the system [61]. Information regarding possible failure is relayed to the operator via the TCS system for corrective action. If no input from the operator is received, the mission is aborted, and a flight plan to the nearest pre-programmed recovery site automatically generated.

9.2 Automatic Nap-of-Earth Guidance System

The guidance system is adopted from a system developed at NASA Ames Research Center [53]. The architecture of this system may be decomposed into three-tiers: far-field mission planning, mid-field planning and automated near-field guidance (Figure 9.2)

The far-field planning consists of either pre-flight or in-flight input of digital maps describing the operating region, along with mission requirements and threat information. Primary and alternate flight paths are defined by vehicle position and velocity at a set of waypoints. Terrain and flight path optimization is performed in the mid-field planning tier using the digital high-resolution map.

RD........ Rate Damping
RCAH... Rate Command Attitude Hold
ACAH... Attitude Command Attitude Hold
TRC..... Translational Rate Command
FDM..... Fault Diagnostic Module

FCS....... Flight Control System
NNHP... Neural Network Hardware Processor
ACC...... Actuator Control Computer
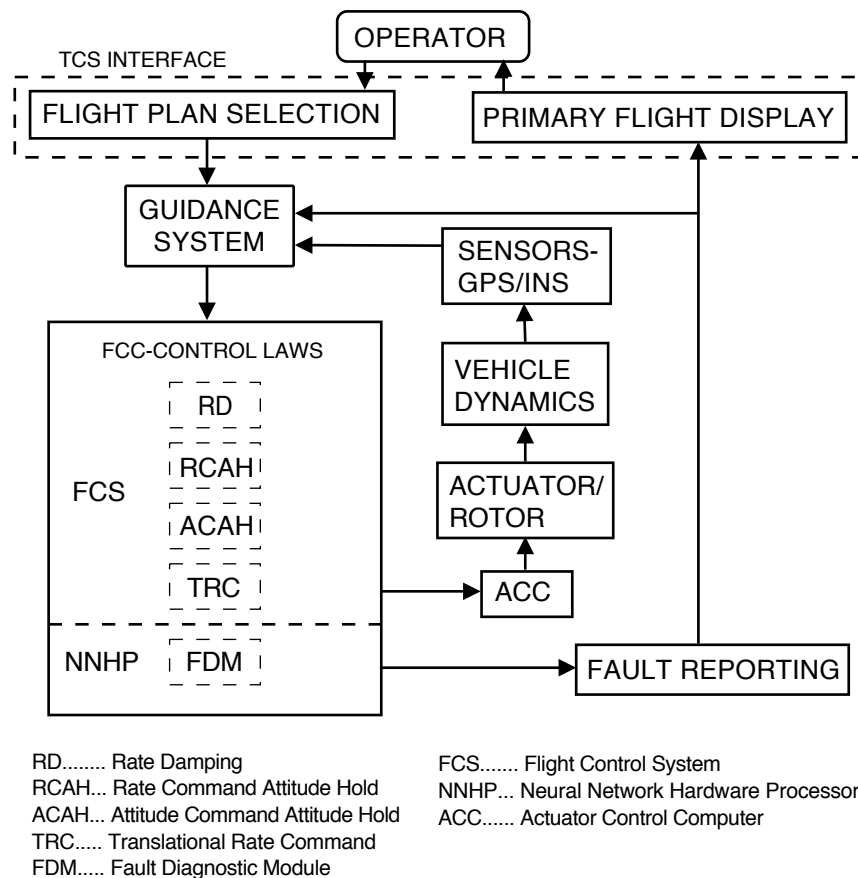
Figure 9.1: Architecture of automatic flight control system

The most critical loop is the automated near-field guidance loop (Figure 9.3). Here, the necessary guidance commands are generated to achieve the desired flight path while avoiding unexpected obstacles or threats. To ensure precision guidance while operating at high speed and low altitude, the system provides compensatory feedforward error reduction by comparison between sensed flight path provided by inertial navigation system, and desired flight path (see Chapter 7 for system information). Upon sensing unexpected changes in the terrain or detection of a new threat, the logic system selects an appropriate response from a predefined suite of avoidance maneuvers. This suite of maneuvers includes: 1) bob-up and down, 2) hover turn, 3) lateral side-step, and 4) longitudinal acceleration/deceleration. Once the obstacle or threat conflict has been resolved, the guidance system seeks an optimal path to return to the pre-planned flight path.

9.3   Stability Analysis

For purpose of stability analysis, a rigid fuselage and rigid bladed rotor model with hinge offset and flap spring was developed. The aerodynamic model for the fuselage consisted of estimated linear aerodynamic coefficients,
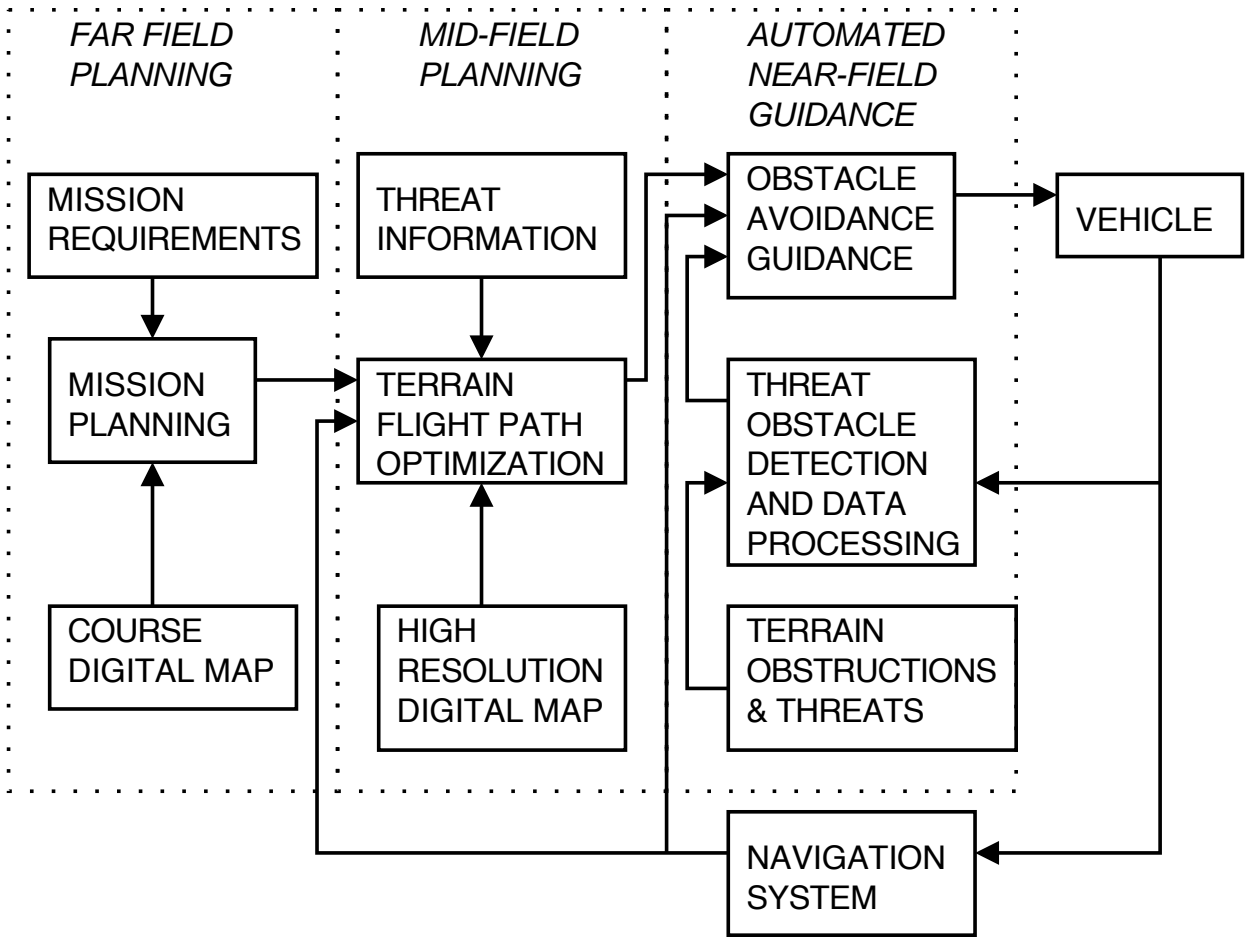
Figure 9.2: Automatic Nap-of-Earth Guidance Architecture

and linear airfoil properties were used for the rotor blades. Estimation of vehicle stability and control derivatives were then numerically estimated using finite differences of the perturb force and moment system corresponding to perturbations of each state from trim. The trim state was determined by performing a full vehicle trim. The resulting stability and control derivatives are given in Tables 9.1 and 9.2, respectively. The force stability derivatives are normalized by vehicle mass, and moment derivatives by corresponding fuselage moment of inertias. Both M_q and L_p are critical parameters because of their close relationship to the short-term and moderate amplitude response. Large negative values of these derivatives are desirable for vehicle stability.

9.4   Tail Sizing

The size of the horizontal tail was driven by both trim and stability considerations. Increasing the planform area of the horizontal tail ensures speed stability and minimizes the tendency of the vehicle to pitch nose down in forward flight. However, as the size of the horizontal stabilizer is increased, the phugoid mode tends to become
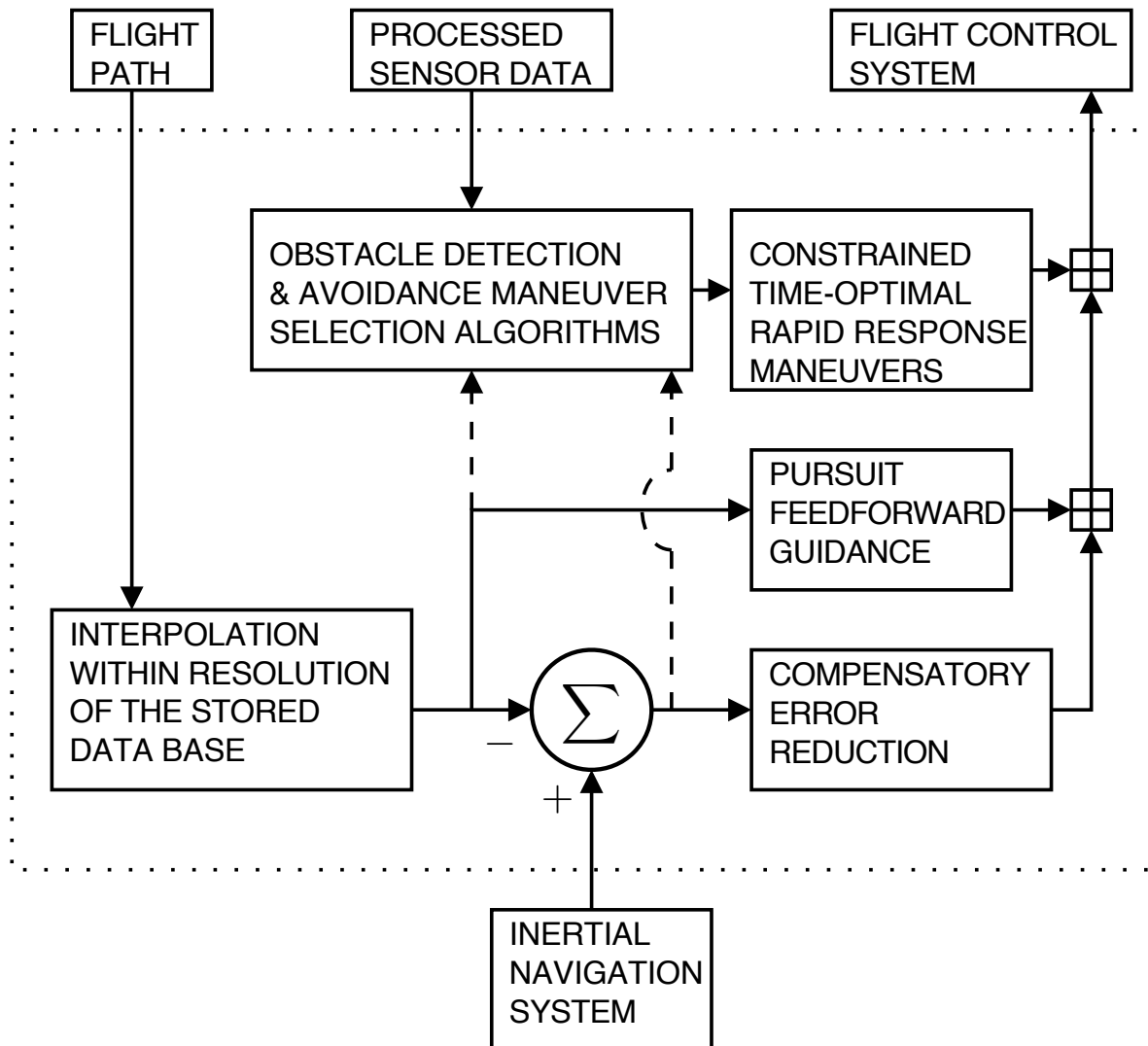
Figure 9.3: Obstacle Avoidance and Guidance System

Table 9.1: Normalized Stability Derivatives in Hover and Forward Flight

Derivative	Hover	Cruise	Units	Derivative	Hover	Cruise	Units
X_u	-0.017	-0.094	1/sec	L_u	0.028	-0.022	rad/sec-ft
X_v	-0.006	0.064	1/sec	L_v	-0.038	-0.073	rad/sec-ft
X_w	-0.062	-0.027	1/sec	L_w	0.002	-0.169	rad/sec-ft
X_p	-0.213	-0.053	ft/rad-sec	L_p	-2.049	-1.964	1/sec
X_q	0.462	0.150	ft/rad-sec	L_q	0.004	-0.753	1/sec
X_r	-0.105	0.578	ft/rad-sec	L_r	-0.126	-0.189	1/sec
Y_u	-0.002	-0.010	1/sec	M_u	0.011	0.029	rad/sec-ft
Y_v	-0.014	-0.241	1/sec	M_v	-0.009	-0.013	rad/sec-ft
Y_w	-0.014	-0.119	1/sec	M_w	-0.014	-0.041	rad/sec-ft
Y_p	-0.474	-0.388	ft/rad-sec	M_p	0.019	0.111	1/sec
Y_q	-0.225	-1.039	ft/rad-sec	M_q	-0.623	-1.881	1/sec
Y_r	-0.024	2.352	ft/rad-sec	M_r	0.012	0.124	1/sec
Z_u	0.047	0.061	1/sec	N_u	-0.003	-0.042	rad/sec-ft
Z_v	-0.005	-0.086	1/sec	N_v	-0.002	0.233	rad/sec-ft
Z_w	-1.247	-1.606	1/sec	N_w	-0.117	-0.175	rad/sec-ft
Z_p	-0.199	-3.901	ft/rad-sec	N_p	-0.582	-0.346	1/sec
Z_q	-0.048	-1.285	ft/rad-sec	N_q	-0.462	-0.862	1/sec
Z_r	1.802	1.728	ft/rad-sec	N_r	-0.084	-3.264	1/sec

Table 9.2: Normalized Control Derivatives in Hover and Forward Flight

Derivative	Hover	Cruise	Units	Derivative	Hover	Cruise	Units
X_{θ_0}	9.495	12.458	ft/sec^2-rad	L_{θ_0}	-0.444	56.078	1/sec^2
$X_{\theta_{1s}}$	30.455	23.529	ft/sec^2-rad	$L_{\theta_{1s}}$	66.736	75.817	1/sec^2
$X_{\theta_{1c}}$	-17.362	-9.287	ft/sec^2-rad	$L_{\theta_{1c}}$	48.353	61.215	1/sec^2
Y_{θ_0}	0.075	2.615	ft/sec^2-rad	M_{θ_0}	0.114	27.755	1/sec^2
$Y_{\theta_{1s}}$	-17.376	-8.402	ft/sec^2-rad	$M_{\theta_{1s}}$	14.101	25.501	1/sec^2
$Y_{\theta_{1c}}$	-30.492	-60.147	ft/sec^2-rad	$M_{\theta_{1c}}$	-19.453	-23.649	1/sec^2
Z_{θ_0}	553.559	809.137	ft/sec^2-rad	N_{θ_0}	-25.724	-38.006	1/sec^2
$Z_{\theta_{1s}}$	-0.936	389.291	ft/sec^2-rad	$N_{\theta_{1s}}$	0.162	-11.924	1/sec^2
$Z_{\theta_{1c}}$	-0.545	-5.564	ft/sec^2-rad	$N_{\theta_{1c}}$	-0.021	-1.648	1/sec^2

unstable. Thus, a planform area of 10 ft^2 was chosen as a compromise.

10 Weight Analysis

This section presents detailed component weight analysis of the vehicle. An estimate of center of gravity (CG) and CG travel in the helicopter over the mission cycle will be presented. Besides discussing the methods of analysis, a detailed weight component breakdown description will be provided.

Table 10.1: Weight Estimate

Weight Category	Weight, lb	% of Empty Weight
Main rotor blade	61.7	5.56
Main rotor hub	42.0	3.78
Tail rotor blade and hub	18.3	1.65
Main and tail rotor gearbox	192.0	17.29
Tail rotor shaft	3.3	0.29
Engine	115.0	10.36
Fuel System	23.7	2.13
Fuselage	181.0	16.31
Horizontal Stabilizer	2.2	0.19
Landing Gear	41.6	3.75
Control System	105.8	9.53
Avionics	300.0	27.03
Mission Oil and Unusable Fuel	24.1	2.17
Empty Weight	1109.9	100.0
Fuel Weight	320.9	–
(UEV)	(660.2)	–
Pilot + Passenger + equipment	800	–
(UEV)	(600)	–
Gross Weight	2230.8	–
(UEV)	2370.8	–

10.1   Weight Estimate

The preliminary weight estimate was performed by making use of a technique developed by Tishchenko [6]. This method uses weight coefficients established for each component, using regression analysis techniques to develop relationships between the component weights and the design parameters that most influence these weights. The weight coefficients for the current analysis were obtained by modifying Tishchenko's values against Robinson R-44 component weights, because the overall GTOW of the current design is comparable to that of R-44. Since, R-44 is an old rotor craft design with structural components composed of metallic materials, it can be claimed that the current analysis gives a conservative estimate. There can be further reduction in weights by use of advanced materials and technologies [62].

10.2   Component Weight Breakdown

Table 10.1 gives a brief component breakdown of the rotorcraft and percentage contribution of each component to the empty weight. Measures were taken to keep the component weights as low as possible by using advanced low weight materials and composites.

10.2.1 Fuselage and Cowling.

The fuselage and cowling of the vehicle is constructed from Kevlar/graphite/epoxy panels and aluminium-lithium metal alloy with a ceramic based (CRYSTALOY) front face plate. Titanium has been used at critically high-demanding stations, such as engine deck. There has been a lot of effort towards keeping the fuselage structures as as streamlines as possible and at the same time maintaining the structural integrity. The weight of this component is 181 lbs.

10.2.2 Fan-in-fin and Empennage.

The structure aft of primary bulkhead is mainly composed of monocoque Kevlar/graphite/epoxy composite panel. Again, the frontal face is composed of CRYSTALOY. The bulkheads are aluminium-lithium rings. Empennage (vertical as well as horizontal fins) are made of composite structures again. The fenestron is also constructed using composite materials, thus ensuring a low weight of 24 lbs.

10.2.3 Engines.

The engine to be used for the vehicle is provided by RFP, which represents an advanced engine design that is likely to be developed by 2020. The engine weight thus computed comes out as 115 lbs.

10.2.4 Transmission.

The gear box is composed of carborized and ground AISI 9310 steel but has a composite casing. This helps in reducing the weight of gear box while sizing. (refer to Section 8.2.5) The weight of the gearboxes for both the main rotor as well as the tail rotor is 192 lbs.

10.2.5 Main Rotor System.

Main rotor materials are Nomex honeycomb and graphite/epoxy composite. The use of such light material provides enough lightweight base for further addition of weights due to actuators, motors and electrical control systems necessary for actuation of trailing edge flaps required for a swashplateless mechanism. Total weight contribution of main rotor is 61.7 lbs. The hub mainly consist of flexbeam, torque tubes, and index splice. Its weight contribution is 42 lbs.

10.2.6 Avionics.

The current design makes use of the latest state of the art in avionics. The avionics are placed inside the vehicle such that their effective CG lies close to the overall helicopter CG. While the overall weight of avionics system is 300 lbs (as required by RFP), around 75 lbs of this is placed near the nose.

10.2.7 Landing Gear.

The landing gear has a nose wheel and two tail wheels, equipped with snow-skids. This explains its higher weight contribution as compared to the conventional ones. But, effort has been taken to keep the weights to minimum by using light weight material. The estimated weight is around 42 lbs.

10.2.8 Fuel and Fuel System.

Fuel requirement is critical from UEV design point of view. The maximum

fuel requirement is 660 lbs. The unusable fuel and the mission oil adds to 24.1 lbs ($\sim 3.7\%$ of total fuel for UEV mission). The weight of the fuel system is 23.7 lbs. The single module design requires two fuel tanks to be used. Since, fuel weight amounts to almost 30% of total gross weight for UEV, the fuel tanks are placed close to the helicopter CG so as to minimize CG travel during the mission.

10.2.9 Control System. The control system consists of automatic control, such as computers, signal cables, and power cables. The shielded cables is a major weight contributor. It also includes the starter batteries (26.4 lbs) and the generators (22.5 lbs) for driving the active flap actuators, de-icing system, the landing gear actuation and all other small or big power requirements of the helicopter. The overall weight contribution is 106 lbs ($\sim 9.53\%$).

10.2.10 Crew. The RFP requires two crews whose weight amount to a total 540 lbs including their equipments.

10.2.11 Empty Weight Fraction. *Empty weight fraction* gives an estimate of useful load in a rotorcraft. It can also be defined in terms of *weight efficiency*, K_{we}, which is defined as:

$$
\begin{aligned}
K_{we} &= \frac{\text{Useful Load}}{\text{Total Weight}} \\
\text{Empty Weight Fraction} &= 1 - K_{we}
\end{aligned}
$$

TRITON has an empty weight fraction of 49.8% for the ARV and 44.5% for the UEV.

10.2.12 Weight and Balance. The longitudinal CG travel envelope of TRITON is shown in Figure 10.1. The extremes of the longitudinal CG are 0.2 to 0.8 ft ahead of rotor shaft (a CG travel 5% of the main rotor diameter). The CG travel due to fuel consumption alone, for a fully loaded ARV, lies within this longitudinal CG envelope.

11   Performance Analysis

It was decided (Chapter 3) that there would be one common modular design for both the vehicles. The major performance requirement difference lies in the added endurance (3 hrs) needed for the UEV to loiter. Other considerations were discussed more in detail in Section 3.2.3. The current chapter discusses the performance capability of this one common design, keeping the performance requirements of both ARV and UEV (Table 11.1 summarizes the vehicle performance). The RFP's specific flight requirements are:
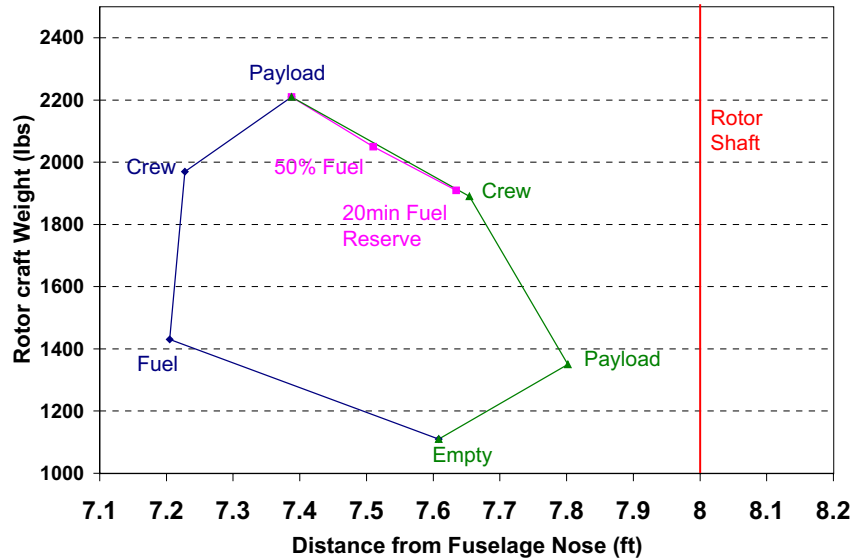
Figure 10.1: Longitudinal CG Travel of TRITON -ARV

Table 11.1: Performance Summary

| Parameters	Estimate
GTOW (UEV)	2230 lbs
GTOW (ARV)	2370 lbs
Optimum Cruise Speed	140 knots
Maximum Cruise Speed	170 knots
HOGE Ceiling (ISA/SL)	6040 ft
Maximum Range (ISA/102°F)	405 nm
Maximum Range (102°F, Extra Fuel Tank)	811 nm
Maximum Endurance (ISA/102°F, Extra Fuel Tank)	6.4 hrs
Best Range Speed (ISA/102°F)	140 knots
Best Endurance Speed (ISA/102°F)	60 knots

- **ARV:** VTOL at the submarine; cruise at AGL ($\leq$ 50 ft, with V_{br}) for 140 nm, mid-mission HOGE, and cruise back.

- **UEV:** VTOL at the submarine; cruise at AGL ($\leq$ 50 ft, with V_{br}) for 140 nm, mid-mission LOITER (3 hrs), and cruise back.

Table 11.2: Airframe Equivalent Flat Plate Area

Components	f_i(ft^2)	% Contribution
Fuselage	1.40	36.36
MR hub & shaft	1.26	32.72
TR hub & shaft	0.15	3.82
Horizontal Stab	0.004	0.09
Vertical Fin	0.007	0.19
Fuselage-body int.	0.73	18.9
Miscellaneous	0.10	2.60
Total	3.85	100%
Total + 20%	4.62	–

11.1   Drag Estimate

The sizing calculation requires an estimate of total drag of the helicopter. For the fuselage drag estimate, the methodology from Prouty [63] was adopted. The method provides a rough estimate of equivalent flat plate area of overall fuselage. The equivalent flat plate area of any component is defined by $f_i = \frac{D_i}{\rho V^2/2} = C_{D_i} S_i$, so that the total drag is $f = \sum_i f_i$. Here, C_{D_i} is drag coefficient of the i'th component and S_i is its equivalent wetted area.
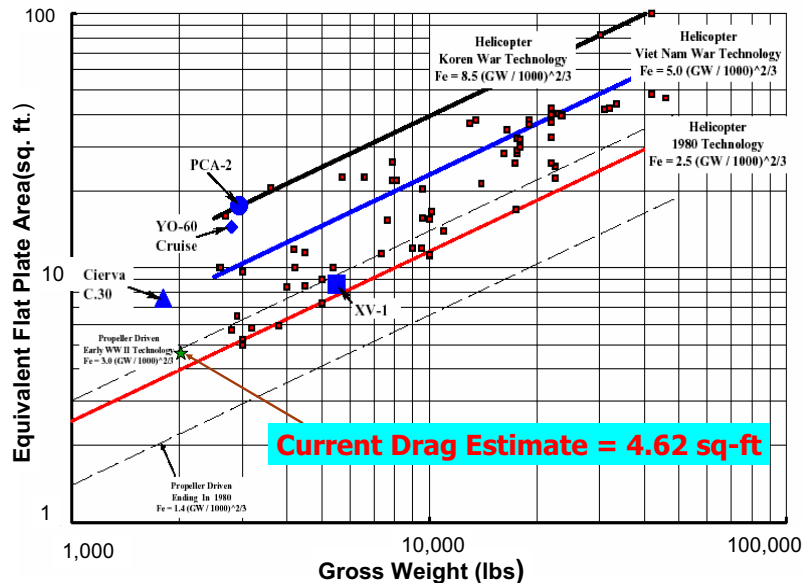
Figure 11.1: Trend in Helicopter Flat Plate Area[64]

The estimate requires a knowledge of helicopter geometry and various table lookups. The fuselage can be broken down into various components: basic fuselage, main rotor hub and shaft, tail rotor hub and shaft, main

landing gear, horizontal stabilizer, vertical fin/stabilizer. The estimated values of drag for the current helicopter fuselage and its components is given in Table 11.2. The estimate also includes drag due to fuselage-body interaction as well as that due to antennas, door handles, lights, and cooling linkages etc. The component drag estimates have been increased by 20% as suggested by Prouty [63] to obtain a conservative estimate. Figure 11.1 compares the current drag value with the general trend among contemporary helicopters. The estimated drag follows the trend [65], i.e, $f = \alpha(GTOW/1000)^{2/3}$, with a value of $\alpha \sim 2.5$ for helicopters of 1980 vintage. For our current configuration the value is $\alpha = 2.8$. Thus, the current value is a conservative estimate, and the total drag of the vehicles would not be expected to exceed this value. The drag can be expected to be lower than the estimated value since the current vehicle design has an aerodynamically clean hub, its landing gears are retractable, and is a swashplateless configuration (no exposed upper pitch links). The estimate of rotor drag is obtained from a code developed by Tishchenko [6].

11.1.1 Drag Reduction Considerations.   Since the vehicle design is mostly driven by forward flight considerations, an effort was made to achieve low drag to give a high cruise speed of 140 knots. The following points were considered to achieve the low equivalent flat plate area of 4.6:

- *Fuselage:* Effort has been taken to make the fuselage well-streamlined. It has no sharp curvatures from nose to hub. The large up sweep behind the fuselage can cause flow separation and is usually a major contributor in parasitic drag. To avoid flow separation, kinetic energy has to be imparted into the flow separation zone. This has been made possible in the current design by having sharp corners at the bottom of the fuselage, which would act as artificial vortex generators [66]. These vortex structures maintain the high momentum even in the adverse pressure region thus reducing the separation bubble. This leads to a smaller overall fuselage drag.

- *Landing Gear:* The landing gears are fully retractable, and thus do not contribute to drag in forward flight.

- *Main Rotor Shaft:* Cowling structures were provided to cover the exposed area of the main rotor shaft. The disk rotates along with the shaft. Moreover, the length of the exposed main rotor shaft height also is kept small (1 ft), thus reducing the drag due to the shaft. The streamlined covering of the shaft cowling will to expected to help in energizing the boundary layer aft of the pylon and will so help in reducing the interference drag between hub and the fuselage.

- *Engine Inlet/exhaust:* The engine exhaust is directed away and to the side of fuselage (starboard side) to reduce bluff body parasitic drag. Same considerations were made while deciding on the inlet of the engine. The inlet was made flush with the fuselage body, thereby maintaining the streamlined structure of the fuselage and reduced drag.

11.2   Hover Performance

The RFP had a hover requirement that both ARV/UEV should have a HOGE capability at 6000 ft /95°F. Figures 11.2 shows variation of excess available power with total gross weight of TRITON when hovering OGE at both ISA/SL as well as 6000 ft/95°F conditions. The large excess power is due to the fact that TRITON is designed for a high cruise speed of 140 knots which leads to an higher installed power than the hover power required. Figure 11.3 shows hover performance forTRITON .The figure shows that the lifting capability of the engine is 2400 lbs at 6000 ft/95°F conditions and 3200 lbs at ISA conditions. The maximum GTOW of TRITON -UEV is 2370 lbs.
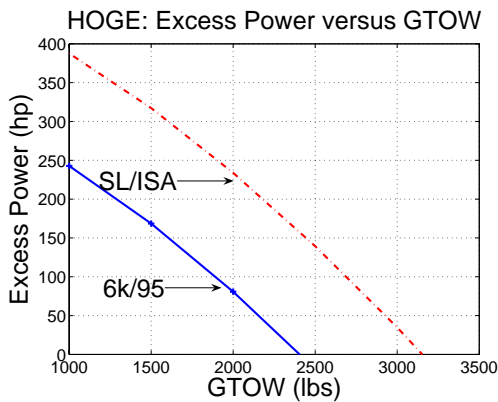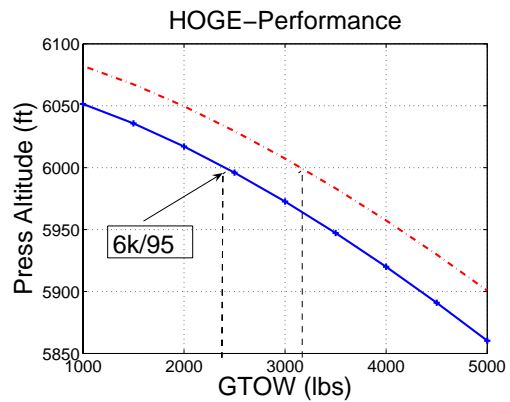
Figure 11.2: Hover Ceiling
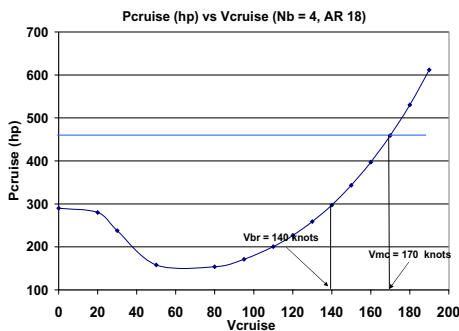
Figure 11.3: Hover Ceiling

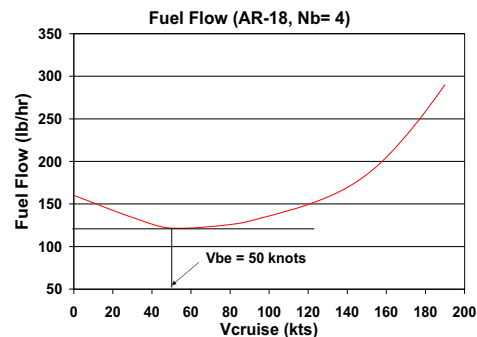**Figure 11.4:** Required Power versus Speed

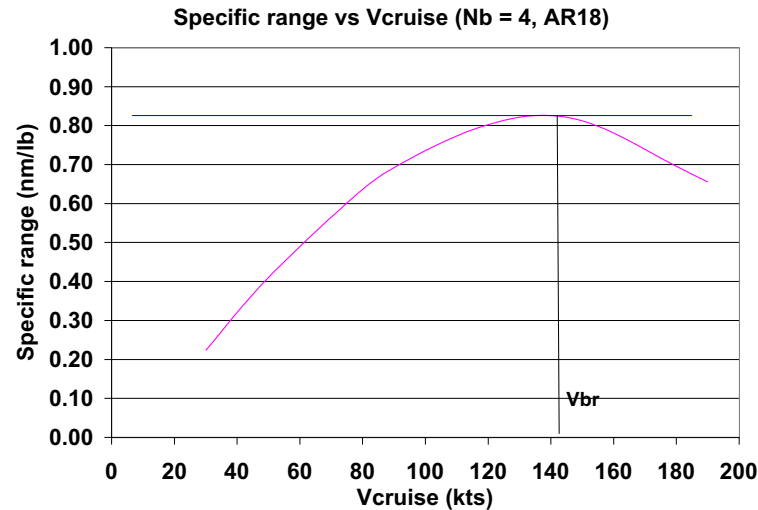**Figure 11.5:** Fuel Flow versus Speed

Figure 11.6: Hover Ceiling

11.3 Forward Flight Performance

Besides a HOGE requirement at 6k/95, the forward flight requirement was to cruise the given range (140 nm) at the *best range* cruise speed for the ARV. For the UEV, there is an added requirement of a 3 hrs loiter time at *best endurance* cruise speed. Since a common modular design is considered for both the helicopters, it had to meet both these requirements together. As discussed the power requirements of UEV is not very different (5% higher) from ARV requirement, though UEV requires larger fuel tank.

Figure 11.4 shows the power required as a function of forward speed. The best range speed is 140 knots and the maximum level speed is 170 knots. To obtain the best range, we used the specific range curve in Figure 11.6. The maximum specific range gives the best range speed as 140 knots.

Figure 11.7 shows the payload-range curve for the vehicle (for the ARV mission profile), where payload implies combined weight of payload and fuel. The maximum range at SL/102°F conditions is 405 nm. This is more than that is required by RFP, and hence the vehicle shows good adaptability to emergency situations. Mission profile for UEV involves a loiter at *best endurance* cruise speed, V_{BE}. This speed is the minimum in fuel flow curve for the vehicle, as shown in Figure 11.5, and the value is, $V_{BE} = 50$ knots. Figure 11.8 shows that the UEV has a large endurance of 6.4 hrs at ISA/102°F. Figure 11.7 also shows payload range characteristics of the UEV (by showing the effect of adding an extra fuel tank). Maximum range shown in the figure for the UEV at

Table 11.3: Mission Profile
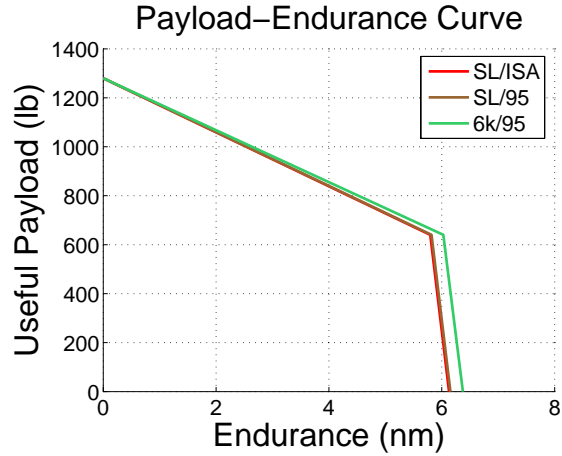
Segment	1	2	3	4 (ARV/UEV)	5	6	7	Total
Type	Idle	HOGE	Cruise	HOGE/Loiter	Cruise	HOGE	Reserve	–
Speed (Knots)	0	0	V_{br-99}	$0/V_{be}$	V_{br-99}	0	V_{be}	–
Time (min)	4	2	–	4/180	–	2	20	–
Range (nm)	-	-	140	–	140	–	–	–
Altitude (ft)	0	0	0	0	0	0	0	–
Temp(°F)	102.9	102.9	102.9/102.9	102.9	102.9	102.9	102.9	–
Engine Rating	IRP	MRP	MCP	MRP/MCP	MCP	MRP	MCP	–
Fuel Req. (lb)	4.1	4.9	128.2	9.8/350	128.2	4.9	39.9	320/660

ISA/102°F is 811 nm.
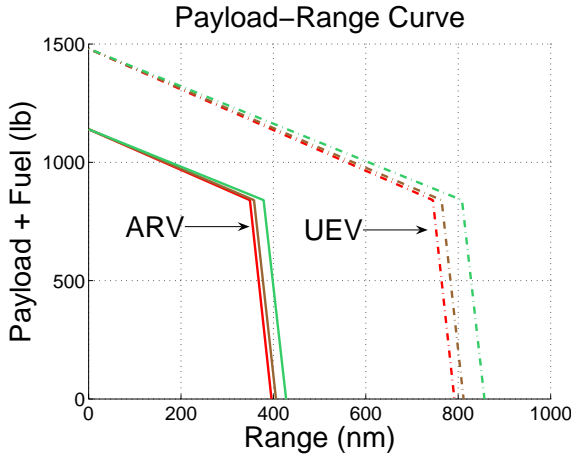
Figure 11.7: Payload-Range (ARV & UEV)

Figure 11.8: Payload-Endurance (UEV)

11.4 Mission Profile and Fuel Requirements

Table 11.3 shows the mission profile and the fuel required for each leg of the mission. The main difference in the two mission profiles is in the extra fuel requirement for loiter (330 lb for the UEV and about 10 lb for the ARV) because of the 180 minutes loiter time needed for UEV. To account for this extra fuel required by UEV mission, an extra fuel tank is added to the modular design, which has a fuel capacity for 680 lbs of fuel (more than the required 623 lbs).

12 Cost Estimate

This chapter gives a quantitative measure of system affordability and provides an estimate of cost of vehicle (acquisition and direct operating). System affordability is a critical index in deciding a new design's potential to succeed or fail. Therefore, for the current design the system affordability is discussed in terms of purchase or

Table 12.1: Acquisition Cost

Cost Category	Cost
Main Rotor System	$70,373
Tail Rotor System	$37,621
Airframe Structure	$126,422
Landing Gear	$10,769
Engine	$42,224
Engine Installation	$64,229
Drive System	$39,553
Flight Control System	$27,379
Airframe Assembly	$72,781
Total (in 2002 Dollars)	$491,358
Total Acquisition (1.5 factor)	$737,038

acquisition cost as well as maintenance and *operational* cost.

12.1   Cost Reduction Considerations

Low Risk Technology: The design incorporates technologically advanced concepts in designing various aspect of helicopter (for example, fan-in-fin, main rotor hub, fuselage design, and landing gear). These are proven concepts and it reduces risk and cost.

Electric Technology: The current design makes use of extensive use electric components to have a more reliable and reduced maintenance intensive design beside ensuring lower overall vehicle weight. This is more effective than using hydraulic or pneumatic components.

Engine size and number of engines: Single engine has been considered for both ARV and UEV design, which is very effective in maintaining overall lower helicopter weight. In addition, it also helps in reducing in acquisition, operational and maintenance related costs.

System Commonality: The major advantage of the current design is the use of one common module for both missions. This is very useful not only in reducing the acquisition and operational cost but also in ensuring reduced mission related maintenance cost.

Room for Future Growth: The estimated weight of the vehicle is a conservative one, which cushions any growth in weight that might result from future developments.
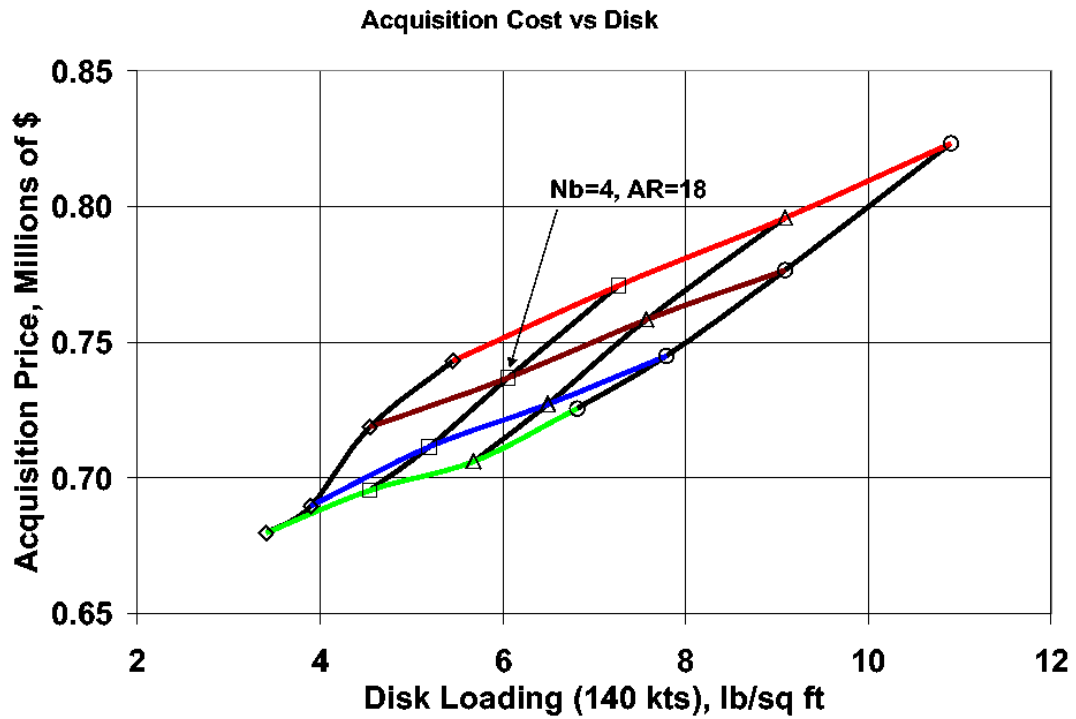
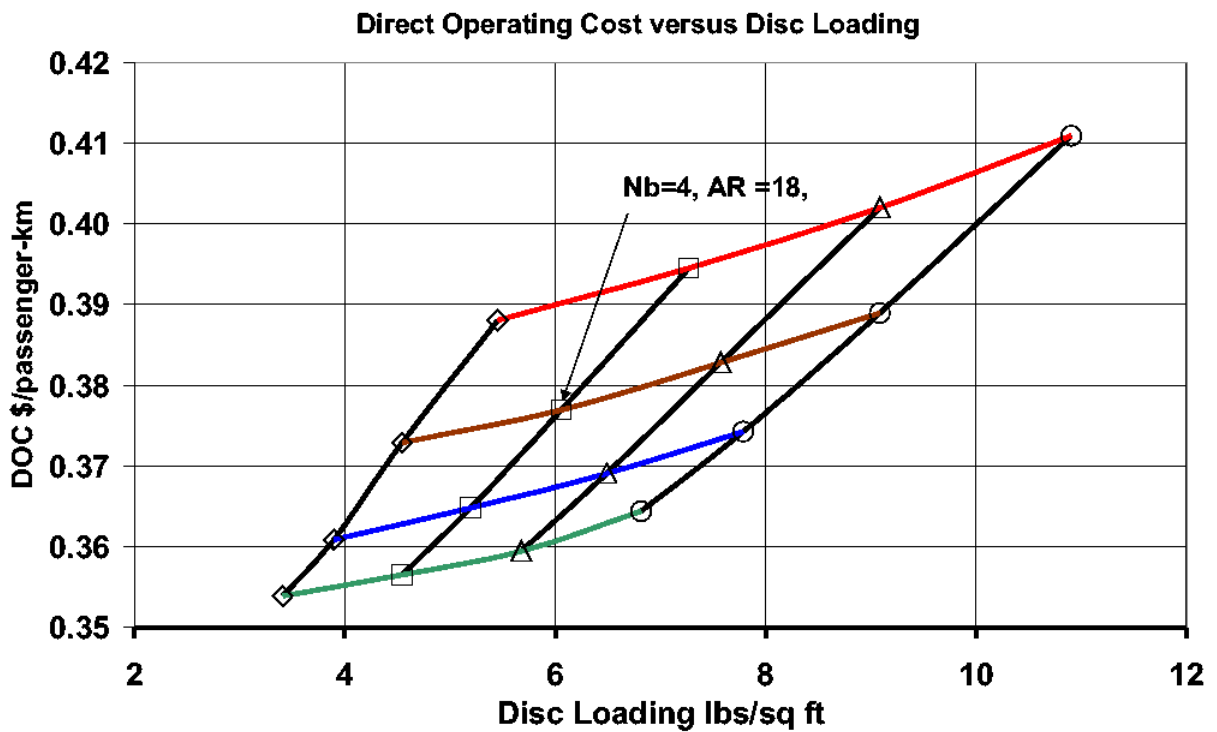**Figure 12.1:** Acquisition Cost vs Disk Loading

Figure 12.2: Direct Operating Cost vs Disk Loading

12.2 Acquisition Cost

The total cost of the helicopter was estimated using the cost estimating relationships given in 2002 AHS design RFP [67] by Bell. This method estimates the costs using the component weight, total production quantity, and production rate as primary cost drivers. Additional variables are used to adjust for differences in manufacturing complexities between various design parameters. To estimate the purchase price of the aircraft, the total cost is increased by 50% to account for tooling, amortization, and profit [67]. The cost thus obtained for the current design is, $0.74 million (Figure 12.1). This cost estimation uses dollar value of 2002. This when adjusted for inflation, using the consumer price index, [68] gives an estimate of $0.847 million in current dollars. Another estimate of acquisition cost using Tishcenko's formula, which takes into account individual cost contributions due to engine weight as well as the empty weight, is 0.817 million. As a comparison, the cost of Bell 206 B111 Jet Ranger-III, which has a comparable GTOW, is $0.835 million.

12.3 Operating Cost

Helicopter cost estimate involves the Direct Operating Cost (*DOC*) per passenger per kilometer. The *DOC* was estimated using Tischenko's formula, which is given by:

$$\text{DOC}_{fh} = \frac{3P}{\text{Total Flight Hours}} + P_{\text{fuel}} \times Q + N_{\text{crew}} \times S_{\text{crew}}$$

where P is the acquisition price, P_{fuel} is the fuel price per gallon, Q is the fuel consumption in gallons per flight hour, N_{crew} is the number of crew members and S_{crew} is the crew salary per flight hour. Figure 12.2 shows *DOC* of the current ARV configuration. For the particular configuration chosen, the DOC is $0.377/passenger/km range. The increase in *DOC* with increasing number of blades for a chosen aspect ratio, was one of the reasons for restricting the blade number to four. It should be mentioned here that *DOC* is an index for civil helicopter from operational point of view and hence is a measure of economic efficiency. Thus, for military vehicles *DOC* may not be a major factor affecting the final design of the vehicle.

13 Conclusion

The TRITON is a compact, high-speed, automonous helicopter designed to fulfill both ARV and UEV mission with a common airframe and modular components. The modular design of TRITON allows a high degree of mission adaptability while reducing manufacturing and maintenance costs.

13.1   Launch and Recovery Strategy

The challenge of transporting TRITON between the submerged SSCN and the water's surface was met with the design of a Submersible Launch and Recovery Pod (SLRP). The SLRP system consists of a tethered, box-like pod which encapsulates a single vehicle during the ascent/descent between the SSCN and water's surface. Upon surfacing, the pod transforms into a floating pad for the vehicle, providing a stable dry platform for take-off and landing. The SOF crew are transported along with the ARV in the SLRP. An umbilical between the SSCN and SLRP provides breathing air for SOF crew, electrical power for powering SLRP and TRITON subsystems, and fuel for hot refueling. A harpoon capturing system ensures safe and reliable landing of TRITON in varying sea and weather conditions. The interior pressure of the pod is maintained at 1-atm to mitigate the risk of decompression sickness during the ascent stage.

13.2   SSCN Hanger Configuration

The proposed SSCN hanger configuration permits up to 9 TRITON helicopters to be stored within the space currenltly occupied by 20-missile silos. The hanger layout consists of 6-storages bays plus two deployment and recovery bays. The relative placement of the dual launch and recovery bays permit simultaneous vehicle deployment and recovery. A central elevator system permits optimal usage of the vertical space previously occupied by Trident missiles. Symmetry within the hanger configuration permits 3-storage bays and one launch and recovery bay to be omitted to yield an alternative configuration with a reduced footprint. This reduced footprint has the advantage of retaining four missile silos.

13.3   Design Features of TRITON

TRITON, a compact, high-speed, autonomous helicopter, was specifically design to be an integral component within the Special Operations structure. In addition to its compact, high-speed design, TRITON is equipped with state-of-the-art avionics and communications equipment that is compatible with all net-centric devices. Salient design features include the following:

- **Modular ARV/UEV design**   Modular ARV/UEV design permits TRITON to be configured for either ARV or UEV missions depending on specific mission needs. This adaptability permits a single SSCN to handle multiple SOF mission scenarios without returning to port. In addition, in-field removal of UEV modular payload enables emergency recovery of SOF team members. Careful attention has also been paid to the mass balance of the vehicle to ensure that CG movement is well within rotor limits for both manned and unmanned flights and all fuel levels.

- **Fully electric control system** Both weight and maintenance are reduced through the use of electric actuation systems in place of traditional hydraulics.

- **Compact design** The compact design of TRITON maximizes the number of vehicles stowed on-board a single SSCN while allowing two TRITON's to be transported in a single C130J without any disassembly.

- **Very Low CG Travel** Designed to have maximum CG travel of about 7 inches between fully loaded and empty conditions.

- **Swashplateless rotor design** Swashplateless rotor design offers reduced weight and maintenance of the main rotor system, while providing the agility required for nap-of-earth flight. Quad trailing edge flaps provide redundant primary control and active vibration reduction.

- **Off-blade automatic blade folding system** Innovative automatic blade folding strategy places the primary actuation mechanism in the fuselage. This provides the distinct advantages of simplified rotor construction and the placement of moving components in a low inertial environment for increased life.

- **Deicing system** Provision made for deicing rotor blades and other critical components have been provided to ensure 100% mission capability in arctic environments.

- **Composite transmission housing** Corrosion proof composite transmission housing for increased operational life in maritime environments, and reduced system weight.

- **Armored composite airframe** Composite airframe ensures continued operation in maritime environments with minimal maintenance. In addition, low altitude flight introduces the risk of sustaining damage due to light arms fire. Thus, the external composite construction also consists of of CRYSTALOY ceramic matrix composite capable of withstanding light arm fire.

- **Self sealing crashworthy fuel tanks** Self sealing capabilities of the fuel tanks prevent the leakage of fuel, in the case of a crash. In addition, fuel tanks have been sized to have a volume 10% greater than required for flight. This provide volume for an air cushion, to prevent tank failure during impact.

- **Retractable wheeled landing gear** Retractable wheeled landing gear provides reduced drag in forward flight while facilitating easy ground handling.

- **Fully sealed fuselage** Fuselage is fully sealed to ensure no ingress of sea water during normal vehicle operation and emergency water landings.

- **Crashworthy fuselage** Dual sine-wave keel beams specially designed to absorb high amounts of energy upon impact. Geometry of fuselage lower body tailored to mitigate earth plowing during a crash, thereby further reducing the severity of impact forces.

- **Health Usage and Monitoring System (HUMS)** HUMS capability is designed into to help track the usage of flight critical components, and provide credits to standard maintenance schedules. The HUMS

will lead to reduced maintenance cost as well as increased reliability, readiness and safety.

- **Low development risks** Usage of proven state-of-the-art technology minimizes development risks. and ensures repeatable mission performance. Recognizing that Special Operations is only as strong as its weakest link, this is a particularly attractive feature.

- **Tactical Control System software** Tactical Control System (TCS) software permits command and control of TRITON helicopters and SLRP launch and recovery pods through a common control network.

The TRITON design is a modular solution that fulfills both ARV and UEV requirements while offering the ability to adapt to the specific needs of the mission. The armored composite skin combined with crashworthy airframe and and fuel system, all electric actuation, and TCS software make the TRIT0N design well adept for SOF missions. TRITON is a compact, high-speed, autonomous helicopter designed to be an integral component of Special Operation Forces.

Bibliograpy

[1] Stephen J. Spadafora. Navair perspective on corrosion prevention and control. Professional paper, NAWCAD, 2000. Accession Number ADA375736.

[2] Macartney group underwater technology systems. http://www.macartney.com/, 2007.

[3] Sierra nevada corporation uav common automatic recovery system. http://www.waveband.com/prod/cnsatm/uav/uav3.shtml, 2007.

[4] Kell-strom light harpoon landing restraint system. http://www.kell-strom.com/tools/dcn/dcnpg01.htm, 2007.

[5] H. A. Jackson. Fundamental of submarine concept design. *Society of Naval Architects and Marine Engineers*, 100, 1992.

[6] M. N. Tischenko, V. T. Nagaraj, and I. Chopra. Preliminary design of transport helicopters. *Journal of the American Helicopter Society*, 48(2):71–79, 2003.

[7] N. Koratkar. *Smart Helicopter Rotor With Peizoelectric Bender Actuated Trailing-Edge Flaps*. PhD Dissertation, University of Maryland, College Park,MD, 2000.

[8] B. Roget. *Individual Blade control for Vibration Reduction of a Helicopter with Dissimlar Blades*. PhD Dissertation, University of Maryland, College Park,MD, 2004.

[9] J. Shen. *Comprehensive Aeroelastic Analysis of Trailing Edge Flap Helicopter Rotors*. PhD Dissertation, University of Maryland, College Park,MD, 2003.

[10] T. P. Arnold Uwe, T. Neuheuser, and R. Bartels. Development of integrated electrical swashplateless primary and individual blade control system. *Proceedings of 63rd Annual American Helicopter Society Forum*, 2006.

[11] J. Falls, A. Datta, and I. Chopra. Integrated trailing-edge flaps and servotabs for helicopter primary control. *Submitted to American Helicopter Society Journal*, 2007.

[12] Maxon motor. High precision drives and system. *http://www.maxonmotorusa.com*, 2007.

[13] V. T. Nagaraj. *ENAE 634, Helicopter Design Lecture Notes*. University of Maryland, College Park,MD, 2007.

[14] J. Bao, V. T. Nagaraj, I. Chopra, and A. P. F. Bernhard. Wind tunnel testing of low vibration mach scale rotor with composite tailored blade. *Proceedings of 60th Annual American Helicopter Society Forum*, 2004.

[15] F. W. Alex and G. A. McCourbrey. Design and structural evaluation of the sh-2f composite main rotor blade. *Journal of American Helicopter Society*, 1986.

[16] Lord Corporation. Lead lag dampers. *http://www.lord.com*, 2007.

[17] J. G. Leishman. *Principles of Helicopter Aerodynamics*. Cambridge University Press, 2006.

[18] Unison. Power generation systems. *http://www.unisonindustries.com*, 2007.

[19] W. Johnson. *Helicopter Theory*. Dover Publications, Inc., New York, 1994.

[20] W.Z. Stepniewski and C.N. Keys. *Rotary Wing Aerodynamics*. Dover Publications, Inc., 1984.

[21] J. Gordan Leishman. *Principles of Helicopter Aerodynamics*. Cambridge University Press, 2000.

[22] William G. Bousman. Airfoil design and rotorcraft performance. In *American Helicopter Society 58th Annual Forum, Montreal, Canada, June 11-13*, 2002.

[23] Kevin W. Noonan. Aerodynamic characteristics of two rotorcraft airfoils designed for application to the inboard region of a main rotor blade. Technical report, NASA, 1990. Technical Paper 3009.

[24] Kevin W. Noonan. Aerodynamic characteristic of a rotorcraft airfoil designed for the tip region of a main rotor blade. Technical report, NASA, 1991. Technical Report 91-B-003.

[25] Preston B. Martin and J. Gordon Leisman. Trailing vortex measurements in the wake of a hovering rotor blade with various tip shapes. In *58th Annual Forum of the AHS International, Montreal Canada, June 11-13*, 2002.

[26] Ki Hoon Chung, Jae Wook Kim, Ki Wahn Ryu, Kyung Tae Lee, and Duck Joo Lee. Sound generation and radiation from rotor tip-vortex pairing phenomenon. *AIAA Journal*, 44(6):1181–1187, 2006.

[27] Kim Chung and Inderjit Chopra. Aeroelastic analysis of helicopter rotor blades with advanced tip shapes. In *AIAA/ASME/ASCE/AHS/ASC Structures, Structural Dynamics and Materials Conference*, pages 1690–1713, 1990. 31st, Long Beach, CA Apr 2-4.

[28] A. Desopper, Lofton P. Philips, and J. Prier. Effect of an anhedral sweptback tip on the performance of a helicopter rotor. In *44th Annual Forum of American Helicopter Society*, June 1988.

[29] O.L. Santa Maria and A.W. Mueller. Acoustics of uh-60 black hawk with growth rotor blades. In *American Helicopter Society 53rd Annual Forum, Virginia Beach, Virginia, April 29 - May 2*, 1997.

[30] Avibank mfg. www.avibank.com.

[31] R. Mouille and F. d'Ambra. The 'fan-in-fin': A shrouded tail rotor concept for helicopters. *Proceedings of 42nd Annual American Helicopter Society Forum*, pages 597–606, 1986.

[32] J. G. Leishman. *Principles of Helicopter Aerodynamics*. Cambridge University Press, 2006.

[33] C. Keys, M. Sheffler, S. Weiner, and R. Heminway. Lh wind tunnel testing: Key to advanced aerodynamic design. *Proceedings of 47th Annual American Helicopter Society Forum*, pages 77–87, 1991.

[34] Charles A. Jr. Yoerkie, Philip H. LeMasurier, and Steven D. Weiner. Helicopter antitorque device, April 11 1991. United States Patent.

[35] Henri-James R. Marze and Vincent J. L. Routhieau. Counter-torque device with rotor and flow straightening stator, both of which are ducted, and inclined flow-straightening vanes, September 30 1996. United States Patent.

[36] Y. Niwa. The development of the new observation helicopter (xoh-1). *Proceedings of 54th Annual American Helicopter Society Forum*, 1998.

[37] Naval Air Systems Command. Aeronautical requirements-structural design requirements (helicopters). Military requirements, U.S. Navy, 1970. AR56 superceding MIL-S-8698.

[38] Jean-Claude Flabel. *Practical Stress Analysis for Design Engineers*. Lake City Publishing Company, 1992.

[39] Daniel P. Raymer. *Aircraft Design: A Conceptual Approach*. AIAA Education Series, third edition, 1999.

[40] Inc. Industrial Ceramic Technology. Composite structures for ballistic protection. http://www.indceramictech.com.

[41] Dupont. http://www.dupont.com.

[42] U.s. navy tactical control system. http://www.raytheon.com/products/stellent/groups/public/documents/legacy_site/cms01_ 2007.

[43] Raytheon products tcs. http://www.raytheon.com/products/tcs/, 2007.

[44] General atomics aeronautical systems ground control station. http://www.ga-asi.com/products/gcs.php, 2007.

[45] Future combat system. http://www.army.mil/fcs/, 2007.

[46] Bae systems identification friend or foe systems. http://www.baesystems.com/ProductsServices/eis_nes_iff.html, 2007.

[47] Dukane underwater acoustic beacons. http://www.aerosystems.com/Showcase/PID142.HTM, 2007.

[48] Honeywell aerospace radar altimeters. http://www.honeywell.com/sites/aero/Military-Aircraft3_CC97F1FA1-ED1D-D7D4-15D8-1272F2E6C702_HFC5482F9-3DD3-2A4F-DE15-0A1BCB4CA9C6.htm, 2007.

[49] H. koch & sons co. emergency egress lighting system. http://www.hkoch.com/eels.cfm, 2007.

[50] Flir systems eo/ir/lrdf. http://www.flir.com/imaging/Airborne/Products/BriteStar.aspx, 2007.

[51] Kearfott gps/ins. http://www.astronautics.com/new/Products/Datasheet.asp?id=153, 2007.

[52] Selex communications laser obstacle avoidance monitoring system. http://www.selex-comms.com/en/wp-content/uploads/2006/02/LOAM.pdf, 2007.

[53] Wayne F. Jewell Warren F. Clement, Peter J. Gorder. Fully automatic guidance and control for rotorcraft nap-of-the-earth flight following planned profiles volumne 1 - real-time piloted simulation. Contractor report, NASA, 1991. Contract Number NAS2-12640.

[54] Martin-baker crashworthy armoured crew seat. http://www.martin-baker.com/crashw_armored.html, 2007.

[55] Atlas devices powered rope ascender. http://atlasdevices.com/index.htm, 2007.

[56] David G. Lewicki. Torque splitting by a concentric face gear transmission. *58th American Helicopter Society Annual Forum*, June 2002.

[57] Darle W. Dudley. *Handbook of Practical Gear Design*. McGraw-Hill Book Company, 1984.

[58] A H. Schmidt. A method of estimating the weight of aircraft transmissions. *35th Annual Conference of the Society of Allied Weight Engineers*, May 1976.

[59] Charley Kilmain Timothy M. Cecil, Ryan T. Ehinger. Application and configuration issues of resin transfer molded composite transmission housings a program overview. *63rd American Helicopter Society Annual Forum*, May 1-3 2007.

[60] N D Phan Scott Maley, J Plets. Us navy roadmap to structural health and usage monitoring—the present and future. *63rd American Helicopter Society Annual Forum*, May 1-3 2007.

[61] J.M. Sr. Unres, J. Cushing, B. Bond, and S. Nunes. "on-board flight fault diagnostics for fly-by-light flight control systems using neural network flight processors. In *Proceedings of SPIE - The International Society for Optical Engineering, Fly-By-Light III, vol. 2840, August*, 1996.

[62] D. K. Unsworth and J. G. Sutton. An assessment of the impact of technology on vtol weight prediction. *Proceedings of 40nd Annual American Helicopter Society Forum*, pages 253–262, 1984.

[63] R. W. Prouty. *Helicopter Performance Stability and Control*. Kreiger Publishing Company, 2005.

[64] Hyeonsoo Yeo and Wayne Johnson. Aeromechanics analysis of a heavy lift slowed-rotor compound helicopter. *Journal of Aircraft*, 44(2):501–508, 2007.

[65] R. V. Harris. An analysis and correlation of aircraft wave drag. Technical report, NASA, 1964. NASA TM X-947.

[66] Daniel P. Raymer. *Aircraft Design: A Conceptual Approach*. AIAA Education Series.

[67] Request for proposals for light helicopter upgrage program. Technical report, AHS, Bell Helicopters and Textron, 2002. 19*th* Annual Student Design Compettition.

[68] http://data.bls.gov/cgi.bin/cpicalc.pl.